Discrete-Time Control Design for Tracking Control Of Piezo-Actuated Positioning Systems

A DISSERTATION SUBMITTED TO THE
GRADUATE SCHOOL OF ENGINEERING AND SCIENCE OF
SHIBAURA INSTITUTE OF TECHNOLOGY

by

NGUYEN MANH LINH

IN PARTIAL FULFILLMENT OF THE REQUIREMENTS
FOR THE DEGREE OF

DOCTOR OF PHILOSOPHY

SEPTEMBER 2018

Acknowledgments

First of all, I would like to convey my special thanks to my supervisor, Professor Xinkai Chen for his kindness, encouragements, enthusiastic guidance, helpful advices and technical supports throughout my research.
I would also like to thank to all students in Systems Control laboratory, Omiya campus, Shibaura Institute of Technology and special thanks to my all Vietnamese friends for their support.

Saitama, September, 2018

Nguyen Manh Linh

Abstract

Recently, the micro-positioning has become an important development target for meeting the requirements of the precision industry, such as in the semiconductor manufacturing process, biotechnology processes and opto-electronics systems. Since the piezoelectric actuator has many advantages, such as high displacement resolution (sub nanometer), large actuating force, fast response time (μs range), tiny size, electric controllable, PEA as well as PEA-driven positioning systems has been extensively used in the fields of micro/nano positioning and being the most commercialized and understood technology in the smart actuator market. However, PEAs also exhibit undesired serious disadvantages such as hysteresis, creep and vibration behaviors, which have shown to be able to significantly degrade the performance of the controlled system.

In this study, precise tracking control of piezo-actuated positioning systems, which is composed by a PEA and a positioning mechanism, is considered due to its important role and popularity in practical applications. In this case, the performance of system is mainly affected by the hysteresis phenomenon. Hence, the goal of this study is to propose control algorithms which have ability to handle the difficulties caused by the nonlinear behavior and achieve excellent tracking performance. In advanced, all the control designs are conducted in discrete-time domain. As a result, the control algorithm can easily be implemented in digital controllers.

In order to achieve the above goals, various advanced control schemes have been proposed and presented in this study. In details, a pseudo

model predictive control which mimics the behavior of its conventional counterpart is presented in *Chapter 2*. In *Chapter 3*, the conventional discrete-time sliding mode control and integral sliding mode control design is introduced in the first two sections. Then, a novel discrete-time prescribed performance sliding mode control is proposed to improve the response in transient-state while remains the tracking performance in steady-state. In *Chapter 4*, the discrete-time fractional order-based controllers are discussed. A new method to approximate the fractional order integral is proposed first. Then, this proposed approximation is applied to a discrete-time fractional order $PI^{\alpha}D^{\beta}$ controller along with the particle swarm optimization to get the best performance. At last, the discrete-time fractional order integral sliding mode control is investigated. Fuzzy tuning is chosen as an effective tool to improve the system performance by adjusting all parameters of the controller simultaneously. The validity and effectiveness of all proposed methods are confirmed by experiments.

Contents

List of Figures

List of Tables

List of Abbreviations

Acronyms

Symbol	Description
AI	Analog input
AO	Analog output
DFISMC	Discrete-time fractional order integral sliding mode control
DISMC	Discrete-time integral sliding mode control
DSMC	Discrete-time sliding mode control
FOD	Fractional order differential
FOI	Fractional order integral
GA	Genetic algorithm
ISMC	Integral sliding mode control
MAXTE	Maximum tracking error
MF	Membership function
MPC	Model predictive control
NMSS	Non-minimal state space model
PEA	Piezoelectric actuator

PI	Prandtl-Ishlinskii
PID	Proportional integral differential
PPC	Prescribed performance control
PPF	Prescribed performance function
PSO	Particle swarm optimization
QSM	Quasi sliding mode
QSMB	Quasi sliding mode band
SISO	Single input single output
SMC	Sliding mode control

Greek Symbols

Symbol	**Description**
α	Fractional order of integral
$\bar{\delta}$, $\underline{\delta}$	Upder and lower bound of prescribed performance function
β	Fractional order of differential
χ	Damping coefficient of the sliding variable
δ_k	Integral of error state variable
ϵ	Positive constant representing the bound of $\hat{p}_k$
γ	Small positive constant
$\hat{\theta}$	Estimation of θ_0
Λ	Strictly increasing function
λ_x,λ_u	Positive definite weighted matrices
μ_0	Initial value of prescribed performance function

μ_∞	Prescribed performance function in steady-state
μ_k	Prescribed performance function at time instance k
Ω,ω	Weighting factors of fractional order integral
τ_k	Revised transformed error
θ_0	Vector of original parameters
ϑ	Original transformed error

Superscripts

Symbol	Description
z^{-1}	Backward shift operator

Subscripts

Symbol	Description
$\hat{p}_k$	Perturbation estimation at time instance k
$\tilde{p}_k$	Perturbation estimation error at time instance k
a_1, a_2, b_1, b_2	Known parameters of piezo-actuated positioning system
c_1,c_2	Cognitive and social coefficient
e_k	Tracking error at time instance k
G_{best}	Global best vector used in PSO
K_D	Differential gain
K_I	Integral gain
K_P	Proportional gain
K_{sw}	Switching gain
N_P	Number of prediction

P_k	Projection matrix at time instance k
p_k	Perturbation at time instance k
P_{best}	Best position used in PSO
S_k	Sliding variable k
T_s	Sampling time
U_F	Vector of future control signals
u_k	Controlse signal at time instance k
W_c	Closed-loop transfer function
W_d	Input disturbance's transfer function
W_p	Plant's transfer function
W_{L_d}	Load disturbance's transfer function
X_F	Vector of future state variables
y_k	Measured output at time instance k
$Y_{d,F}$	Vector of future desired outputs

Other Symbols

Symbol	**Description**
${}^{\alpha}\zeta_{e,k}$	Fractional order integral of tracking error at time instance k
${}_{t_0}^{\beta}D_t e(t)$	Fractional order differential of tracking error $e(t)$
$B(z^{-1})$, $A(z^{-1})$	Numerator and denominator polynomial of plant's transfer function, respectively
$D_{ref}(z^{-1})$	Desired characteristic polynomial
$O(T_s^2)$	Same order with T_s^2

NumofIter	Number of iterations
NumofPo	Number of population
AvgGain	Average gain

Chapter 1

Introduction and Objectives

This chapter starts out by describing the working principle of PEA and its important characteristics. Then, challenges and objective of this dissertation are discussed. The end of this chapter presents the outline of its organization.

1.1 Working Principle of Piezoelectric Actuator

1.1.1 Piezoelectric Effect

The piezoelectric effect was discovered by the Curie Brothers in 1880. The direct piezoelectric effect contains the ability of certain materials, which are called piezo-materials, to generate electric charge in proportion to externally applied force. The effect is reversible and then is called as an inverse piezoelectric effect (Fig. 1.1). The piezoelectric actuator (PEA) is based on the inverse piezoelectric effect. In this case, the deformation of PEA can be adjusted by varying the applied input voltage.

1.1.2 Properties of PEA

The main properties of the PEAs are briefly introduced in this sub-section.

1. **Unlimited Resolution**: Piezo actuators convert electrical energy directly into mechanical energy and vice versa and allow for motions in the sub-nanometer range. There are no friction elements that limit resolution.

2. **Rapid Response**: Piezo actuators allow response times of a few microseconds.

3. **High Force Generation**: High-load piezo actuators capable of moving loads of several tons are available.

4. **No Magnetic Fields**: The piezoelectric effect is related to electric fields, piezo actuators do not produce magnetic fields nor are they affected by them.

5. **Low Energy Consumption**: Static operation, even holding heavy loads for long periods, consumes virtually no power. A piezo actuator behaves very much like an electrical capacitor. When at rest, no heat is generated.

6. **No Wear and Tear**: A piezo actuator has no moving parts as gears or bearings. Its displacement is based on crystalline solid-state dynamics and shows no wear and tear. For example, PEAs of Physical Instrument have gone through several billion cycles in endurance tests without measurable changes in their behavior.

7. **Vacuum and Clean Room Compatible**: Piezo actuators neither cause abrasion nor do they require lubrications. The all-ceramic insulated actuators have no polymer coating and are thus ideal for ultrahigh vacuum applications.

8. **Operation at Cryogenic Temperatures**: The piezo effect continues to operate even at very low temperatures close to 0 Kelvin.

9. **Wide Operating Voltage Range**: Two types of PEAs have become established: Monolithic-sintered multilayer actuators (low-voltage actuators) operate at voltages up to about 130 V and are made of ceramic layers from 20µm to 100µm in thickness. Classical high-voltage actuators (high-power

actuators) are made from ceramic layers of 0.5 to 1mm thickness and operate at voltages of up to 1000V. PICA actuators can be manufactured with larger cross-sections, making them suitable for larger loads than the more compact monolithic multilayer piezo actuators.

10. **Stiffness, Load Capacity, Force Generation**: To a first approximation, a PEA is a spring-and-mass system. The stiffness of the actuator depends on the elasticity module of the ceramic (approx. 25% of that of steel), the cross-section and length of the active material and other nonlinear parameters. Typical actuators have stiffnesses between 1 and 20000N/µm and compressive limits between 10N and 100000N. For tensile stresses, a casing with integrated preload or an external preload spring is required. Adequate measures must be taken to protect the piezo ceramic from shear and bending forces and from torque.

11. **Travel Range**: The travel ranges of piezo actuators are typically in between a few 10µm to a few 100µm for linear actuators. Bending actuators can achieve a few millimeters.

12. **Position Resolution**: The piezoceramic itself works free of friction and theoretically has unlimited resolution. In practice, the resolution actually attainable is limited by electrical and mechanical factors:
    a) Sensor and servo-control electronics, amplifiers: Amplifier noise and sensitivity to electromagnetic interferences (EMI) affect positional stability.
    b) Mechanical parameters: Design and mounting precision issues concerning the actuator, preload and sensor can induce microscopic friction which limits resolution and accuracy. PEAs reach sub-nanometer resolution and stability

Given above properties, the PEAs have been extensively used in a variety of industrial, automotive, medical, aviation, aerospace and consumer electronics applications. PEAs are found in precision knitting machinery and braille machines. The silent drive characteristics make piezo actuators an excellent auto focusing mechanism in microphone-equipped video cameras and mobile phones. Finally,

since PEAs require no lubrication to operate, they are also used in cryogenicand vacuum environments.

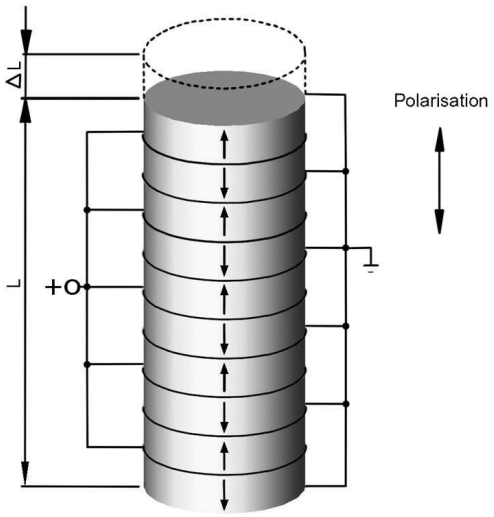

Figure 1.1: Inverse piezoelectric effect

1.2 Behaviors of PEA

In micro- and nanopositioning applications, typical behaviors of PEAs concerned include hysteresis, creep, and vibration dynamics.

1.2.1 Hysteresis

Hysteresis is the nonlinear dependence of a system not only on its current input but also on its past input. In PEAs, hysteresis exists in voltage-displacement relationship as shown in Fig. 1.2(a) [59]. It can be seen that the hysteresis is composed of three types of components, which are the major loop that spans the whole input range, the minor loop that only spans portions of input range, and the initial loading curve.

Hysteresis occurs in both relatively static operations and dynamic operations. If the influence of the rate of change of the input can be ignored, then the hysteresis is referred to as rate independent, otherwise rate dependent. As hysteresis being the major nonlinearity of PEAs, compensation of hysteresis has always been a major concern in modeling and control of PEAs.

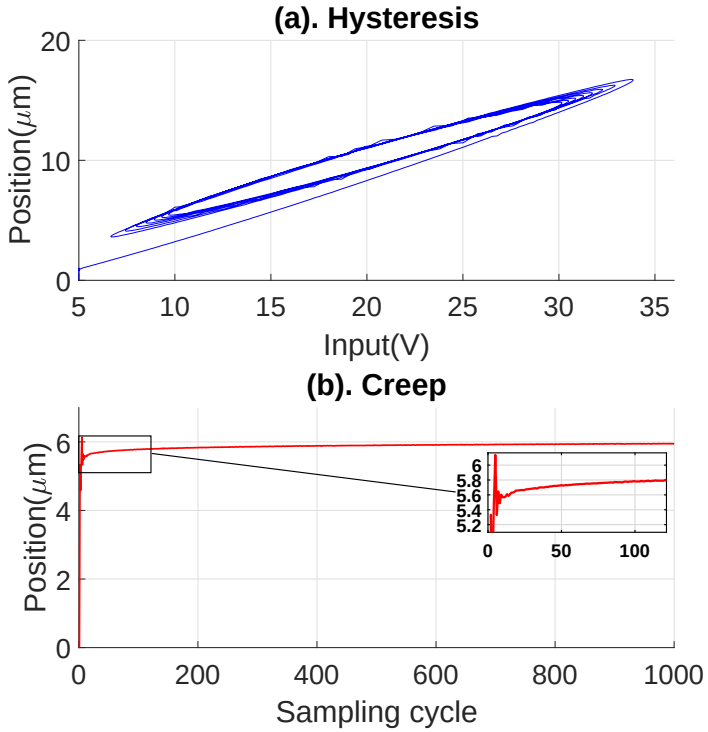

Figure 1.2: Hysteresis and creep of a PEA

1.2.2 Creep

Creep is the slow variation in the PEA displacement that occurs without any accompanying change in the input voltage as shown in 1.2(b). Being a slow and a small effect, creep is sometimes neglected in closed loop and high frequency operations. However, for slow and open-loop operations of PEAs, creep must be considered to avoid large positioning error.

1.3 An Overview of Modeling and Control Design

1.3.1 Modeling of PEAs

Significant efforts have been made to mathematically represent the complicated behaviors of PEAs and mainly focus on modeling the hysteresis phenomenon which has strong influence on the accuracy of the positioning systems. The linear electromechanical model reported in [**?**] is an early example. However, the nonlinear behavior including hysteresis and creep have not been well reflected due to the linear and static nature of the model. Then, advanced mathematical models which are able to describe the hysteresis curve directly have been proposed. These advanced models can be classified as operator-based and nonlinear differential equation-based hysteresis models. In the former approach, Preisach hysteresis model [53, 69], the Prandtl-Ishlinskii(PI) hysteresis model [4, 40, 41], and the Maxwell slip hysteresis model [29, 46] are the most widely used. In the latter approach, Bouc-Wen model [3, 31, 81] can be regarded as typical examples. These above mentioned models are briefly reviewed as follows.

1.3.1.1 Preisach Hysteresis Model

The Preisach model reflects the behavior of the hysteresis by combining infinite number of the Preisach hysteresis operators $\delta_P[\alpha, \beta, u(t)]$. Each operator is characterized by two parameters including a up switching value α and a down switching value β, with $\alpha \geq \beta$. Two saturation values: -1 and 1 are used to restrict the output of the operator. The model output is adjusted by an additional weighting function $\mu(\alpha, \beta)$. As such, the final formulation of the Preisach model is expressed by

$$Pr(t) = \int\int \mu(\alpha, \beta)\delta_P[\alpha, \beta, u(t)]\, d\alpha d\beta \tag{1.1}$$

where $u(t)$ is the input and $Pr(t)$ is the output of the model.

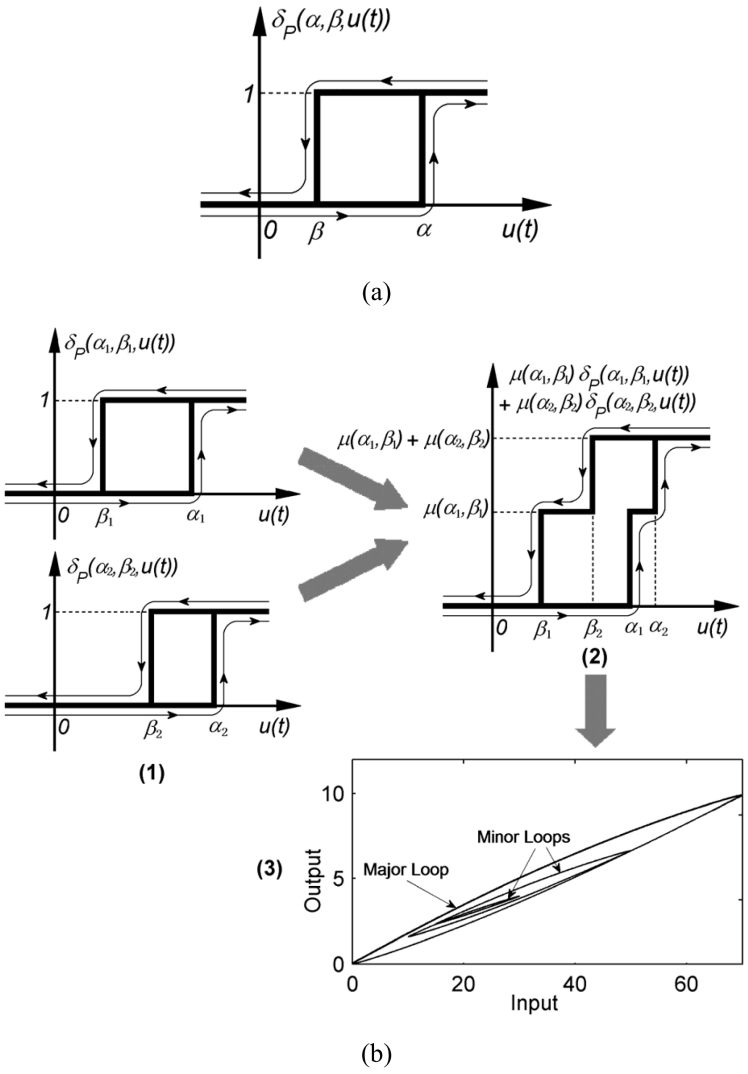

Figure 1.3: (a) Preisach hysteresis operators; (b) Combination of operators; (c) Result hysteresis curve

By using infinite number of operators, the Preisach model can describe a wide range of hysteresis precisely as illustrated in Fig. 1.3 [59]. However, large computational effort and rate-independent are major concerns of this approach.

1.3.1.2 Prandtl-Ishlinskii Hysteresis Model

The PI model describes the behaviour of the hysteresis by the combined effect of large number of back-lash operators.

Let $C[0, t_E]$ stands for a space of piecewise monotone continuous functions. For any input $u(t) \in C[0, t_E]$ with $0 = t_0 < t_1 < \cdots < t_N = t_E$ such that $u(t)$ is monotone on each sub-interval $[t_i, t_{i+1}]$, the output of the backlash operator is defined by

$$\begin{aligned} B_r[u](0) &= f_r(u(0), 0) = w(0) \\ w(t) &= B_r[u](t) = f_r(u(t), B_r[u](t_i)) \\ &\text{for } t_i < t \leq t_{i+1} \text{ and } 0 \leq i \leq N-1 \end{aligned} \tag{1.2}$$

in which

$$f_r(v, w) = max(v - r, min(v + r, w)) \tag{1.3}$$

and r is the threshold of the operator.

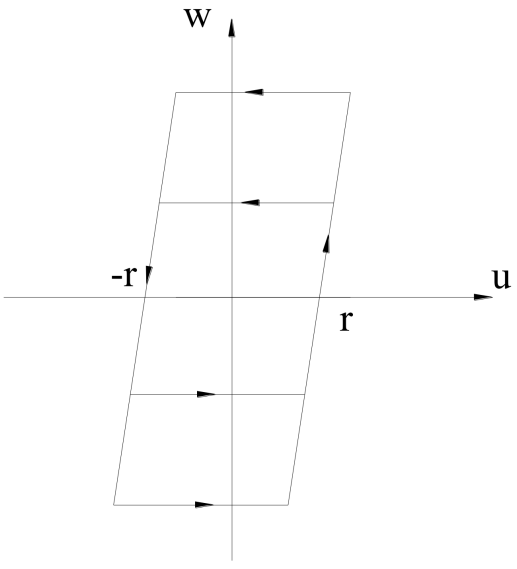

Figure 1.4: Back-lash operator with threshold r

The PI model combines the play operator and a linear function of input $u(t)$

to describe the hysteresis as follows

$$H[u](t) = Ku(t) + \int_0^R d(r) B_r[u](t) dr \tag{1.4}$$

where $d(r) \geq 0$ is a density function, $K > 0$ is a desired gain and R is a positive constant.

In practice, the discrete form of the classical PI model is prefered

$$H[u]_k = Ku_k + \sum_{j=1}^{N} d_j B_{r,j}[u]_k \tag{1.5}$$

where N is the number of used back-lash operator.

As can easily be seen in Fig. 1.4, the classical PI model can only reflect the behaviour of the symmetrical hysteresis. To describe the asymmetrical hysteresis, this model must be modified.

1.3.1.3 Maxwell Slip Hysteresis Model

Similar to the PI model, the Maxwell slip hysteresis model describe the hysteresis by putting a finite number of elasto-slide elements in parallel as shown in Fig. 1.5 [47]. Each element is composed of a mass sliding on a surface with a Coulomb friction $\mu_i N_i$ where μ_i is the friction coefficient and N_i is the normal force between the mass ans the surface, and a linear spring with stiffness k_i with one connected to the mass and the other end is free. As such, the hysteresis exists between the displacement and the force of the spring and expressed by

$$\dot{x}_i(t) = \begin{cases} 0 & for \quad k_i \left[x(t) - x_i(t)\right] sgn\left[\dot{x}(t)\right] < \mu_i N_i \\ \dot{x}(t) & for \quad k_i \left[x(t) - x_i(t)\right] sgn\left[\dot{x}(t)\right] \geq \mu_i N_i \end{cases} \tag{1.6}$$

$$F(t) = \sum_{i=1}^{n} k_i \left[x(t) - x_i(t)\right] \tag{1.7}$$

where x is the input displacement, F is the output force and x_i is the block position.

As the displacement increases or decreases continuously, the gain between the force and the displacement changes piecewise linearly which represents the

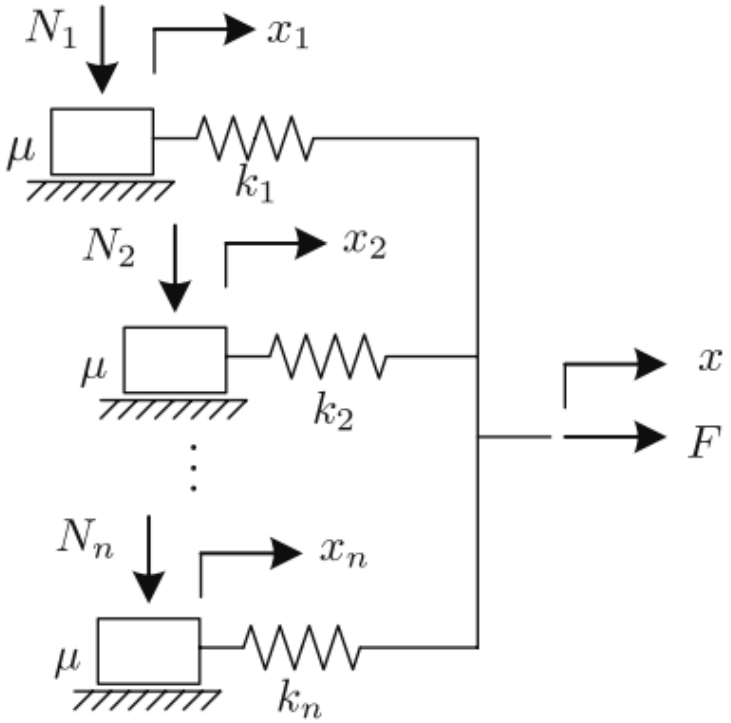

Figure 1.5: Maxwell slip hysteresis model

nonlinear gain of the hysteresis. If the movement changes the direction, the sliding elements come to stick. Hence, the sudden switch of the gain at the endpoint of the hysteresis loop can be reflected.

1.3.1.4 Bouc-Wen Hysteresis Model

This nonlinear differential equation-based model was first proposed by Bouc early in 1971 and subsequently generalized by Wen in 1976. Since then, it was known as the Bouc-Wen model and extensively used not only in modeling the hysteresis but also in control design. The most popular form of the Bouc-Wen model is expressed by

$$\begin{aligned} \Phi_{BW}[x(t)] &= \alpha k x(t) + (1-\alpha) D k z(t) \\ \dot{z}(t) &= D^{-1}\left(A\dot{x} - \beta|\dot{x}||z|^{n-1}z - \gamma\dot{x}|z|^{n}\right) \end{aligned} \tag{1.8}$$

in which z is the shape function, $n > 1$, $D > 0$, $k > 0$, $0 < \alpha < 1$ and $\beta + \gamma \neq 0$ are desired constants. By tuning these parameters appropriately, the hysteresis

curve can be obtained. A typical example of the Bouc-Wen model is depicted in Fig. 1.6.

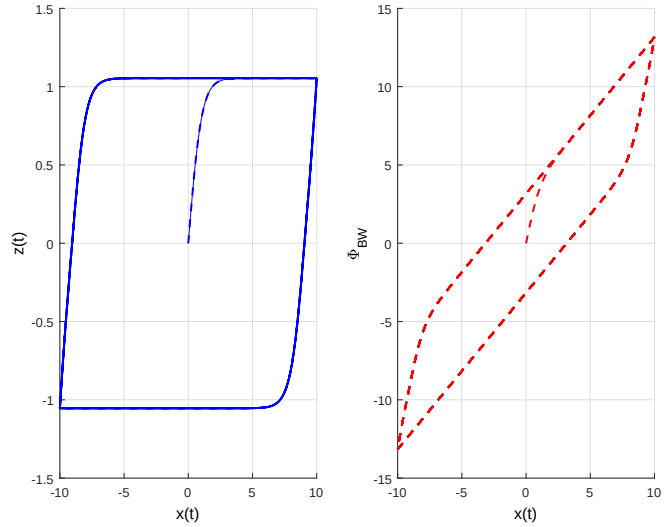

Figure 1.6: An example of hysteresis based on Bouc-Wen model

1.3.2 A Survey of Control Design

Over the years, a large number of control methods have been proposed for control of piezo-actuated positioning systems. Due to the detrimental influences of the hysteresis on the performance of the control systems, compensation of the hysteresis becomes the major concern in all studies. The typical control schemes are briefly introduced as following.

1.3.2.1 Open-Loop Control

This is the simplest control scheme in which the control signal is computed from the inverse model of the control plant. The way to obtain the inverse hysteresis has been reported in numerous studies [5, 35, 38, 42, 62]. The parameters of the controller is obtained based on the open-loop input/output data. Hence, the control system can only show acceptable performance in specific conditions. In

general, this method is very sensitive to the modeling error and the changes of working condition.

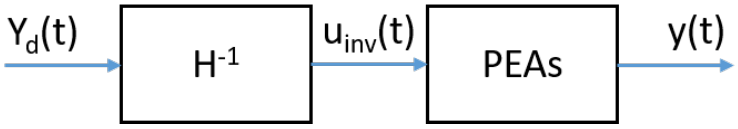

Figure 1.7: Inverse control scheme

1.3.2.2 Feedback Control

Until now, feedback control is still the most popular control scheme in practice due to its ability to suppress the unknown effects such as modeling error, external load and disturbances. The typical configuration of a feedback control system is shown inf Fig. 1.8.

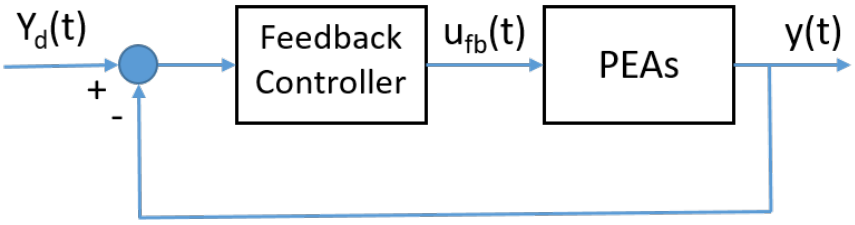

Figure 1.8: Feedback control scheme

In static or low tracking frequency, classical proportional-integral-differential (PID) controller is widely used because of its simplicity in implementation as well as its capable of compensating the steady-state error. The parameters of the PID controller can be obtained by various techniques such as "trial and error" [27], optimal linear quadratic regulation [68], auto tuning [94], etc. However, the performance of the PID controller is significantly degraded in high frequency tracking applications due to its limited bandwidth while dealing with uncertainties.

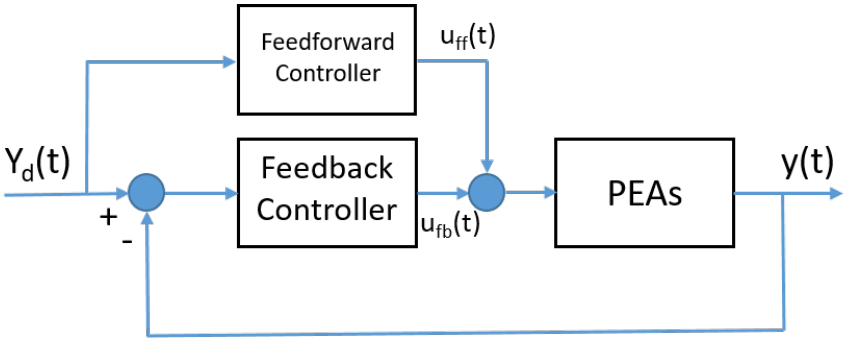

Figure 1.9: Feedforward control scheme

1.3.2.3 Feedback with Feedforward Control

To improve the tracking performance, the conventional feedback scheme can be augmented by a feedforward controller as seen in Fig. 1.9. The merit of this approach is that the gain margin of the control system can be enhanced. Typical researches which adopt this control scheme are [27, 45] in which an inverse Preisach hysteresis model is used as the feedforward controller to compensate the hysteresis while a PID is used as feedback controller to handle other effects.

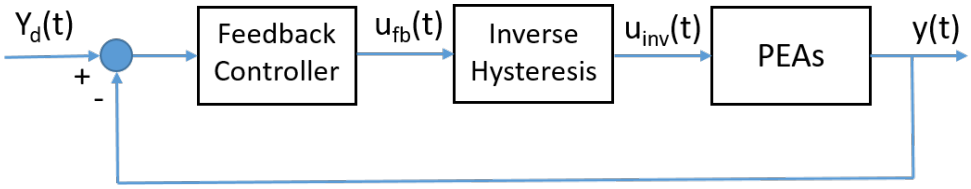

Figure 1.10: Feedback with inverse feedforward control scheme

Another control scheme which involves feedback and feedforward is reported in [23, 82]. The block diagram of this approach is shown in Fig. 1.10. In this case, an inverse hysteresis is used to mitigate the hysteresis effect first. Then, a feedback controller is used to suppress the remaining nonlinearity. However, as other hysteresis-based methods, identification procedure is a time consuming task and the existence of the modeling error is inevitable.

1.3.2.4 Advanced control techniques

To overcome the aforementioned drawbacks of the conventional control scheme, handle the nonlinearities as well as improve the tracking performance in broadband applications, advanced control techniques are extensively studied in recent years.

Among all of such advanced control techniques, sliding mode control (SMC) shows itself a very effective approach due to its capable of rejecting the effects of so-call matched uncertainties which results in strong robustness of the control system. In advance, the fast dynamic of the PEAs also suit well the deadbeat response of the closed-loop system-based SMC. A lot of results based on this control scheme have been reported, e.g, in [84] a second order discrete-time terminal SMC is adopted to guarantee that the quasi-sliding mode is reached in finite time and high accuracy output tracking is achieved, in [88] a novel model predictive SMC is proposed to further attenuating the positioning error, in [83] the discrete-time integral sliding mode control is used to achieve an $O(T^2)$ tracking precision with respect to the sampling interval T, etc. In these researches, the control design is conducted based on a nominal mathematical model of the PEAs whist the hysteresis, creep and other uncertainties are treated as a lump disturbance. This lump disturbance is then estimated by a disturbance observer and embedded into the control action such that the chattering can be mitigated.

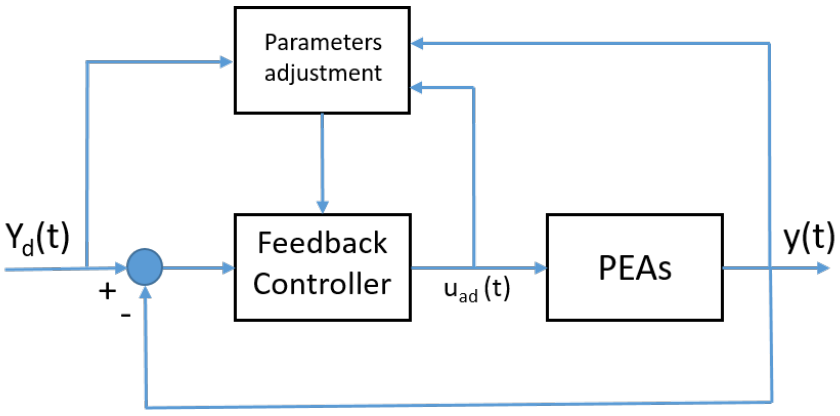

Figure 1.11: Adaptive control scheme

Adaptive control technique has also been applied to control PEAs and achieved good tracking performance [14, 43, 86]. An adaptive control system can be thought as having two loops: one loop is a normal feedback loop with the plant and the controller, the other is the parameter adjustment loop. The typical block diagram of the adaptive control system in shown in Fig. 1.11. The advantage of this technique is that it does not rely on system identification since all unknown parameters are automatically updated by adaptive law during control process. The variation in uncertainty that an adaptive system can handle depends directly on the speed of the parameter adjustment loop. However, fast adaptation may lead to high frequency oscillations in control signal.

1.4 Challenges and objective

Figure 1.12: E-712 Digital piezo controller of *physikinstrumente*

Although PEAs have been extensively used in many practical applications, the most popular commercial controller used in motion control of PEAs still based on the conventional proportional-integral-differential (PID) algorithm [1]. An typical example is the digital servo controller *E72* of *physikinstrumente* shown in Fig. 1.12. The block diagram and sample response of a PEA is shown in

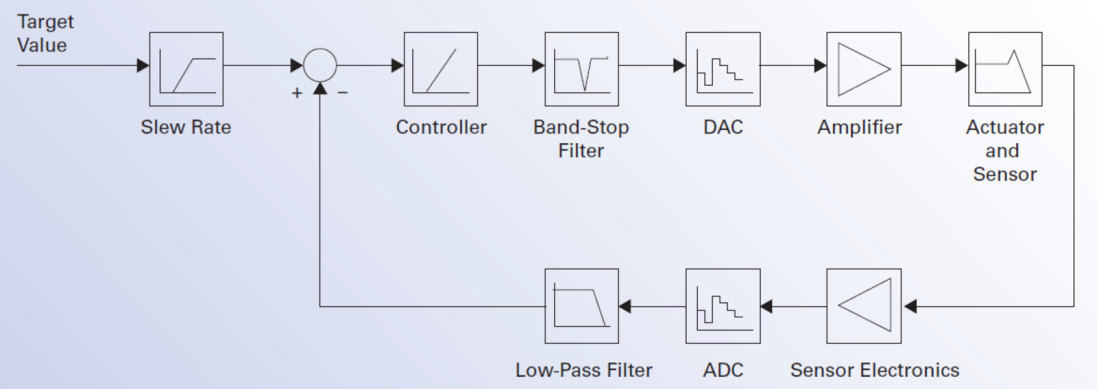

Figure 1.13: Block diagram of a digital piezo servo controller of *physikinstrumente*

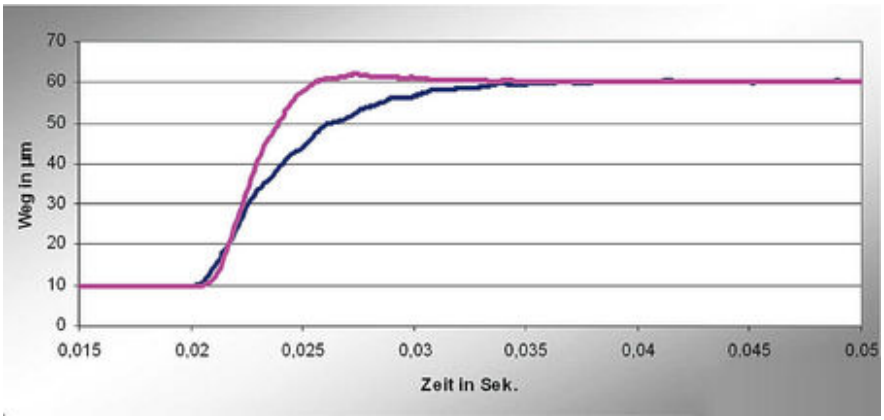

Figure 1.14: Settling behavior of a system with optimized PID parameters (blue) and Advanced Piezo Control (pink)

Fig. 1.13 and Fig. 1.14, respectively. As will be seen in the next sections, this simple controller can only give good tracking performance with simple desired trajectories. For complicated desired ones, the tracking error increases significantly due to the phase-shift, gain reduction and finite sampling time. To handle this problem, very high sampling rate or advanced control techniques are needed. The former solution requires a high speed controller which results in a high cost system. Hence, the overall objective for the thesis work is to investigate and develop advanced control schemes, which are practical and implementable, to achieve excellent tracking performance. The control designs are also conducted in discrete-time domain so that the algorithms can easily be implemented by dig-

ital controllers directly. The algorithms are also not too complicated to avoid using expensive hardware.

1.5 Structure of This Dissertation

To this end, the remaining of this dissertation is organized as following:

Chapter 2 presents the design of the model predictive control (MPC) using non-minimal state-space (NMSS) model for tracking control of single input single output (SISO) system. By inspecting the block diagram of the conventional MPC, it can be seen that tuning the MPC parameters to achieve high tracking performance is a challenging task. Hence, a pseudo MPC which has same structure and set of parameters with MPC is proposed. However, the way to get the parameters of this proposed controller is clear. Besides, robustness against parameters variation is also improved.

Chapter 3 discusses the discrete-time sliding mode control (DSMC) for SISO uncertain systems. First, conventional DSMC and discrete-time integral sliding mode control (DISMC) are applied to the piezo-actuated positioning system. By analyzing the experimental results, it can be said that the both DSMC and DISMC can give a good tracking performance in steady-state. Nevertheless, it is impossible to adjust the transient response in practice due to the uncertainties. Thus, a novel prescribed performance DSMC is proposed. The novel method offers additional parameters to adjust the transient response. In advance, the tracking error is always kept inside a pre-defined area.

Chapter 4 concerns so-called fractional order-based controllers which is based on the generalized differential and integral of fractional order instead of integer order. These controllers offers more degree of freedom in comparison with their integer order-based counterparts. Therefore, the control performance may be improved. First, the numerical approximation of the fractional order differential (FOD) and integral (FOI) is introduced. Then, a new method to approximate the FOI is proposed such that the FOI can be computed recursively. Based on this proposed approximation, the design of discrete-time $PI^{\alpha}D^{\beta}$ of fractional order

α, β is discussed. The particle swarm optimization (PSO) is also used to obtain the best set of parameters. In advance, the PSO run directly with real system instead of a mathematical model to remove the influences of the modeling error. Finally, discrete-time fractional order integral sliding mode control (DFISMC) with variant switching gain and fuzzy tuning is investigated. This DFISMC is able to achieve high tracking performance with no chattering in steady-state.

The dissertation ends with conclusions and future works in Chapter 5.

Chapter 2

Tracking Control of Piezo-Actuated Positioning Systems Based On Pseudo Model Predictive Control

2.1 Introduction

In recent years, the PEAs become more and more important in many key technologies such as semiconductor, optoelectronic devices production, biological manipulation, etc., where ultrahigh precision motion is required because of many advantages mentioned in the first chapter. However, the nonlinear relationship between the applied input voltage and the output displacement may cause difficulties in control design.

Numerous control strategies have been developed in the literature to cope with nonlinear behavior of the PEAs [21]. In general, these methods can be divided into two groups: hysteresis model-based and hysteresis model-free approaches. In the first approach, the hysteresis phenomenon is reconstructed by using nonlinear hysteresis operators or nonlinear differential equations, leading to the proposal of many famous models such as: Preisach model [28], Prandtl-Ishlinskii model [39],

Bouc-Wen model [34], etc. Then, inverse compensation technique is employed to reject the influence of the hysteresis. However, these method are quite sensitive to the modeling error as well as require high computational cost. Thus, this chapter focuses on the second approach in which the hysteresis is regarded as an unknown disturbance to a nominal model. Then, robust control techniques are employed to handle this disturbance.

For tracking applications where the desired trajectory is normally known, MPC has been shown to be a good candidate [64]. Nevertheless, the main drawback of the MPC is how to tune the parameters to get the desired performance. Conventionally, these parameters are found by solving a quadratic cost function with weighted matrices to minimizes the future tracking error. The problem is that the relationship between the weighted matrices and the stability criterion is not straightforward which makes tuning of MPC become a challenging task [26]. Furthermore, the conventional MPC itself is also sensitive to the modeling error since the predictive tracking error is inaccurate if the mathematical model is imperfect.

2.2 Contributions

This chapter presents a different approach to obtain the parameters of the MPC for SISO system. Based on the block diagram of the conventional MPC, a closed-loop transfer function is obtained. Then, pole-placement and adaptive techniques are employed to directly find all the necessary parameters of the MPC without using the quadratic cost function. Since this method utilizes the closed form representation of the conventional MPC in control design, it is named pseudo MPC. The experimental results show that the proposed method can achieve better tracking performance than its conventional counterpart. In advanced, the control system is also robust against the external load disturbance and the tunning procedure is simplified.

2.3 System Description

In this section, the system hardware and formulation which are used throughout this research are introduced.

2.3.1 System Hardware

A positioning system named PS1H80-030U which is composed of a moving table, a piezoelectric actuator (PEA) and a built-in displacement sensor is used in experiment. The travel range of this positioning system is 30µm and the resolution of the sensor is 2nm. The sensor's output is connected to a signal conditioning device named SAB101, which converts 0µm $\sim$ 100µm displacement to 0V$\sim$ 10V voltage signal. The PEA is supplied by PH301 power amplifier, which has able to provide a wide voltage range from 0V to 150V with 6kHz bandwidth. All above devices are produced by Nano Control Co, Ltd. An analog interface board named AIO-163202F-PE is employed to collect the data from the displacement sensor and control the power amplifier. This board is equipped with 32 analog inputs (AIs) and 2 analog outputs (AOs) with 16bits resolution and 500kHz sampling rate. The control algorithm is implemented on a personal computer (PC) by C language. The sampling time T_s of the controller is 0.5ms. The block diagram of the control system is shown in Fig. 2.1. The image of the experimental devices can be seen in Fig. 2.2.

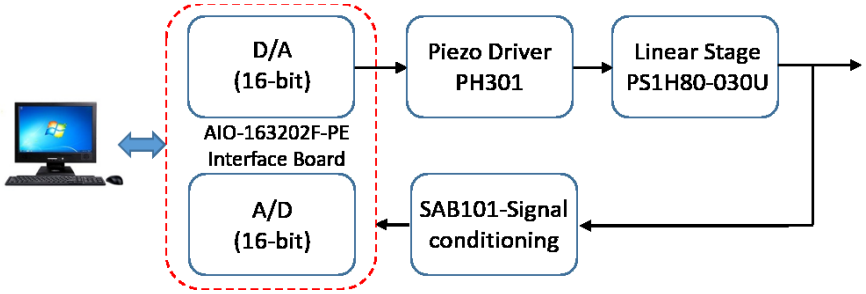

Figure 2.1: Block diagram of experimental system

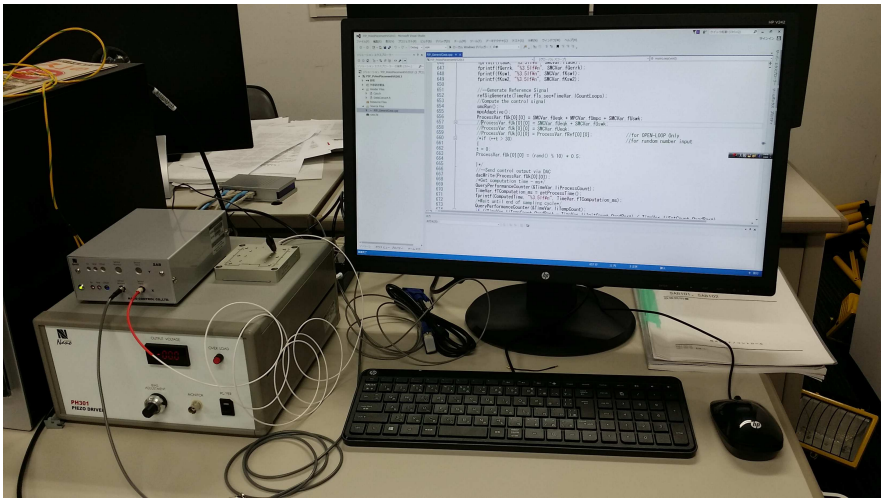

Figure 2.2: Experimental devices

2.3.2 Modeling and Identification

Consider the following uncertain SISO dynamical system as the nominal model of the above piezo-actuated positioning system

$$y_{k+1} = -\sum_{i=1}^{n} a_i y_{k-i+1} + \sum_{j=1}^{m} b_j u_{k-j+1} + p_k \tag{2.1}$$

in which, u_k is control voltage, y_k is output displacement, a_i and b_j are known parameters of the plant and p_k is the disturbance including unknown modeling errors and nonlinearities, n and m are two positive integers satisfying $m \leq n$.

By inspecting the collected open-loop input/output data as depicted in Fig. 2.3, int can be seen that the static gain of the positioning system is amplitude dependent. Besides, a small overshoot also occurs in transient-state which means the order n of (2.1) must satisfy $n \geq 2$ to be able to represent the behavior of the positioning system. In this work, to show the effectiveness of the proposed controller designed in the next sections, a second order system is chosen. The remaining nonlinearities are treated as the lump disturbance p_k. To find the parameters of the nominal model, a square voltage with random amplitude from 0-5V is applied to the PEA first. Then, the output displacement is measured with 2kHz sampling rate. On the basis of this input/output data, the parameters

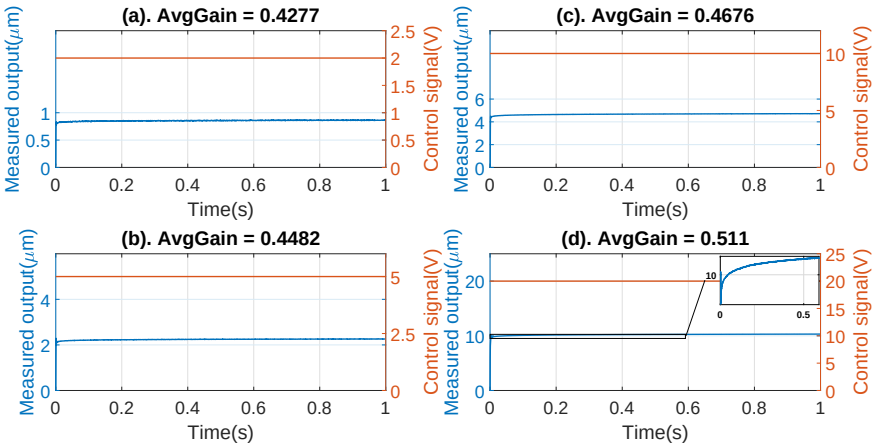

Figure 2.3: Open-loop input-output experimental data

are identified by least square technique. It would be noted that the identification result is governed by the type of excitation signal. Besides, it is impossible to get a precise model which fits the real system perfectly in practice, especially for piezo-actuated positioning systems. A good controller should be capable of handling all the modeling error and uncertainties.

For this specific system, the identification result is shown in Fig. 2.4 and the plant can be described by (2.2).

$$y_{k+1} = -0.1993y_k - 0.3411y_{k-1} + 0.4283u_k + 0.2873u_{k-1} + p_k \tag{2.2}$$

2.3.3 Related Definitions

The tracking error at time instance k is defined as

$$e_k = y_{d,k} - y_k \tag{2.3}$$

in which $y_{d,k}$ is the desired output at time instance k.

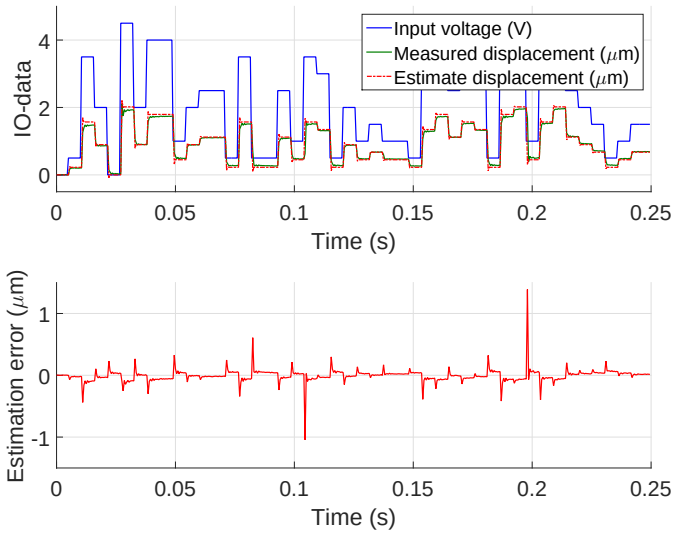

Figure 2.4: Systems identification by random step input

The one step ahead tracking error is then derived from (2.1) and (2.3) as

$$\begin{aligned} e_{k+1} &= y_{d,k+1} - y_{k+1} \\ &= y_{d,k+1} + \sum_{i=1}^{n} a_i y_{k-i+1} - \sum_{j=1}^{m} b_j u_{k-j+1} - p_k \end{aligned} \tag{2.4}$$

In (2.4), the disturbance p_k is unknown. Hence, the one step delayed technique is employed to estimate this unknown term. This technique is based on the following assumptions:

Assumption 2.1: The disturbance p_k is bounded and the sampling time T_s is sufficient small such that the difference in two consecutive sampling instance is also bounded, i.e,

$$p_k - p_{k-1} = O(T_s) \tag{2.5}$$

$$p_k - 2p_{k-1} + p_{k-2} = O(T_s^2) \tag{2.6}$$

which means there alway exists constant A and B such that

$$|p_k - p_{k-1}| \leq AT_s \tag{2.7}$$

$$|p_k - 2p_{k-1} + p_{k-2}| \leq BT_s^2 \tag{2.8}$$

$\forall\ k > 0$. These above mentioned assumptions are based on the Taylor expansion and can be explained as following.

For a very small constant T_s we have

$$p(t - T_s) = p(t) - \frac{dp(t)}{dt}T_s + \sum_{i=2}^{\infty}(-1)^i \frac{d^{(i)}p(t)}{dt^i}\frac{T_s^i}{i!} \tag{2.9}$$

Then it can be derived from (2.9) that

$$\begin{aligned} p(t) - p(t - T_s) &= \frac{dp(t)}{dt}T_s - \sum_{i=2}^{\infty}(-1)^i \frac{d^{(i)}p(t)}{dt^i}\frac{T_s^i}{i!} \\ &\approx \frac{dp(t)}{dt}T_s + O(T_s^2) \end{aligned} \tag{2.10}$$

Assume that the signal $p(t)$ is smooth and its differential is bounded, then there exists a constant A such that

$$|p(t) - p(t - T_s)| \leq AT_s + O(T_s^2) \tag{2.11}$$

which means

$$p(t) - p(t - T_s) = O(T_s) \tag{2.12}$$

and (2.5) holds.

Now, ignore the small term $O(T_s^2)$ and differentiate both sides of (2.10), it gives

$$\frac{dp(t)}{dt} - \frac{dp(t - T_s)}{dt} \approx \frac{d^2p(t)}{dt^2}T_s \tag{2.13}$$

By using (2.10) on the left side of (2.13), it results in

$$p(t) - 2p(t - T_s) + p(t - 2T_s) \approx \frac{d^2p(t)}{dt^2}T_s^2 \tag{2.14}$$

Again, assume that the second order differential of $p(t)$ is bounded by a constant B, then it leads to

$$|p(t) - 2p(t - T_s) + p(t - 2T_s)| \leq BT_s^2 \tag{2.15}$$

which means (2.8) holds.

The estimation $\hat{p}_k$ of the disturbance p_k can be computed based on (2.1) as

$$\hat{p}_k = 2p_{k-1} - p_{k-2} \tag{2.16}$$

in which

$$p_{k-1} = y_k + \sum_{i=1}^{n} a_i y_{k-i} - \sum_{j=1}^{m} b_j u_{k-j} \tag{2.17}$$

Hence, the disturbance estimation error $\tilde{p}_k$ is

$$\begin{aligned} \tilde{p}_k &= p_k - \hat{p}_k \\ &= p_k - 2p_{k-1} + p_{k-2} = O(T_s^2) \end{aligned} \tag{2.18}$$

Finally, the one step ahead tracking error (2.4) can be expressed by

$$e_{k+1} = y_{d,k+1} + \sum_{i=1}^{n} a_i y_{k-i+1} - \sum_{j=1}^{m} b_j u_{k-j+1} - \hat{p}_k - \tilde{p}_k \tag{2.19}$$

2.4 Problem Statement

2.4.1 MPC Based on Non-Minimal State Space (NMSS) Model

Considering the following discrete-time SISO dynamical system as the nominal model of a piezo-actuated stage

$$y_k = -\sum_{i=1}^{n} a_i y_{k-i} + \sum_{j=1}^{m} b_j u_{k-j} \tag{2.20}$$

where y_k and u_k are output displacement and input voltage at time instance k, $m \leq n$ are two integers stand for the order of the plant. System (2.20) can also be represented by the following transfer function

$$W_p = \frac{B(z^{-1})}{A(z^{-1})} \tag{2.21}$$

in which z^{-1} is the backward shift operator; $A(z^{-1})$ and $B(z^{-1})$ are relatively prime polynomials of degree n and m, respectively.

$$B(z^{-1}) = b_1 z^{-1} + b_2 z^{-2} + ... + b_m z^{-m} \tag{2.22}$$

$$A(z^{-1}) = 1 + a_1 z^{-1} + a_2 z^{-2} + ... + a_n z^{-n} \tag{2.23}$$

To conduct the MPC design for discrete-time SISO system, an extended non-minimal state space (NMSS) model [79] is employed as follows:

$$\begin{aligned} x(k) &= \mathbf{A}x(k-1) + \mathbf{b}u(k-1) + \mathbf{d}y_d(k) \\ y(k) &= \mathbf{c}x(k) \end{aligned} \tag{2.24}$$

with,

$$x(k) = \begin{bmatrix} y_k & \cdots & y_{k-n+1} & u_{k-1} & \cdots & u_{k-m+1} & \delta_k \end{bmatrix}^T \tag{2.25}$$

$$\mathbf{A}^{(n+m)\times(n+m)} = \begin{bmatrix} -a_1 & \cdots & -a_{n-1} & -a_n & b_2 & \cdots & b_{m-1} & b_m & 0 \\ 1 & \cdots & 0 & 0 & 0 & \cdots & 0 & 0 & 0 \\ \vdots & \ddots & \vdots & \vdots & \vdots & \ddots & \vdots & \vdots & \vdots \\ 0 & \cdots & 1 & 0 & 0 & \cdots & 0 & 0 & 0 \\ 0 & \cdots & 0 & 0 & 0 & \cdots & 0 & 0 & 0 \\ 0 & \cdots & 0 & 0 & 1 & \cdots & 0 & 0 & 0 \\ \vdots & \ddots & \vdots & \vdots & \vdots & \ddots & \vdots & \vdots & \vdots \\ 0 & \cdots & 0 & 0 & 0 & \cdots & 1 & 0 & 0 \\ a_1 & \cdots & a_{n-1} & a_n & -b_2 & \cdots & -b_{m-1} & -b_m & 1 \end{bmatrix} \tag{2.26}$$

$$\mathbf{b}^{(n+m)\times 1} = \begin{bmatrix} b_1 & 0 & \cdots & 0 & 1 & 0 & \cdots & 0 & -b_1 \end{bmatrix}^T \tag{2.27}$$

$$\mathbf{d}^{(n+m)\times 1} = \begin{bmatrix} 0 & \cdots & 0 & 1 \end{bmatrix}^T \tag{2.28}$$

$$\mathbf{c}^{1\times(n+m)} = \begin{bmatrix} 1 & 0 & \cdots & 0 \end{bmatrix} \tag{2.29}$$

$$\delta_k = \delta_{k-1} + y_{d,k} - y_k \tag{2.30}$$

In (2.30), δ_k is an additional integral of output error state variable and $y_{d,k}$ is the desired output at time instance k.

Based on (2.24), the predictive state vector in next N_p sampling cycles is

$$X_F = \mathbf{F}x(k) + \mathbf{H}U_F + \mathbf{G}Y_{dF} \tag{2.31}$$

where,

$$U_F = \begin{bmatrix} u_k & u_{k+1} & \cdots & u_{k+N_p-1} \end{bmatrix}^T \tag{2.32}$$

$$Y_{dF} = \begin{bmatrix} y_{d,k+1} & y_{d,k+2} & \cdots & y_{d,k+N_p} \end{bmatrix}^T \tag{2.33}$$

$$X_F = \begin{bmatrix} x^T(k+1) & x^T(k+2) & \cdots & x^T(k+N_p) \end{bmatrix}^T \tag{2.34}$$

$$\mathbf{F} = \begin{bmatrix} \mathbf{A} \\ \vdots \\ \mathbf{A}^{N_p} \end{bmatrix} \tag{2.35}$$

$$\mathbf{H} = \begin{bmatrix} \mathbf{b} & 0_{(n+m)\times 1} & \cdots & 0_{(n+m)\times 1} \\ \mathbf{Ab} & \mathbf{b} & \cdots & 0_{(n+m)\times 1} \\ \vdots & \vdots & \ddots & \vdots \\ \mathbf{A}^{N_p-1}\mathbf{b} & \mathbf{A}^{N_p-2}\mathbf{b} & \cdots & \mathbf{b} \end{bmatrix} \tag{2.36}$$

$$\mathbf{G} = \begin{bmatrix} \mathbf{d} & 0_{(n+m)\times 1} & \cdots & 0_{(n+m)\times 1} \\ \mathbf{Ad} & \mathbf{d} & \cdots & 0_{(n+m)\times 1} \\ \vdots & \vdots & \ddots & \vdots \\ \mathbf{A}^{N_p-1}\mathbf{d} & \mathbf{A}^{N_p-2}\mathbf{d} & \cdots & \mathbf{d} \end{bmatrix} \tag{2.37}$$

In conventional MPC, the optimal control sequences is obtained by minimizing the following quadratic cost function:

$$J = U_F^T \lambda_u U_F + X_F^T \lambda_x X_F \tag{2.38}$$

where λ_x and λ_u are two positive definite weighted matrices of dimensions $(n+m)N_p \times (n+m)N_p$ and $N_p \times N_p$, respectively. Without constraints, by substituting (2.31) into (2.38) and differentiating J with respect to U_F, the solution for (2.38) is

$$U_F = -\mathbf{Q}x(k) - \mathbf{R}Y_{dF} \tag{2.39}$$

with,

$$\mathbf{Q} = (\lambda_u + \mathbf{H}^T \lambda_x \mathbf{H})^{-1} \mathbf{H}^T \lambda_x \mathbf{F} \tag{2.40}$$

$$\mathbf{R} = (\lambda_u + \mathbf{H}^T \lambda_x \mathbf{H})^{-1} \mathbf{H}^T \lambda_x \mathbf{G} \tag{2.41}$$

In (2.39), only the first element of U_F is used as actual control signal while the others are ignored. This process is repeated in every consequent sampling cycles.

2.4.2 Properties of MPC based on NMSS and Integral of Error State Variable

Let $Q^{r1} = [q_1 \cdots q_{n+m}]$ and $R^{r1} = [r_1 \cdots r_{Np}]$ be the first row of matrix $\mathbf{Q}$ and $\mathbf{R}$, respectively. The control signal of the MPC at each sampling cycle can be written in detail as

$$u_k = -\sum_{i=1}^{N_p} r_i y_{d,k+i} - \sum_{i=1}^{n} q_i y_{k-i+1} - \sum_{i=1}^{m-1} q_{n+i} u_{k-i} - q_{n+m}\delta_k \tag{2.42}$$

By using backward shift operator, (2.42) can also be represented in polynormial form as

$$L(z^{-1})u_k = -S(z^{-1})y_k - R(z^{-1})y_{d,k+N_p} + K_I\delta_k \tag{2.43}$$

in which

$$S(z^{-1}) = \quad q_1 + q_2 z^{-1} + \cdots + q_n z^{-n+1} \tag{2.44}$$

$$R(z^{-1}) = \quad r_{N_p} + r_{N_p-1} z^{-1} + \cdots + r_1 z^{-N_p+1} \tag{2.45}$$

$$L(z^{-1}) = \quad l_0 + l_1 z^{-1} + \cdots + l_{m-1} z^{-m+1} \tag{2.46}$$

and $l_0 = 1$, $l_i = q_{n+i}$, $K_I = -q_{n+m}$.

The extended variable δ_k described by (2.30) can also be transformed into polynomial form as

$$\delta_k = \frac{y_{d,k} - y_k}{1 - z^{-1}} \tag{2.47}$$

Now, substitute (2.47) into (2.43), it yields

$$u_k = \frac{1}{L(z^{-1})}\{\frac{K_I}{1 - z^{-1}}(y_{d,k} - y_k) - S(z^{-1})y_k - R(z^{-1})y_{d,k+N_p}\} \tag{2.48}$$

From (2.48), the block diagram of the MPC-based NMSS is reconstructed as in Fig. 2.5. Based on this block diagram, the transfer functions from the reference input to output (W_c), from the input disturbance to the output ($W_{p_{in}}$) and from the output disturbance to the output ($W_{p_{out}}$) can easily be obtained.

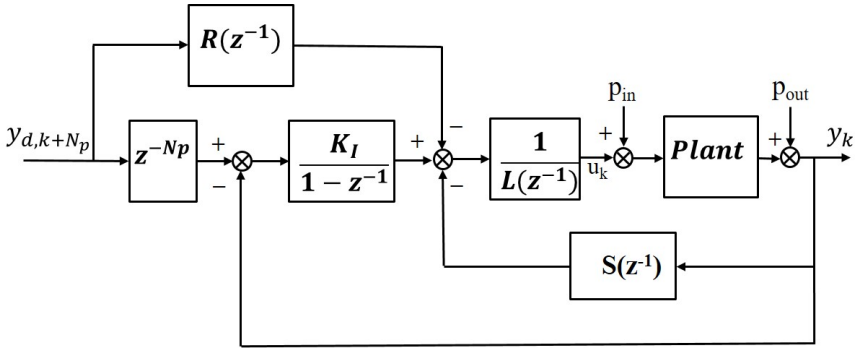

Figure 2.5: Block diagram of MPC based NMSS

$$W_c = \frac{y_k}{y_{d,k}} = \frac{K_I B(z^{-1}) - (1-z^{-1}) z^{N_p} R(z^{-1}) B(z^{-1})}{K_I B(z^{-1}) + (1-z^{-1}) \left[S(z^{-1}) B(z^{-1}) + L(z^{-1}) A(z^{-1}) \right]} \tag{2.49}$$

$$W_{p_{in}} = \frac{y_k}{p_{in,k}} = \frac{(1-z^{-1}) L(z^{-1}) B(z^{-1})}{K_I B(z^{-1}) + (1-z^{-1}) \left[S(z^{-1}) B(z^{-1}) + L(z^{-1}) A(z^{-1}) \right]} \tag{2.50}$$

$$W_{p_{out}} = \frac{y_k}{p_{out,k}} = \frac{(1-z^{-1}) L(z^{-1}) A(z^{-1})}{K_I B(z^{-1}) + (1-z^{-1}) \left[S(z^{-1}) B(z^{-1}) + L(z^{-1}) A(z^{-1}) \right]} \tag{2.51}$$

The characteristic equation of (2.49), (2.50) and (2.51) is

$$K_I B(z^{-1}) + (1-z^{-1}) \left[S(z^{-1}) B(z^{-1}) + L(z^{-1}) A(z^{-1}) \right] \tag{2.52}$$

If all the roots of (2.52) are inside the unit circle, the closed-loop system is stable following that

$$\lim_{z \to 1} W_c = 1 \tag{2.53}$$

$$\lim_{z \to 1} W_{p_{in}} = 0 \tag{2.54}$$

$$\lim_{z \to 1} W_{p_{out}} = 0 \tag{2.55}$$

From (2.53),(2.54) and (2.55), it can be concluded that the output of the closed loop system will track any constant reference and reject other constant input and output disturbances.

Remark 2.1: In order to get the desired performance, the parameters of the controller including the predictive horizon N_p, the weighted matrices λ_x and λ_u must be tuned. It can be observed from (2.39) that the first row of $\mathbf{Q}$ decides the position of the closed loop poles and the first row of $\mathbf{R}$ decides the contribution

of the feedforward loop to the system performance. However, the relationship between $\mathbf{Q}$, $\mathbf{R}$ and the two weighted matrices λ_x and λ_u described by (2.40), (2.41) are not straightforward.

2.5 Pseudo MPC Design

In this section, a simple and effective method is proposed to obtain the parameter of the MPC directly without complicated tuning procedure related to the weighted matrices. The first row of $\mathbf{Q}$ is computed by pole-placement method such that the stability of the closed loop system is guaranteed. Then, the first row of $\mathbf{R}$ is automatically computed on-line by recursive least square (RLS) technique to minimize the predictive tracking error. The details of the control design is as following.

2.5.1 Pole Placement Design

From (2.52), the characteristic polynomial of the closed loop system can be rewritten as

$$K_I B(z^{-1}) + B_1(z^{-1})S(z^{-1}) + A_1(z^{-1})L(z^{-1}) \tag{2.56}$$

in which,

$$B_1(z^{-1}) =(1 - z^{-1})B(z^{-1}) = b_0 + \sum_{i=1}^{m} \tilde{b}_i z^{-i} - b_m z^{-m-1} \tag{2.57}$$

$$A_1(z^{-1}) =(1 - z^{-1})A(z^{-1}) = a_0 + \sum_{i=1}^{n} \tilde{a}_i z^{-i} - a_n z^{-n-1} \tag{2.58}$$

with,

$$\tilde{a}_i = a_i - a_{i-1} \tag{2.59}$$

$$\tilde{b}_i = b_i - b_{i-1} \tag{2.60}$$

Denote $D_{ref}(z^{-1})$ as the designed characteristic polynomial

$$D_{ref}(z^{-1}) = 1 + d_1 z^{-1} + \cdots + d_{n+m} z^{-(n+m)} \tag{2.61}$$

The unknown parameters of (2.56) can be found by equating both sides of the following equation

$$K_I B(z^{-1}) + B_1(z^{-1})S(z^{-1}) + A_1(z^{-1})L(z^{-1}) = D_{ref}(z^{-1}) \tag{2.62}$$

The explicit solution of (2.62) can be obtained by solving the following algebraic equation

$$\mathbf{M}_c \mathbf{p}_c = \mathbf{d}_c \tag{2.63}$$

with,

$$\mathbf{p}_c^{(n+m+1)} = \begin{bmatrix} l_0 & \cdots & l_{m-1} & q_1 \cdots & q_n & K_I \end{bmatrix}^T \tag{2.64}$$

$$\mathbf{d}_c^{(n+m+1)} = \begin{bmatrix} 1 & d_1 \cdots & d_{n+m+1} \end{bmatrix}^T \tag{2.65}$$

$$\mathbf{M}_c^{(n+m+1)\times(n+m+1)} = \begin{bmatrix} a_0 & 0 & \cdots & 0 & b_0 & 0 & \cdots & 0 & b_0 \\ a_1' & \ddots & \ddots & \vdots & b_1' & \ddots & \ddots & \vdots & b_1 \\ \vdots & & \ddots & 0 & \vdots & & \ddots & 0 & \vdots \\ \vdots & & & a_0 & \vdots & & & b_0 & \vdots \\ a_n' & & & \vdots & b_m' & & & \vdots & b_m \\ -a_n & \ddots & & \vdots & -b_m & \ddots & & \vdots & 0 \\ 0 & \ddots & \ddots & \vdots & 0 & \ddots & \ddots & \vdots & \vdots \\ \vdots & \ddots & \ddots & a_n' & \vdots & \ddots & \ddots & b_m' & \vdots \\ 0 & \cdots & 0 & -a_n & 0 & \cdots & 0 & -b_m & 0 \end{bmatrix} \tag{2.66}$$

Theorem 2.1: Given the closed-loop characteristic polynomial described by (2.56), arbitrary closed-loop pole-placement can only be achieved if [17]:

(i). $A(z^{-1})$ and $B(z^{-1})$ are co-prime.

(ii). $\sum_{i=0}^{m} b_i \neq 0$.

Remark 2.2: It can be seen from *Theorem 2.1* that the first condition means there is no pole-zero cancellation in the transfer function of the controlled plant (2.21). The second condition guarantees that the static gain of the plant differs from zero.

2.5.2 Adaptive Minimum Tracking Error Design

2.5.2.1 Without External Disturbance

The control design is based on the following assumptions:

Assumption 1: The desired output and its difference between two consecutive sampling cycles are bounded.

Assumption 2: After pole-placement design, all the poles of the closed-loop system (2.49) are inside the unit disk which means the closed-loop system is bounded-input bounded-output (BIBO) stable.

Then, the closed-loop transfer function (2.49) can be rewritten as

$$W_c = \frac{y_k}{y_{d,k}} = \frac{[K_I - (1-z^{-1})z^{Np}R(z^{-1})]B(z^{-1})}{1 + d_1 z^{-1} + \cdots + d_{n+m}z^{-(n+m)}} \tag{2.67}$$

From (2.67) and note that

$$y_{d,k}(1-z^{-1}) = y_{d,k} - y_{d,k-1} = \tilde{y}_{d,k} \tag{2.68}$$

it yields

$$\begin{aligned} y_{k+1} = &- \sum_{i=1}^{n+m} d_i y_{k-i+1} + K_I \sum_{i=1}^{m} b_i y_{d,k-i+1} \\ &+ \sum_{i=1}^{N_p} \left(\sum_{j=1}^{m} \tilde{y}_{d,k+1+i-j} b_j \right) r_i \end{aligned} \tag{2.69}$$

By defining

$$\Gamma_k = - \sum_{i=1}^{n+m} d_i y_{k-i+1} + K_I \sum_{i=1}^{m} b_i y_{d,k-i+1} \tag{2.70}$$

$$\tilde{\epsilon}_{d,k+i} = \sum_{j=1}^{m} \tilde{y}_{d,k+1+i-j} b_j \tag{2.71}$$

equation (2.69) can be rewritten as

$$y_{k+1} = \Gamma_k + \Phi_k^T \theta_0 \tag{2.72}$$

with,

$$\Phi_k^T = \begin{bmatrix} \tilde{\epsilon}_{d,k+1} & \tilde{\epsilon}_{d,k+2} & \cdots & \tilde{\epsilon}_{d,k+N_p} \end{bmatrix} \tag{2.73}$$

$$\theta_0 = \begin{bmatrix} r_1 & r_2 & \cdots & r_{N_p} \end{bmatrix}^T \tag{2.74}$$

In order to force the tracking error to zero, the control signal u_k must satisfy

$$y_{d,k+1} = \Gamma_k + \Phi_k^T \theta_0 \tag{2.75}$$

Since θ_0 is unknown, a sequence of estimated parameter $\hat{\theta}_k$ is used instead. Then, (2.75) is replaced by

$$y_{d,k+1} = \Gamma_k + \Phi_k^T \hat{\theta}_k \tag{2.76}$$

Because the relation (2.76) is linear, $\hat{\theta}_k$ can be obtained by minimizing the following quadratic cost function using the recursive least square (RLS) method

$$\begin{aligned} J_N(\theta) = & \frac{1}{2} \sum_{k=1}^{N} (y_k - \Gamma_{k-1} - \Phi_{k-1}^T \theta)^2 \\ & + \frac{1}{2} \left(\theta - \hat{\theta}_0 \right)^T P_0^{-1} \left(\theta - \hat{\theta}_0 \right) \end{aligned} \tag{2.77}$$

where the first term of (2.77) actually represents the sum of squares of the tracking error e_k and the second term is included to account for the initial condition. The square diagonal matrix P_0 is considered as a measure of confidence in the initial estimate $\hat{\theta}_0$.

Without constraint, the solution for the optimization problem (2.77) can be obtained recursively as follows [**?**]

$$\begin{aligned} \hat{\theta}_k = & \hat{\theta}_{k-1} \\ & + \frac{P_{k-1}\Phi_{k-1}}{1 + \Phi_{k-1}^T P_{k-1} \Phi_{k-1}} \left(y_k - \Gamma_{k-1} - \Phi_{k-1}^T \hat{\theta}_{k-1} \right) \end{aligned} \tag{2.78}$$

$$P_k = P_{k-1} - \frac{P_{k-1}\Phi_{k-1}\Phi_{k-1}^T P_{k-2}}{1 + \Phi_{k-1}^T P_{k-1} \Phi_{k-1}} \tag{2.79}$$

in which $\hat{\theta}_k$ represents the estimation of θ; P_k is a projection matrix with the initial value $P_0 = \lambda I$ where I is an unity matrix and λ is a positive constant representing the convergence speed of the algorithm.

Based on (2.78) and (2.42), the final control action is

$$u_k = -\sum_{i=1}^{N_p} \hat{r}_{i,k} y_{d,k+i} - \sum_{i=1}^{n} q_i y_{k-i+1} - \sum_{i=1}^{m-1} l_i u_{k-i} + K_I \sigma_k \tag{2.80}$$

2.5.2.2 Properties of the Update Laws

The update laws (2.78) and (2.79) result in the following properties [**?**]

$$\text{(i)} ||\hat{\theta}_k - \theta_0||^2 \leq \kappa_1 ||\hat{\theta}_0 - \theta_0||^2 \tag{2.81}$$

where κ_1 is the condition number of P_0^{-1} and defined by

$$\kappa_1 = \frac{\lambda_{max}(P_0^{-1})}{\lambda_{min}(P_0^{-1})} \tag{2.82}$$

in which λ_{max} and λ_{min} are the maximum and minimum eigenvalue of P_0^{-1}.

$$\text{(ii)} \lim_{N\to\infty} \sum_{k=1}^{N} \frac{e_k^2}{1 + \Phi_{k-1}^T P_{k-1} \Phi_{k-1}} < \infty \tag{2.83}$$

which implies

$$(a) \lim_{k\to\infty} \frac{e_k}{\left(1 + \lambda_{max} \Phi_{k-1}^T \Phi_{k-1}\right)^{\frac{1}{2}}} = 0 \tag{2.84}$$

$$(b) \lim_{N\to\infty} \sum_{k=1}^{N} \frac{\Phi_{k-1}^T P_{k-1} \Phi_{k-1} e_k^2}{\left(1 + \Phi_{k-1}^T P_{k-1} \Phi_{k-1}\right)^2} < \infty \tag{2.85}$$

$$(c) \lim_{N\to\infty} \sum_{k=1}^{N} ||\hat{\theta}_k - \hat{\theta}_{k-1}||^2 < \infty \tag{2.86}$$

$$(d) \lim_{N\to\infty} \sum_{k=n}^{N} ||\hat{\theta}_k - \hat{\theta}_{k-i}||^2 < \infty \tag{2.87}$$

$$(e) \lim_{k\to\infty} ||\hat{\theta}_k - \hat{\theta}_{k-i}|| = 0 \tag{2.88}$$

where i is a finite positive integer.

On the basis of *Assumption 1*, (2.71) and (2.73), it can be realized that $\Phi_k^T \Phi_k$ is bounded which means the denominator of (2.84) is also bounded. As a result, it yields

$$\lim_{k\to\infty} e_k = 0 \tag{2.89}$$

It also follows from (2.83) that the square of the tracking error is summable. Besides, (2.88) shows that the estimated parameter converges to minimize the tracking error as $k \to \infty$.

2.5.2.3 Under External Disturbance

In practice, the system may be affected by a bounded external disturbance $\Delta\Gamma$. In that case, the predictive output is

$$y_{k+1} = \Gamma_k + \Phi_k^T \theta_0 + \Delta\Gamma_k \tag{2.90}$$

As a result, the update law (2.78) is rewritten as

$$\begin{aligned}\hat{\theta}_k = \hat{\theta}_{k-1} \\ + \frac{P_{k-1}\Phi_{k-1}}{1 + \Phi_{k-1}^T P_{k-1}\Phi_{k-1}} \left(y_k - \Gamma_{k-1} - \Phi_{k-1}^T \hat{\theta}_{k-1} - \Delta\Gamma_{k-1} \right)\end{aligned} \tag{2.91}$$

Although the external disturbance $\Delta\Gamma_{k-1}$ in (2.91) is unknown, it would be noted that

$$y_{d,k} = \Gamma_{k-1} + \Delta\Gamma_{k-1} + \Phi_{k-1}^T \hat{\theta}_{k-1} \tag{2.92}$$

which means

$$y_k - \Gamma_{k-1} - \Delta\Gamma_{k-1} - \Phi_{k-1}^T \hat{\theta}_{k-1} = y_k - y_{d,k} = -e_k \tag{2.93}$$

Hence, the update law (2.91) is revised as follows

$$\hat{\theta}_k = \hat{\theta}_{k-1} + \frac{P_{k-1}\Phi_{k-1}}{1 + \Phi_{k-1}^T P_{k-1}\Phi_{k-1}}(-e_k) \tag{2.94}$$

2.6 Experiment Results

In this section, the validity of the proposed method is confirmed by experiments on the positioning system (2.2). To show the advantages of the proposed method over the conventional MPC, comparative experiments are also conducted and discussed. The parameters of the proposed controller are provided in Table 2.1.

Table 2.1: Parameters of the pseudo model predictive controller

Symbol	Quantity	Value
p_i	Desired closed-loop poles	0.1
$\hat{\theta}_0$	Initial value of $R(z^{-1})$	0.1
λ	Adaptive gain	10
T_s	Sampling time	0.5ms

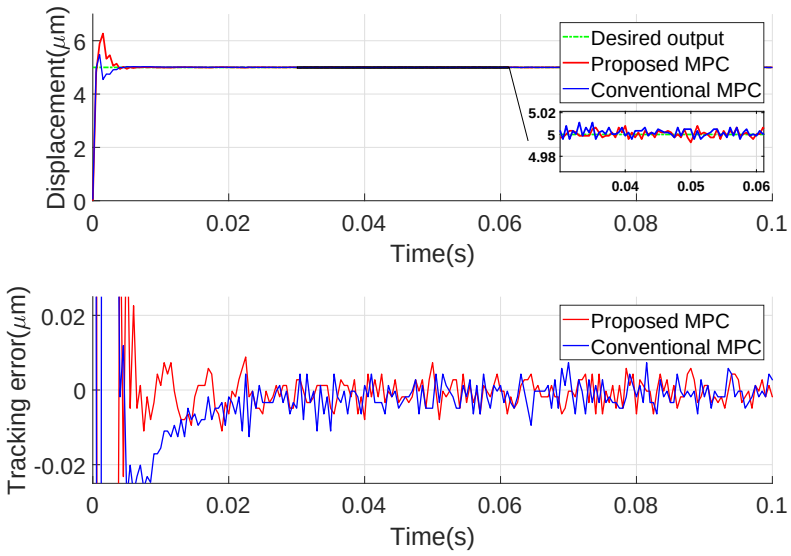

Figure 2.6: The comparative step responses of the closed-loop systems

2.6.1 Transient Response of the Control System

In order to evaluate the transient response, a step desired output which value changes from 0µm to 5µm suddenly is employed. The experiment results getting from the conventional MPC and the proposed one are shown in Fig. 2.6. In both cases, the real outputs quickly reach the desired one in just 0.004ms corresponding to 8 sampling cycles. The maximum tracking error (MAXTE) and the root mean

square tracking error (RMSTE) in steady-state are extremely small, i.e, 0.01µm and 0.0035µm, respectively. These error are corresponding to 0.2% and 0.07% of the desired one, almost same as noise level. The RMSTE is computed by

$$RMSTE = \sqrt{\frac{\sum_{k=k_{ss}}^{N} e_k^2}{N - k_{ss}}} \tag{2.95}$$

in which N is the total number of sampled data and the system is in steady-state after k_{ss} steps.

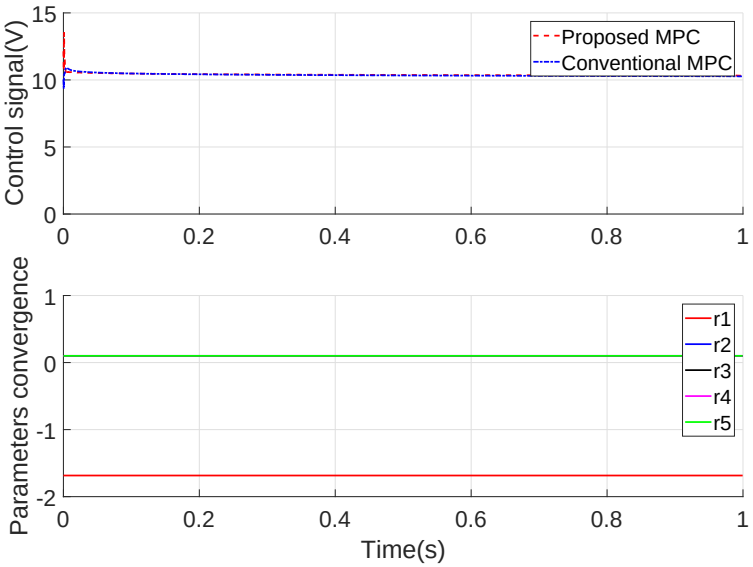

Figure 2.7: The control signal and parameters convergence of the proposed MPC with step input

The control signals and the parameters convergence of the proposed method are provided in Fig. 2.7. Since the desired output is constant, all the elements of vector Φ_k described by (2.73) are zeros. Hences, the parameters of polynomial $R(z^{-1})$ are not changed and have no influence on the control system. The performance in this case is decided by the position of the desired closed-loop poles.

The computation time of the proposed control method and the conventional one are also compared and shown in Fig. 2.8. Due to the update law which

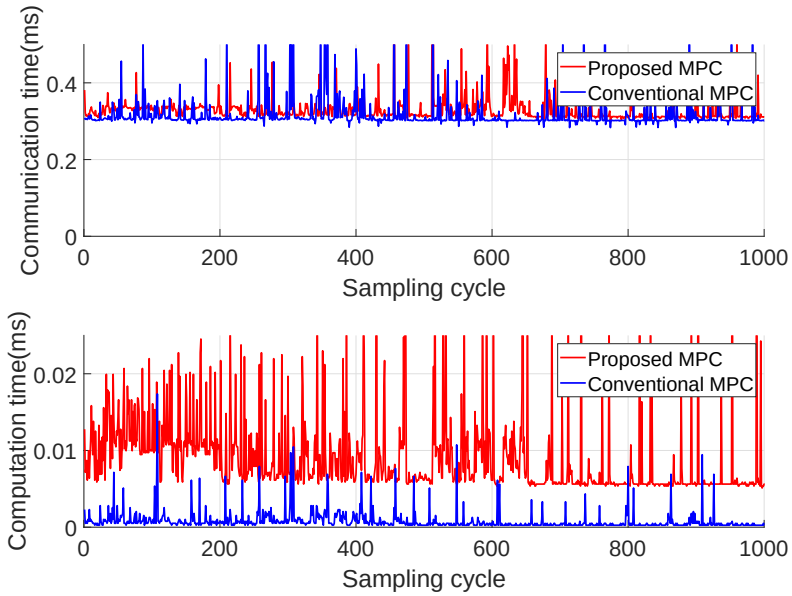

Figure 2.8: The comparative computation times of the MPC algorithms

requires matrix multiplications, the computation time of the proposed method is larger than its conventional counterpart. In return, the quality of control in tracking mode is significantly improved as will be shown in the next subsection.

2.6.2 Tracking performance

To evaluate the tracking performance, various complicated desired outputs such as mixed amplitude-frequency, time-varying amplitude-frequency and sawtooth are employed. The experimental results getting from both methods are shown in Fig. 2.9 $\rightarrow$ Fig. 2.14. As can be observed, the tracking error of the proposed method always smaller then the conventional MPC because the parameters of the feedforward polynomial $R(z^{-1})$ are automatically updated to minimized the tracking error. The experiment results also show that these parameters also converge in finite time.

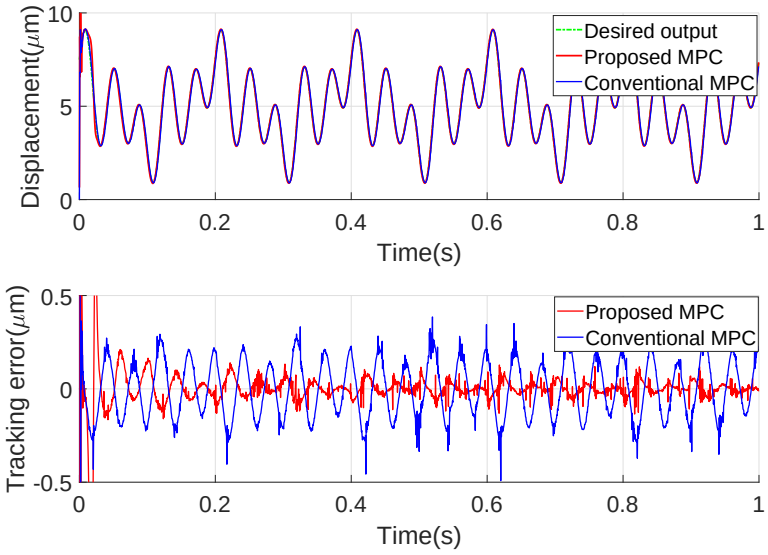

Figure 2.9: Comparative tracking performances of the MPC with mixed amplitude-frequency desired output

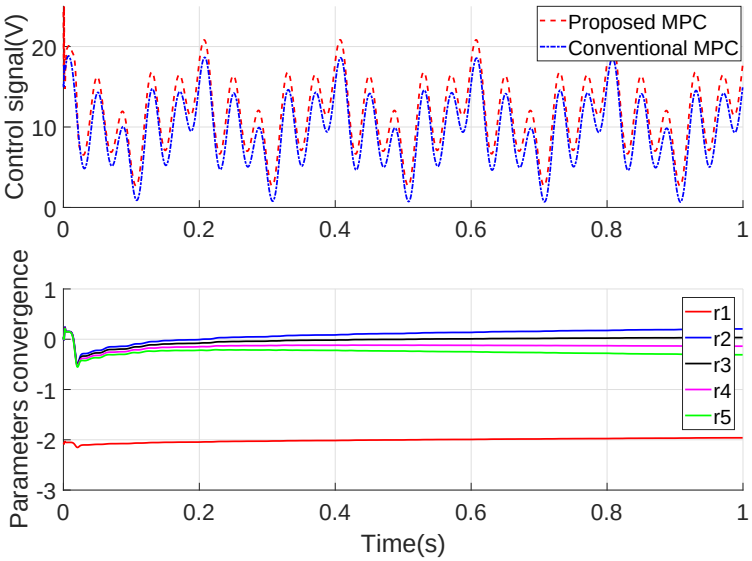

Figure 2.10: The parameters convergence of the proposed MPC with mixed amplitude-frequency desired output

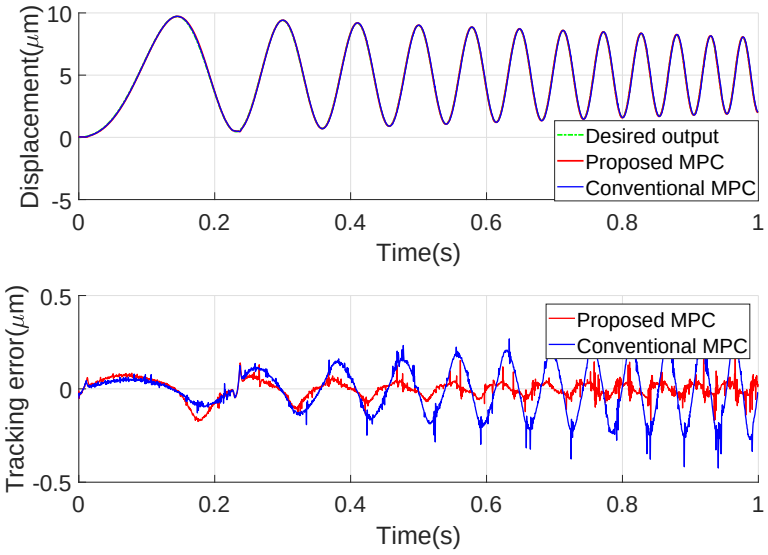

Figure 2.11: Comparative tracking performance of the MPC with time-varying amplitude frequency desired output

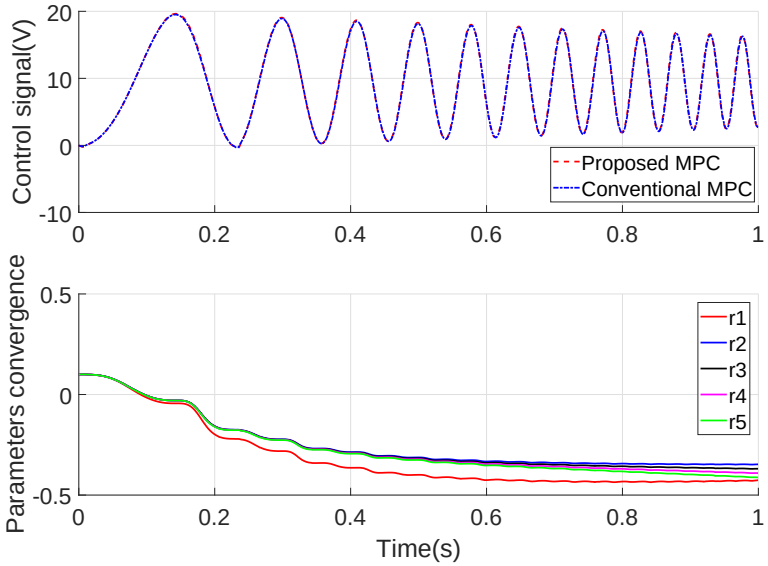

Figure 2.12: The parameters convergence of the proposed MPC with time-varying amplitude frequency desired output

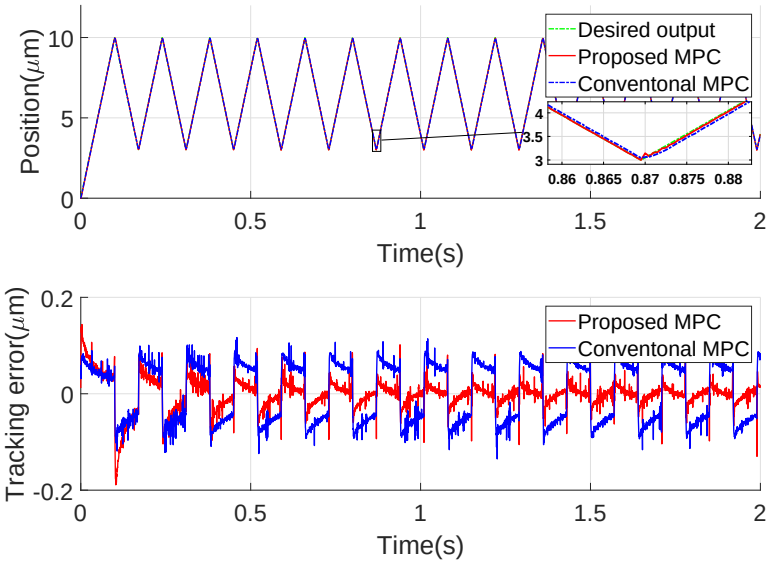

Figure 2.13: Comparative tracking performance of the MPC with sawtooth desired output

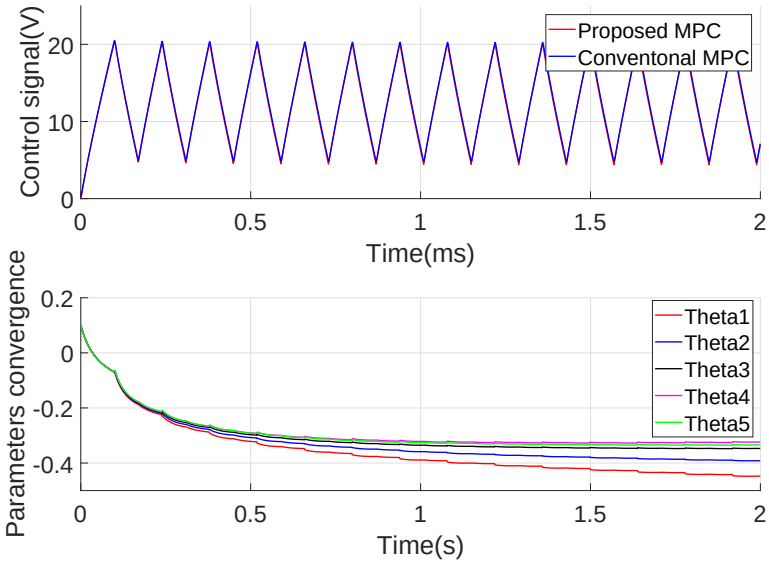

Figure 2.14: The parameters convergence of the proposed MPC with sawtooth desired output

2.6.3 Robustness of the control system

To show the robustness of the proposed controller, an external force is used to impact the positioning system. The experimental results for constant desired output and sinusoidal desired output under external disturbance are shown in Fig. 2.15 and Fig. 2.16, respectively. It can be observed that the control voltage is automatically changed to compensate the external disturbance. And by inspecting the tracking error, it can be said that the influence of the external disturbance is completely removed since there are no sudden changes in the position error.

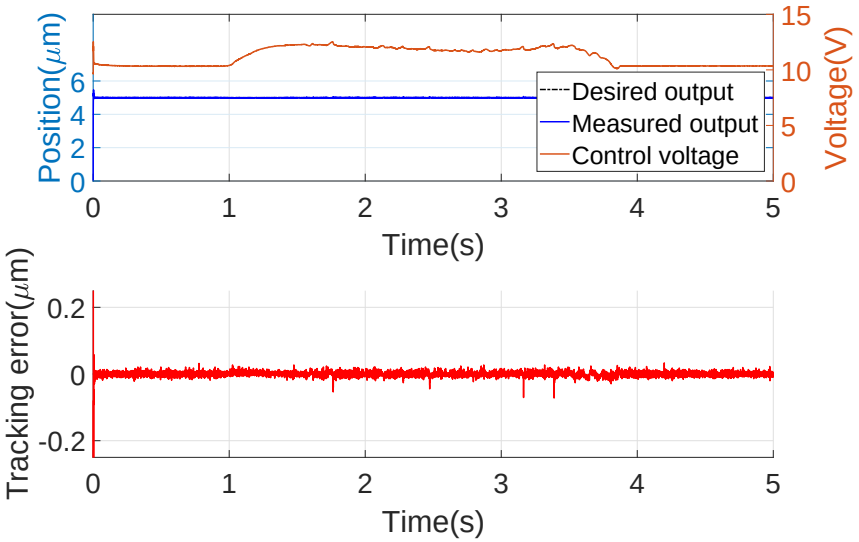

Figure 2.15: System response with constant desired output and external disturbance

2.7 Conclusion

In this chapter, the design of the pseudo MPC for SISO plants is presented. The parameters concerned with the control action of the conventional MPC are obtained directly by using pole-placement and adaptive techniques without complicated tuning procedure involving the weighted matrices. This proposed method

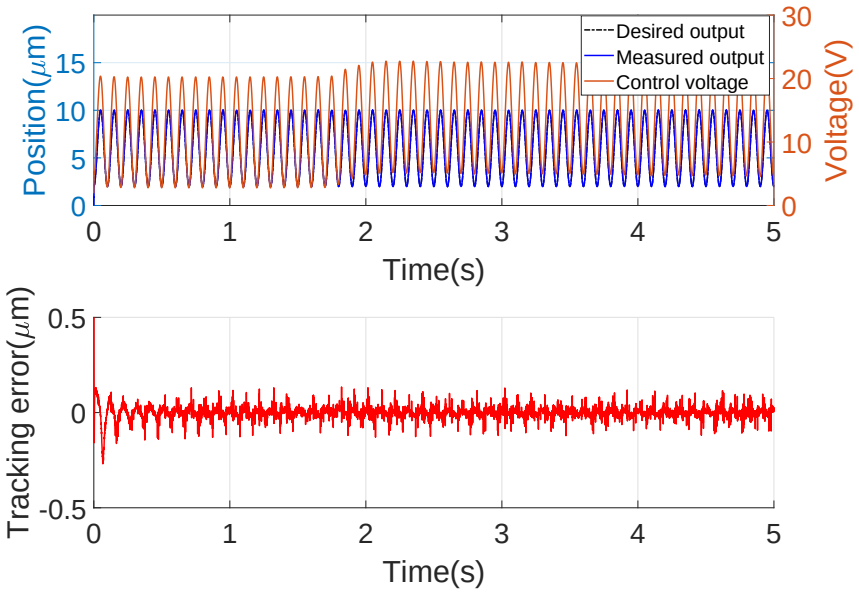

Figure 2.16: System response with sinusoidal desired output and external disturbance

is capable of minimizing the tracking error and robust against the external disturbance. The effectiveness of the proposed method is confirmed by various experiments on the piezo-actuated positioning system in which complicated desired outputs are employed. Although the computation time is increased, the tracking performance of the proposed method is significantly improved in comparison with its conventional counterpart. The experiment results also prove that the control system is immune against the influence of the external disturbances.

Chapter 3

Integer Order Sliding Mode Control Design

3.1 Introduction

The sliding mode control (SMC) is well known as one of the most famous robust control technique due to its insensitivity to matched uncertainties [90]. The main idea of the SMC is to force the system state trajectory to approach a specified manifold by a nonlinear switching control signal (reaching phase) and to keep it on the manifold afterward by an equivalent control signal (sliding phase) [91]. Due to its simplicity and robustness, SMC has been used for a vast of applications such as motor control [18, 55, 77, 78, 83], positioning and motion control [13, 65, 85], power electronic converters [19, 66], robotic [10, 20, 33], etc. At first, most results are achieved in continuous time domain [32, 74]. Then, due to the explosive development of digital-based control devices, which is flexible and capable of implementing complex control algorithm at high speed, the studying on discrete-time sliding mode control (DSMC) has attracted a great attention.

In general, the design of SMC can be accomplished by either assuming a certain control algorithm and show that this algorithm guarantees the stability of the sliding motion on the hyper surface, or applying the reaching law approach, in which the evolution of the sliding variable is designed first and the control action

is then determined. In the former approach, the sliding variable can be driven to the $O(T_s^2)$ boundary layer in just one step [70]. However, such rapid action may require a large control effort if the initial state is far from the sliding manifold. Hence, a discrete-time integral sliding mode control (DISMC) scheme is proposed in [2] to prevent the overlarge control action and to improve the tracking accuracy.

The latter approach is however preferred in the literature due to its systematic design procedure. Besides, the two major concerns of the DSMC including the dynamic in reaching phase and chattering can be considered in the reaching law. This approach was first introduced by Gao in [25]. In that article, the quasi-sliding mode (QSM) motion and quasi-sliding mode band (QSMB) are strictly defined. The obtained control action is composed of a discrete-time equivalent control signal, which maintains the sliding variables on the sliding manifold, and a switching control action which drives the sliding variable to the sliding manifold as well as enhance the robustness of the system. Then, the idea has been extensively used in many other researches [6, 7, 11, 12, 22, 50, 58]. To reduce the chattering in DSMC, the disturbance is estimated by the one step delayed technique with assumption that the sampling frequency is sufficient high. Consequently, the amplitude of the switching control action is small since it only has to deal with the remaining disturbance estimation error. However, the small switching gain may result in long reaching time. To achieve both low chattering and to accelerate the reaching speed, different techniques are considered. For example, an exponential reaching law is proposed in [50] in which the switching gain is an exponential function of the sliding variable, or fuzzy technique can also be used to smoothly change the switching gain according to the value of the sliding variable as in [30].

Recently, the DSMC has also been succesfully exploited in tracking control of pieazo-actuated positioning systems [83, 85, 87, 88] due to the fact that the fast dynamic of the piezoelectric actuators suit well the deadbeat response of the closed-loop systems based DSMC.

This chapter focuses on DSMC design for the pieazo-actuated positioning system. The conventional DSMC and DISMC are first investigated in Section 3.2 and 3.3. Then, the proposed strategy which combines DSMC with prescribed

performance control (PPC) is introduced in Section 3.4. At the end of this chapter is the conclusions.

3.2 Contributions

In this chapter, a novel prescribed performance DSMC in which a nonlinear sliding variable based on a prescribed performance function (PPF) is proposed. Theoretical analysis shows that the DSMC based on the proposed sliding variable is capable of maintaining the tracking error inside a predefined convergence zone formed by the PPF under certain initial conditions. Furthermore, the transient response of the closed-loop system can easily be adjusted to avoid the overshoot without affecting the steady-state performance. The effectiveness of the proposed method is confirmed by experimental results on a piezo-actuated positioning system.

3.3 DSMC Design

3.3.1 Control Design

In this section, the robust DSMC design for tracking control of system (2.1) is presented.

Define the first-order sliding variable S_k as

$$S_k = e_k - \lambda e_{k-1} \tag{3.1}$$

where $0 < \lambda < 1$ is a desired parameter which decides the convergent rate of e_k as $S_k = 0$.

The one-step forward value of the sliding variable is

$$S_{k+1} = e_{k+1} - \lambda e_k \tag{3.2}$$

By substituting (2.19) into (3.2), it gives

$$S_{k+1} = -\lambda e_k + y_{d,k+1} + \sum_{i=1}^{n} a_i y_{k-i+1} - \sum_{j=1}^{m} b_j u_{k-j+1} - \hat{p}_k - \tilde{p}_k \tag{3.3}$$

The equivalent control action u^{eq} which maintains the sliding variable S_k on the sliding manifold is computed by solving the following equation

$$S_{k+1} = 0 \tag{3.4}$$

The solution of (3.4) can only be obtained as the unknown term $\tilde{p}_k$ is ignored. Then, it results in

$$u_k^{eq} = \frac{1}{b_1}\left[-\lambda e_k + y_{d,k+1} + \sum_{i=1}^{n} a_i y_{k-i+1} - \sum_{j=2}^{m} b_j u_{k-j+1} - \hat{p}_k\right] \tag{3.5}$$

Assume that the remaining disturbance estimation error $\tilde{p}_k$ satisfies

$$|\tilde{p}_k| \leq \epsilon \tag{3.6}$$

Then, the robustness of the system against the remaining disturbance estimation error $\tilde{p}_k$ can be improved by introducing an additional switching control action u_k^{sw}

$$u_k^{sw} = \frac{1}{b_1} K_{sw} sign(S_k) \tag{3.7}$$

where K_{sw} is the switching gain satisfying

$$K_{sw} = \gamma + \epsilon \tag{3.8}$$

in which γ is a small positive number, and

$$sign(S_k) = \begin{cases} 1 & for \quad S_k > 0 \\ 0 & for \quad S_k = 0 \\ -1 & for \quad S_k < 0 \end{cases} \tag{3.9}$$

Then, the final control action is

$$\begin{aligned} u_k &= u_k^{eq} + u_k^{sw} \\ &= \frac{1}{b_1}\left[-\lambda e_k + y_{d,k+1} + \sum_{i=1}^{n} a_i y_{k-i+1} - \sum_{j=2}^{m} b_j u_{k-j+1} - \hat{p}_k + K_{sw} sign(S_k)\right] \end{aligned} \tag{3.10}$$

Theorem 3.1: Given a nominal system described by (2.1) with the sliding function (3.1). If the control signal (3.10) is employed, then the sliding variable S_k will reach a bounded QSMB described by (3.11) in one step and stays within this band afterward. The ultimate bound of the tracking error in steady-state is described by (3.12).

$$QSMB = \{e : |S(e)| < 2\epsilon + \gamma\} \tag{3.11}$$

$$\sup_k(|e_k|) = \frac{2\epsilon + \gamma}{1 - \lambda} \tag{3.12}$$

Proof of Theorem 3.1: Substitute (3.10) into (3.3), a fundamental operation gives

$$S_{k+1} = -\tilde{p}_k - K_{sw} sign(S_k) \tag{3.13}$$

If $S_k \geq 0$, it is derived from (3.13) that

$$S_{k+1} = -\tilde{p}_k - K_{sw} \tag{3.14}$$

In view of (3.8) and (3.14), it yields

$$-(2\epsilon + \gamma) < S_{k+1} < -\gamma \tag{3.15}$$

If $S_k < 0$ and in view of (3.8), it gives

$$S_{k+1} = -\tilde{p}_k + K_{sw} \tag{3.16}$$

Again, from (3.8) and (3.16), it yields

$$\gamma < S_{k+1} < (2\epsilon + \gamma) \tag{3.17}$$

From (3.15) and (3.17), it can be concluded that

$$|S_{k+1}| < (2\epsilon + \gamma) \tag{3.18}$$

Relation (3.18) also means that once the control signal (3.10) is employed, the sliding variable will approach and cross the switching plane in every successive sampling cycle. The size of the quasi-sliding mode band in this case is non increasing and specified by (3.11).

To obtain the ultimate bound of the tracking error e_k, substitute (3.10) into (2.19) and in view of (3.13), then a fundamental operation gives

$$e_{k+1} = \lambda e_k + S_{k+1} \tag{3.19}$$

The solution of (3.19) is

$$e_k = \lambda^k e_0 + \sum_{i=0}^{k-1} \lambda^i S_{k-i} \tag{3.20}$$

in which e_0 is the initial error. From (3.18), it can be deduced that

$$|e_k| \leq \lambda^k e_0 + (2\epsilon + \gamma) \sum_{i=0}^{k-1} \lambda^i = \lambda^k e_0 + (2\epsilon + \gamma) \frac{\lambda^k - 1}{\lambda - 1} \tag{3.21}$$

Since $0 < \lambda < 1$, it yields

$$\sup_k(|e_k|) = \frac{2\epsilon + \gamma}{1 - \lambda} \tag{3.22}$$

This ends the proof.

3.3.2 Experimental Results

To confirm the validity of the DSMC design, various experiments on the piezo-actuated positioning system described in section 3.2 are conducted.

The step responses of the DSMC design are shown in Fig. 3.1 and Fig.3.2. It can be observed that the settling time increases as λ increases, as analyzed in the control design section. The sliding variable S_k also quickly moves to the sliding surface and maintains there afterward. The tracking error in steady-state in these cases are extremely small, i.e, $RMSTE = 0.0039$µm, and does not affected by the coefficient λ.

For sinusoidal desired output, the steady-state error is affected by the coefficient λ. As seen in Fig. 3.4 and Fig. 3.5, the tracking error is increased as λ increases. Hence, a negotiation between the transient and steady-state performance should be considered when selecting λ.

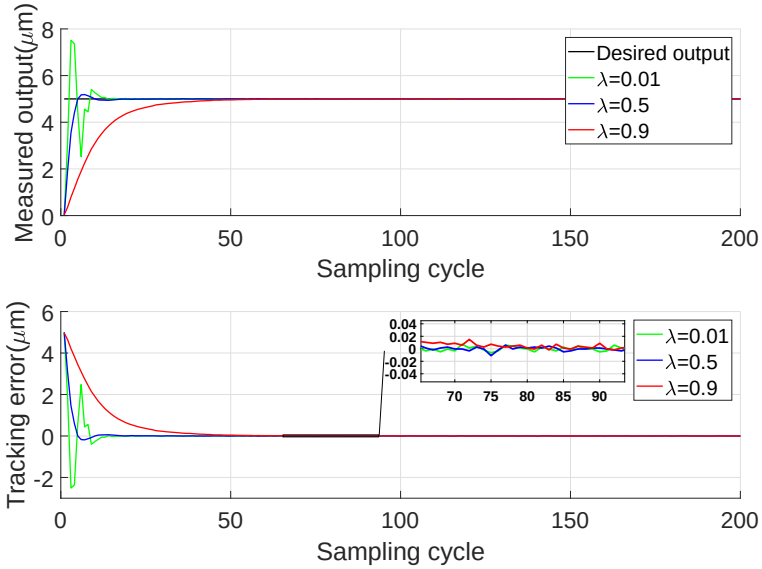

Figure 3.1: Step responses of DSMC

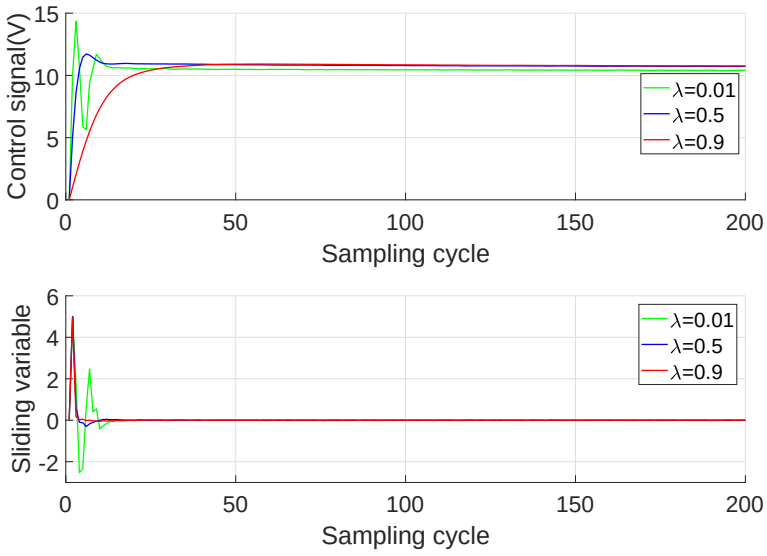

Figure 3.2: Control signal and sliding variable of DSMC with step desired output

The tracking performance of the DSMC design is also test with other complicated desired outputs such as multiple frequency, time-varying amplitude and frequency and sawtooth as seen in Fig. 3.6, Fig. 3.7 and Fig. 3.8, respectively. In

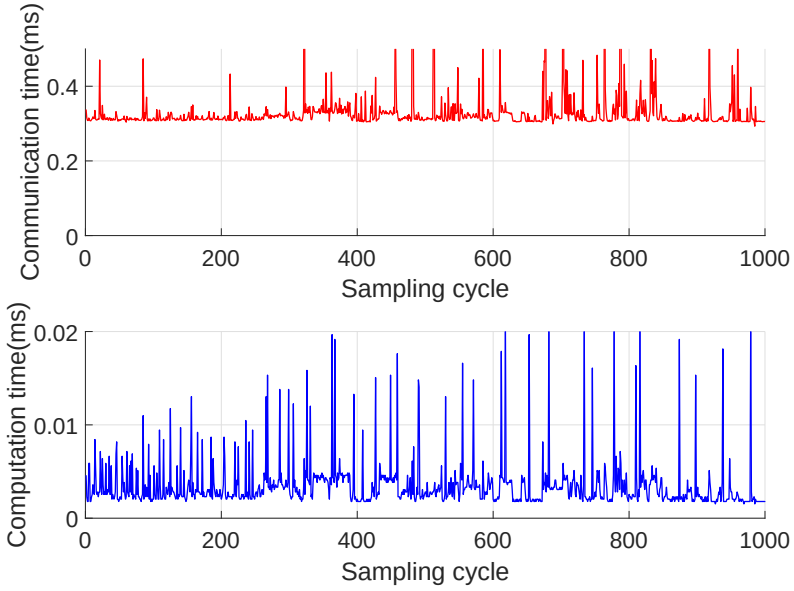

Figure 3.3: The computation time of DSMC algorithm

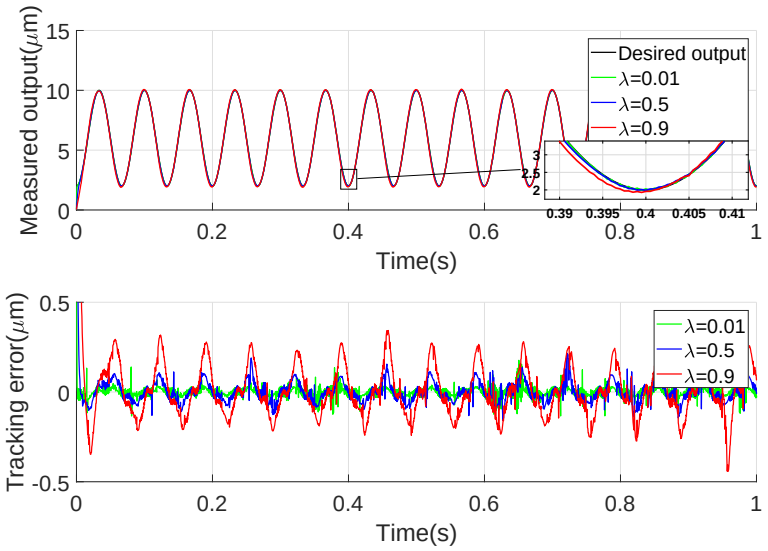

Figure 3.4: Tracking performance of DSMC with sinusoidal desired output

every cases, the RMSTE is less than 0.1µm corresponding to 1% of the maximum set-point.

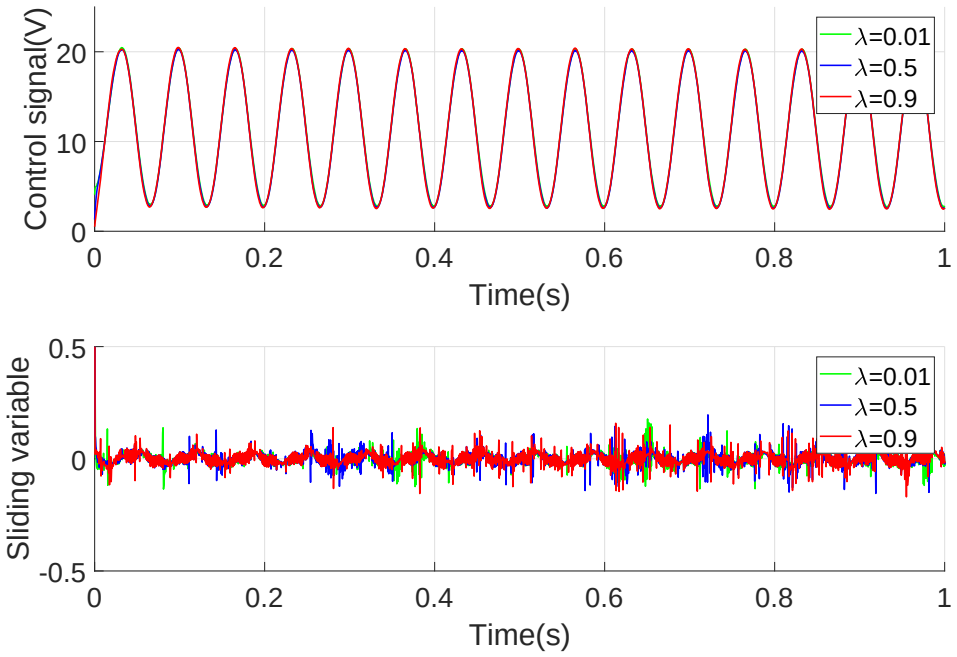

Figure 3.5: Control signal of DSMC with sinusoidal desired output

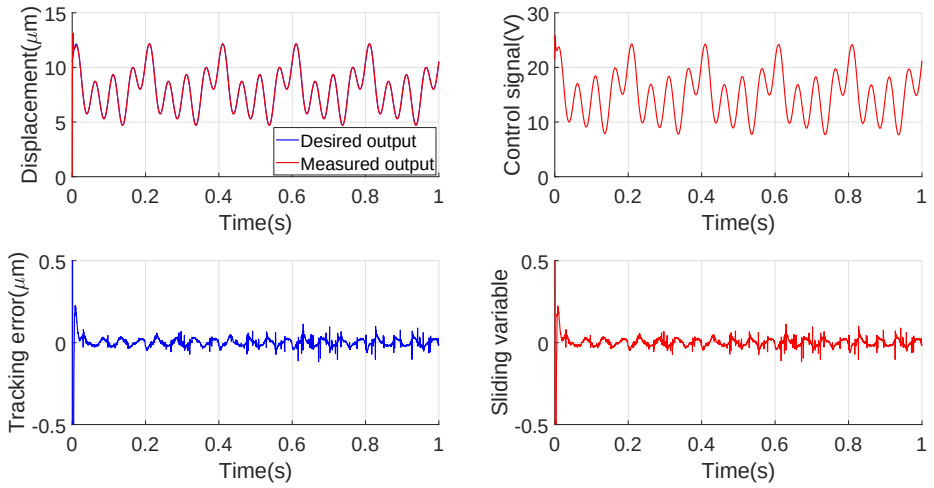

Figure 3.6: DSMC with multiple frequency desired output

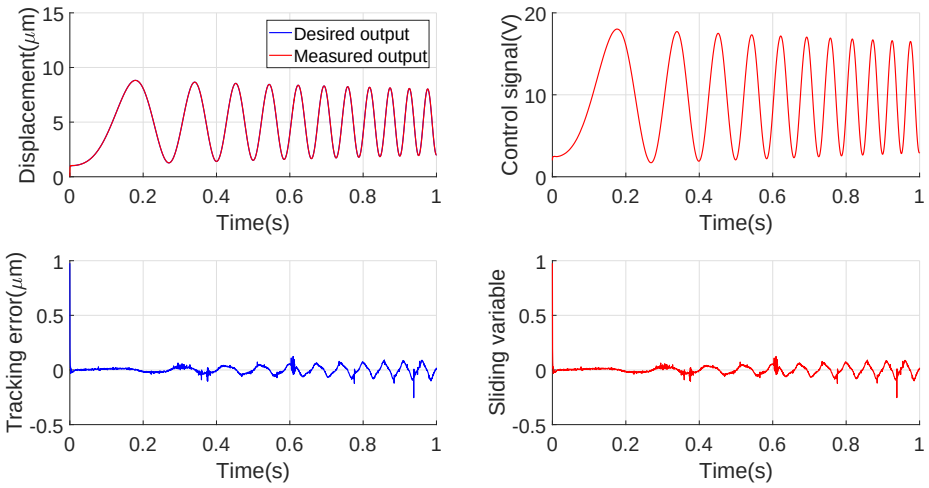

Figure 3.7: DSMC with time-varying amplitude and frequency desired output

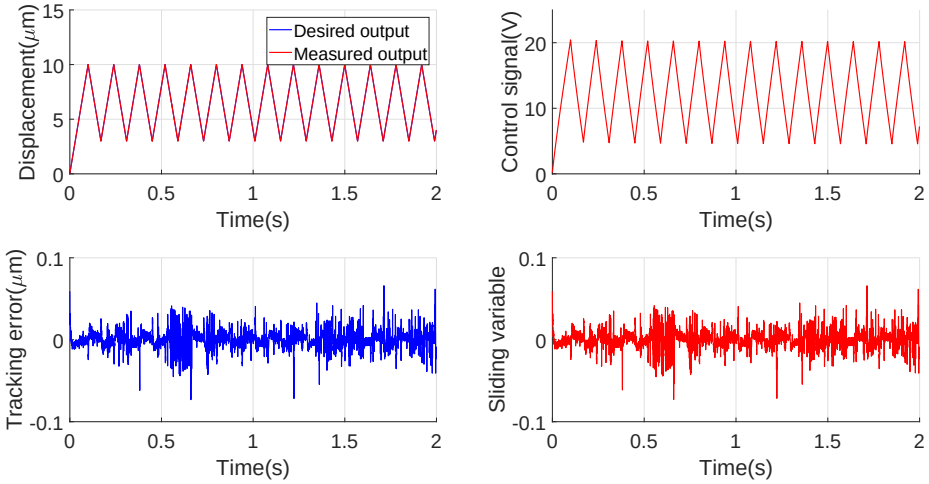

Figure 3.8: DSMC with sawtooth desired output

3.4 DISMC Design

In this section, a free chattering DISMC design which is based on *Assumption 2.1* is introduced.

3.4.1 Control Design

Consider the following sliding variable

$$S_k = e_k + \varepsilon_k \tag{3.23}$$

$$\varepsilon_k = \varepsilon_{k-1} + K_I T_s e_k \tag{3.24}$$

in which ε_k is the integral of the tracking error and K_I is the integral gain.

The one step ahead value of S_k is

$$S_{k+1} = e_{k+1} + \varepsilon_{k+1} \tag{3.25}$$

From (3.23) and (3.24), it can easily be deduced that

$$S_{k+1} = S_k + (1 + K_I T_s)e_{k+1} - e_k \tag{3.26}$$

Consider the following reaching law

$$S_{k+1} - \chi S_k = 0 \tag{3.27}$$

where $0 < \chi < 1$ is a desired constant.

By substituting (2.4), (3.25) into (3.27) and neglecting the unknown term $\tilde{p}_k$, the solution of (3.27) is

$$u_k^I = \frac{1}{b_1}\left[y_{d,k+1} + \sum_{i=1}^{n} a_i y_{k-i+1} - \sum_{j=2}^{m} b_j u_{k-j+1} - \hat{p}_k\right] - \frac{[e_k - (1-\chi)S_k]}{b_1(1 + K_I T_s)} \tag{3.28}$$

Theorem 3.2: Given a nominal system described by (2.1) with the sliding variable (3.25). If the control signal (3.28) is used, then the ultimate bound of the sliding variable and the tracking error in steady-state are described by (3.29) and (3.30), respectively.

$$\sup(|S|) = O(T_s^2) \tag{3.29}$$

$$\sup(|e|) = O(T_s) \tag{3.30}$$

Proof of Theorem 3.2:

Substitute the control action (3.28) into (3.25), a simple manipulation gives

$$S_{k+1} = \chi S_k - (1 + K_I T_s)\tilde{p}_k \tag{3.31}$$

The solution of (3.31) is

$$S_k = \chi^k S_0 + \sum_{i=0}^{k-1} \chi^i \left[-(1 + K_I T_s)\tilde{p}_i\right] \tag{3.32}$$

Based on (2.18) and (2.8), it can be deduced that

$$\begin{aligned} S_k &= \chi^k S_0 + \sum_{i=0}^{k-1} \chi^i \left[O(T_s^2) + K_I O(T_s^3)\right] \\ &\approx \chi^k S_0 + \sum_{i=0}^{k-1} \chi^i O(T_s^2) \end{aligned} \tag{3.33}$$

which means there exists a constant A such that

$$|S_k| \leq \chi^k S_0 + A T_s^2 \sum_{i=0}^{k-1} \chi^i \tag{3.34}$$

Note that if $0 < \chi < 1$, then

$$\sum_{i=0}^{k-1} \chi^i = \frac{\chi^k - 1}{\chi - 1} \tag{3.35}$$

following that,

$$|S_k| \leq \chi^k S_0 + A T_s^2 \left(\tfrac{\chi^k - 1}{\chi - 1}\right), \quad \forall k > 0 \tag{3.36}$$

Since $0 < \chi < 1$, it can be deduced from (3.36) that

$$\begin{aligned} \lim_{k \to \infty} |S_k| &= \frac{A T_s^2}{1 - \chi} \\ &= O(T_s^2) \end{aligned} \tag{3.37}$$

As a result, (3.29) holds.

The ultimate bound of the tracking error e_k is obtained similarly. Substitute (3.28) into (2.19), it gives

$$e_{k+1} = \frac{1}{1 + K_I T_s} e_k - \left[\frac{(1 - \chi)}{(1 + K_I T_s)} S_k + \tilde{p}_k\right] \tag{3.38}$$

Since S_k approaches $O(T_s^2)$ monotonically, for sufficient large k (3.38) can be rewritten as

$$\begin{aligned} e_{k+1} &= \frac{1}{1+K_I T_s} e_k - \left[\frac{(1-\chi)}{(1+K_I T_s)} O(T_s^2) + O(T_s^2) \right] \\ &= \frac{1}{1+K_I T_s} e_k - O(T_s^2) \end{aligned} \tag{3.39}$$

The solution of (3.39) is

$$e_k = \left(\frac{1}{1+K_I T_s} \right)^k e_0 + O(T_s^2) \sum_{i=0}^{k-1} \left(\frac{1}{1+K_I T_s} \right)^i \tag{3.40}$$

Based on (2.18) and (2.8), it can be deduced that

$$|e_k| \leq \left(\frac{1}{1+K_I T_s} \right)^k e_0 + A T_s^2 \sum_{i=0}^{k-1} \left(\frac{1}{1+K_I T_s} \right)^i \tag{3.41}$$

Again, since $\left(\frac{1}{1+K_I T_s} \right) < 1$, it yields

$$\sum_{i=0}^{k-1} \left(\frac{1}{1+K_I T_s} \right)^i = \frac{\left(\frac{1}{1+K_I T_s} \right)^k - 1}{\left(\frac{1}{1+K_I T_s} \right) - 1} \tag{3.42}$$

following that

$$|e_k| \leq \left(\frac{1}{1+K_I T_s} \right)^k e_0 + A T_s^2 \frac{\left(\frac{1}{1+K_I T_s} \right)^k - 1}{\left(\frac{1}{1+K_I T_s} \right) - 1} \tag{3.43}$$

Finally,

$$\begin{aligned} \lim_{k \to \infty} |e_k| &= \frac{A T_s^2}{1 - \frac{1}{1+K_I T_s}} \\ &= A T_s^2 + \frac{A T_s}{K_I} \\ &= O(T_s^2) + O(T_s) \end{aligned} \tag{3.44}$$

Hence, it can be concluded that in steady-state

$$\lim_{k \to \infty} |e_k| \approx O(T_s) \tag{3.45}$$

which means (3.30) holds. This ends the proof.

The stability of the closed-loop system can also be analyzed based on state-space representation as following.

From (3.31) and (3.38), it gives

$$\begin{bmatrix} e_{k+1} \\ S_{k+1} \end{bmatrix} = \begin{bmatrix} \frac{1}{1+K_I T_s} & -\frac{1-\chi}{1+K_I T_s} \\ 0 & \chi \end{bmatrix} \begin{bmatrix} e_k \\ \chi_k \end{bmatrix} + \begin{bmatrix} O(T_s^2) \\ O(T_s^2) \end{bmatrix} \tag{3.46}$$

It can easily seen from (3.46) that the system has two real poles: $\frac{1}{1+K_I T_s}$ and χ. As long as $K_I > 0$ and $0 < \chi < 1$, the system is stable.

3.4.2 Experimental Results

To verify the validity of the control method, various experiments are carried out in this section.

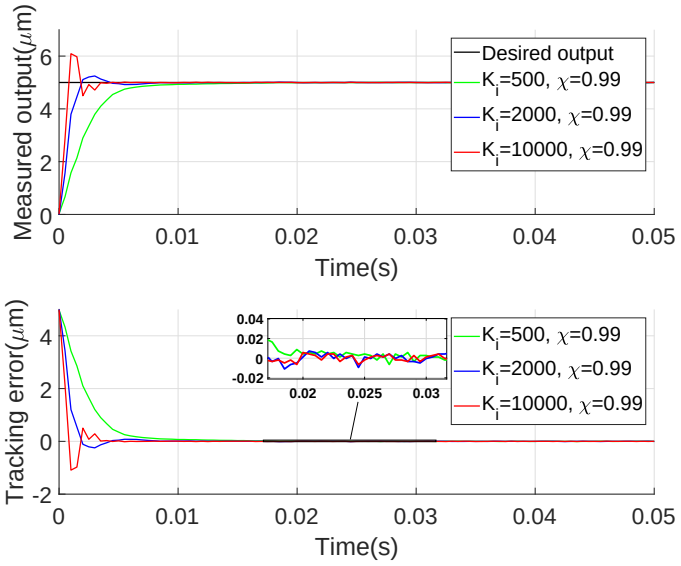

Figure 3.9: The step responses of the DISMC in with various integral gains

The influence of the integral gain K_I on the response of the closed-loop system is shown in Fig. 3.9 and Fig. 3.10 whilst the influence of the damping coefficient χ is shown in Fig. 3.11 and Fig. 3.12. The desired output in this experiment is

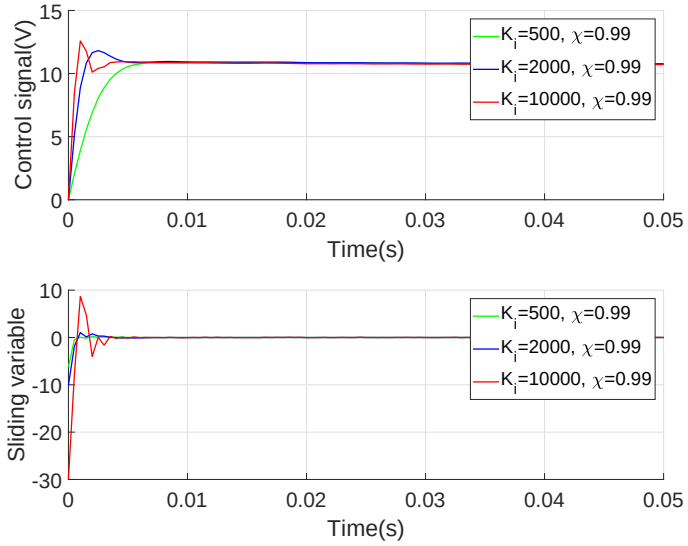

Figure 3.10: The control signal and sliding variable of the DISMC with various integral gain

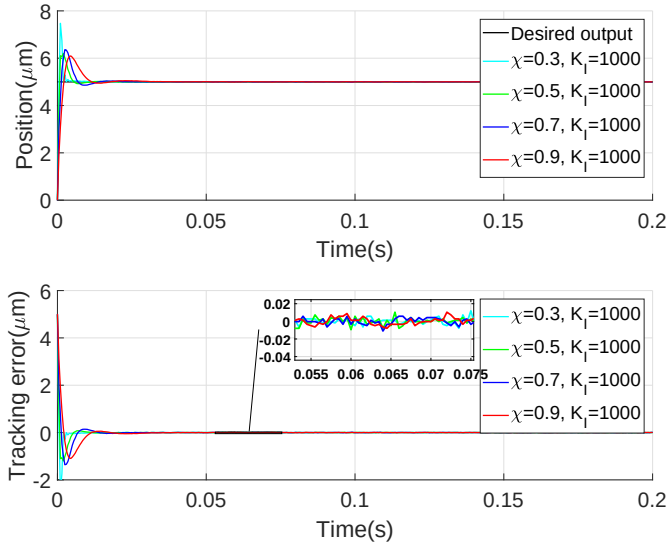

Figure 3.11: The step responses of the DISMC in with various damping coefficients

$y_d = 5$. The computation time of the DISMC is provided in Fig. 3.13. As can be

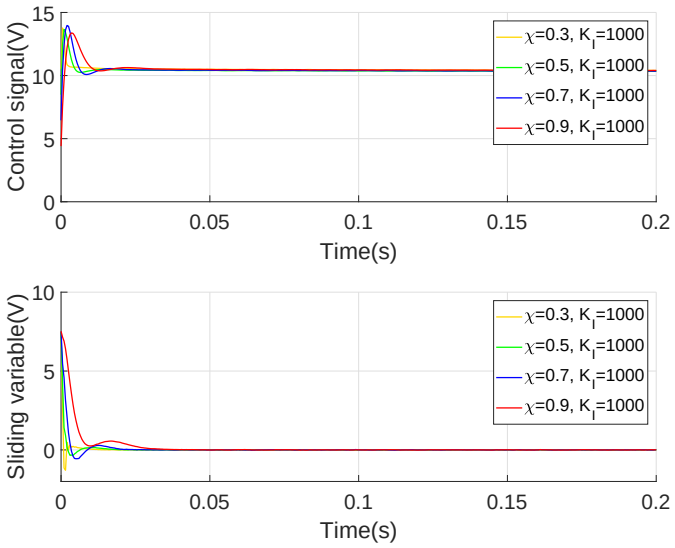

Figure 3.12: The control signal and sliding variable of the DISMC with various damping coefficients

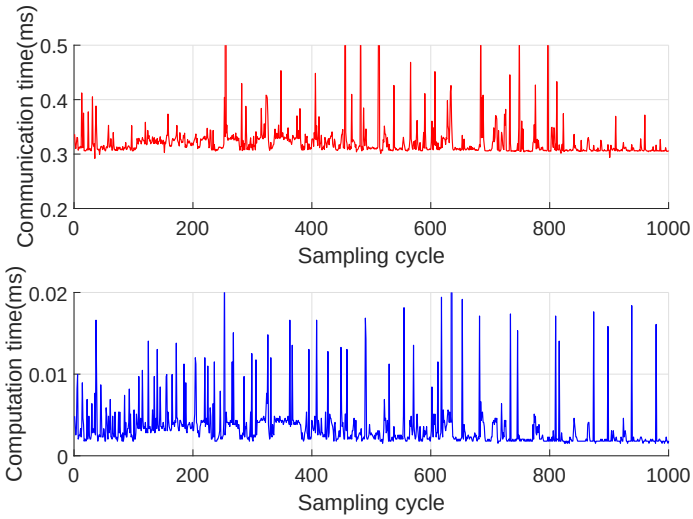

Figure 3.13: The computation time of the DISMC algorithm

observed, the response speed is proportional to the integral gain K_I and inverse proportional to the damping coefficient χ. However, to achieve quick response, the overshoot is inevitable.

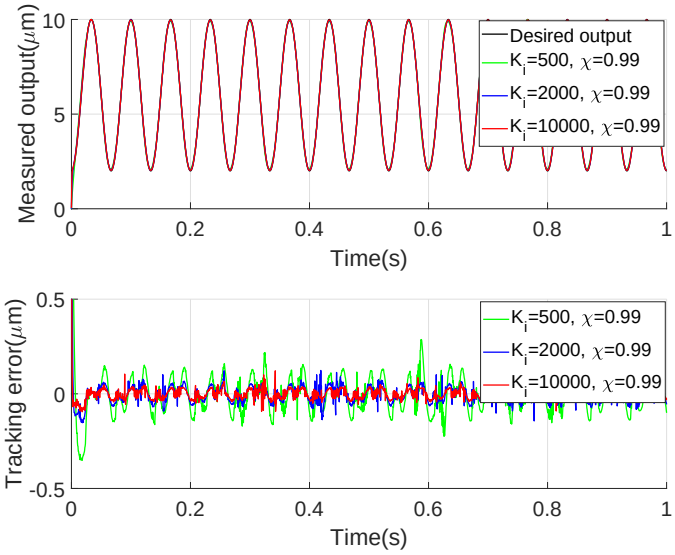

Figure 3.14: The tracking performance of the DISMC with various integral gains

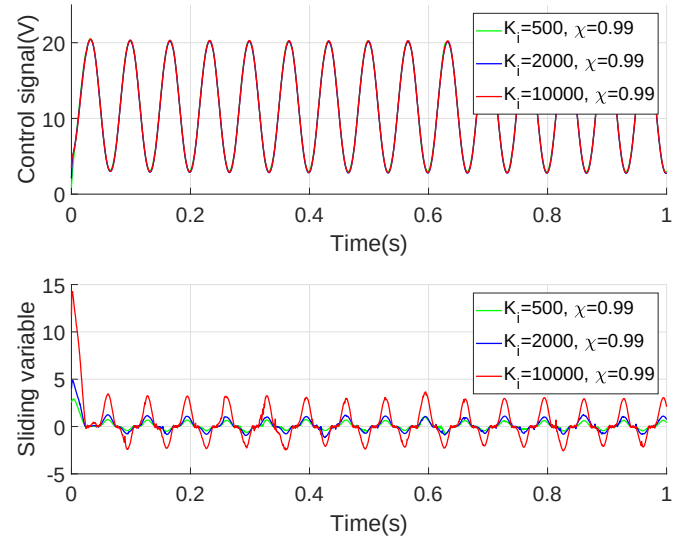

Figure 3.15: The control signal and sliding variable of the DISMC with various integral gains

To show the influence of the parameters on the tracking performance, sinusoidal $y_d = 4\sin(2\pi 10t - \frac{\pi}{2}) + 6$ is adopted. By inspecting the experimental results

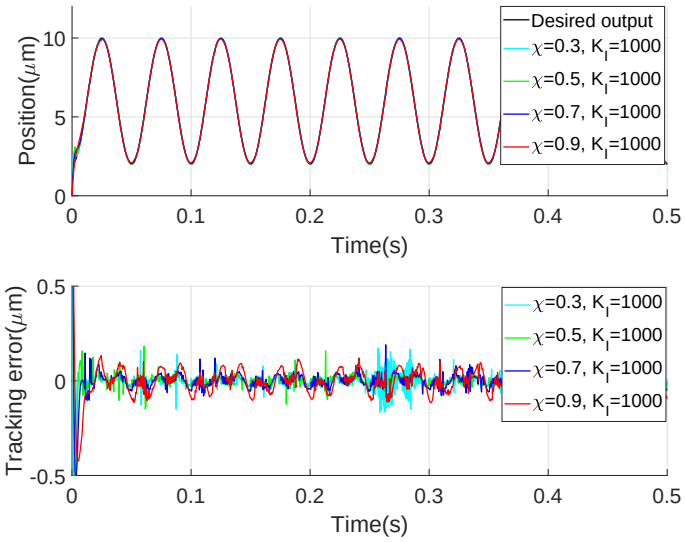

Figure 3.16: The tracking performance of the DISMC with various damping coefficients

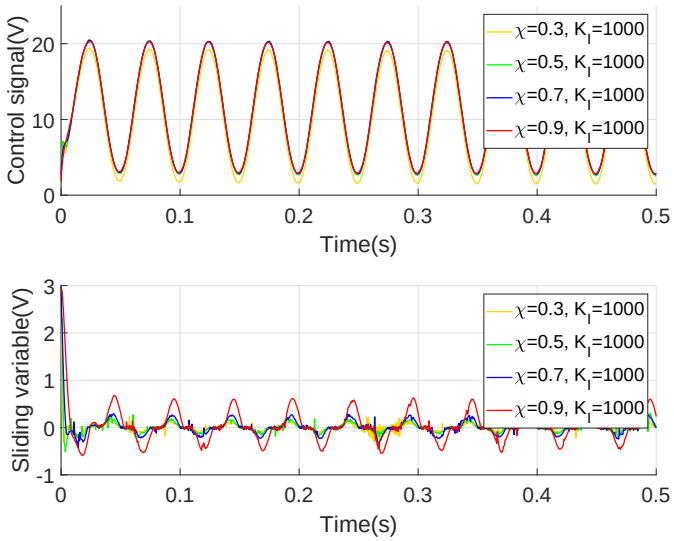

Figure 3.17: The control signal and sliding variable of the DISMC with various damping coefficients

depicted in Fig. 3.14 to Fig. 3.17, it can be realized that if the parameters are

chosen such that the step response is smooth with low overshoot, then the tracking error is large and vice versa. So, similar to the DSMC, a negotiation between transient and steady-state performance should be taken into account when tuning the parameters.

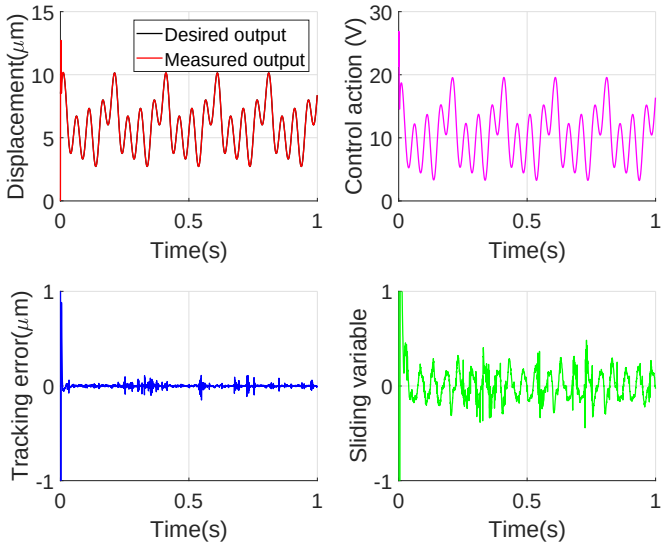

Figure 3.18: Tracking performance of DISMC with multiple frequency desired output

Finally, complicated desired outputs are employed to investigate performance of the control system. The experimental results with $y_d = 0.5\cos(2\pi 5t) + 2\cos(2\pi 15t) + 1.5\sin(2\pi 30t) + 8$ and $y_d = (5 - 5t)\sin[2\pi(10 + 10t) - \pi/2] + 8$ are shown in Fig. 3.18 and Fig. 3.19, respectively. The experiment results with sawtooth desired output is shown in Fig. 3.20. The parameters are $K_I = 1000$ and $\chi = 0.9$ in these experiments. Similar to the DSMC, the tracking error is proportional to the tracking frequency. As long as the ratio between the sampling and the tracking frequency are larger than 100, the RMSTE is kept below 1%. This result is acceptable in most practical application.

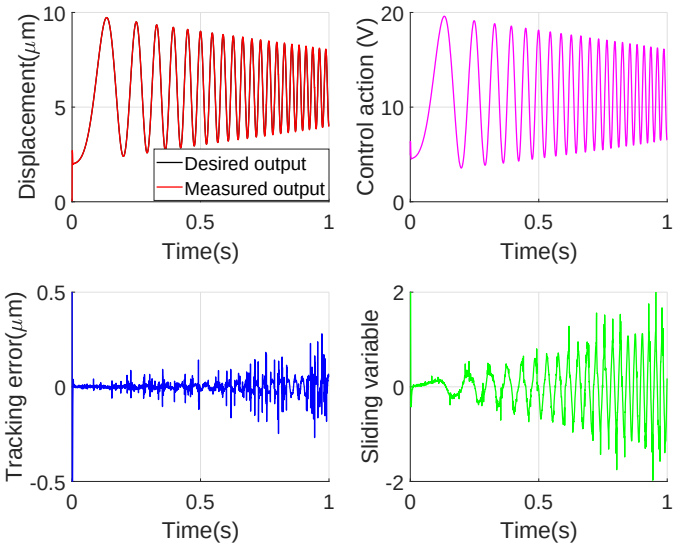

Figure 3.19: Tracking performance of DISMC with time-varying amplitude and frequency desired output

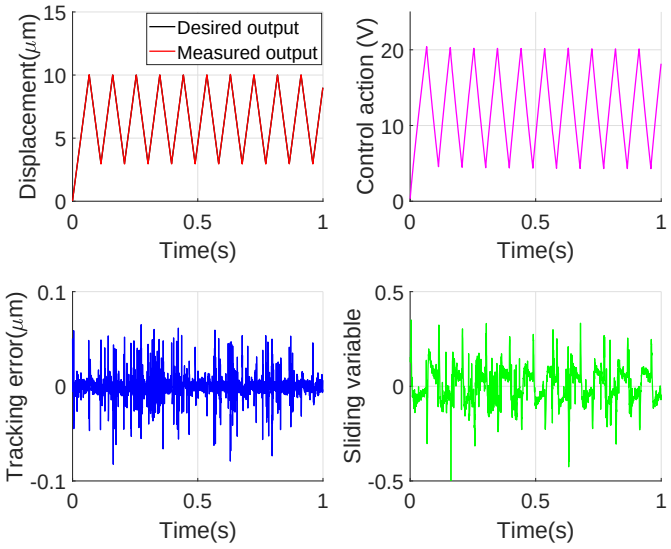

Figure 3.20: Tracking performance of DISMC with sawtooth desired output

3.5 Prescribed Performance DSMC

3.5.1 Introduction

Recently, a new technique named prescribed performance control (PPC) has been proposed in the literature [8, 9, 44, 57, 61, 72, 80]. The main idea of the PPC is to guarantee the convergence of the tracking error in an arbitrarily small predefined zone/region. The merit of this technique is that both transient and steady-state performance of the closed-loop system can be assured, i.e, the tracking error converges to a predefined arbitrarily small zone with convergence rate no less than a preassigned value and the maximum overshoot less than a desired constant. This control problem is normally solved by transforming the constrained tracking error into an unconstrained equivalent form. Then, the controller is designed to stabilize the unconstrained transformed error. Until now, most researches on PPC are conducted in continuous-time domain. Further analysis in this paper also shows that the conventional PPC may produce offset error in steady-state if the transient response is adjusted.

To handle the two above mentioned problems of the PPC, the design of PPC for the discrete-time uncertain system (2.1) is presented in this section. First, the convergence zone is modified such that the transient response of the closed-loop system can be adjusted without producing the offset error in steady-state. Then, a novel sliding variable based on a prescribed performance function (PPF) is proposed. Theoretical analysis shows that the DSMC based on the proposed sliding variable is capable of maintaining the tracking error inside the convergence zone formed by the PPF under certain initial conditions. Since the PPC is designed in discrete-time domain, the algorithm can easily be implemented by any digital controllers without using numerical approximation. Particularly, the computation time of the control algorithm is also reduced since the traditional transformed error which is based on a logarithm function is not employed in the control action. The effectiveness of the proposed method is confirmed by experiments.

3.5.2 Prescribed Performance Function

The performance function is used to describe a convergence zone where the control algorithm must assure that once starting from a point inside the convergence zone, the tracking error trajectory will remain in this zone afterward. In this section, a positive decreasing discrete-time prescribed performance function (DPPF) is chosen as

$$\mu_{k+1} = (1 - \kappa)\mu_k + \kappa\mu_\infty \tag{3.47}$$

with

$$\begin{aligned} &0 < \mu_\infty < \mu_0 \\ &0 < \kappa < 1 \end{aligned} \tag{3.48}$$

This DPPF satisfies

$$\lim_{k\to\infty} \mu_k = \mu_\infty \tag{3.49}$$

with the initial value μ_0 and convergence rate relating to κ are restricted by (3.48).

3.5.3 Conventional Convergence Zone and Transformed Error

By simply changing the continuous-time case in [57] to discrete time case, the convergence zone can be formulated as follows,

$$-\underline{\delta}\mu_k < e_k < \bar{\delta}\mu_k \tag{3.50}$$

where $\bar{\delta}$, $\underline{\delta}$ represent the upper and lower bounds, respectively

To deal with the constrained control problem (3.50), the tracking error e_k is transformed into an unconstrained equivalent form by employing a strictly increasing function $\Lambda(\vartheta_k)$ of a transformed error ϑ_k. The strictly increasing function must satisfy the two following properties:

Property 1. $-\underline{\delta} < \Lambda(\vartheta_k) < \bar{\delta}$, for arbitrary real number ϑ_k

Property 2. $\lim_{\vartheta_k\to+\infty} \Lambda(\vartheta_k) = \bar{\delta}$ and $\lim_{\vartheta_k\to-\infty} \Lambda(\vartheta_k) = -\underline{\delta}$

From the two above properties, the constraint (3.50) is same as

$$e_k = \mu_k \Lambda(\vartheta_k) \tag{3.51}$$

Since $\Lambda(\vartheta_k)$ is strictly increasing, its inverse function always exists and described by

$$\vartheta_k = \Lambda^{-1}[\frac{e_k}{\mu_k}] \tag{3.52}$$

For control design purpose, a strictly increasing function is chosen as

$$\Lambda(\vartheta_k) = \frac{\bar{\delta}e^{\vartheta_k} - \underline{\delta}e^{-\vartheta_k}}{e^{\vartheta_k} + e^{-\vartheta_k}} \tag{3.53}$$

The transformed error is then derived from (3.53) and results in

$$\vartheta_k = \frac{1}{2}\ln(\frac{\underline{\delta}\mu_k + e_k}{\bar{\delta}\mu_k - e_k}) \tag{3.54}$$

From (3.52), it can be deduced that for any initial tracking error e_0, if parameters μ_0, $\underline{\delta}$, $\bar{\delta}$ are selected such that $-\underline{\delta}\mu_0 < e_0 < \bar{\delta}\mu_0$ and ϑ_k can be controlled to be bounded, then $-\underline{\delta} < \Lambda(\vartheta_k) < \bar{\delta}$ holds and (3.50) is guaranteed.

3.5.4 Modified Convergence Zone and Transformed Error

In view of (3.49) and (3.54), if the transformed error ϑ_k is well controlled, i.e., $\vartheta_k = 0$, the tracking error at steady-state is

$$e_{ss} = \lim_{k\to\infty} \mu_k(\frac{\bar{\delta} - \underline{\delta}}{2}) = \mu_\infty(\frac{\bar{\delta} - \underline{\delta}}{2}) \tag{3.55}$$

If $\bar{\delta} \neq \underline{\delta}$, i.e., for transient response tuning, the offset error will exist in steady-state. To overcome this problem, two dynamical functions $\underline{\delta}_k$ and $\bar{\delta}_k$ are proposed:

$$\underline{\delta}_{k+1} = (1-\kappa)\underline{\delta}_k + \kappa \tag{3.56}$$

$$\bar{\delta}_{k+1} = (1-\kappa)\bar{\delta}_k + \kappa \tag{3.57}$$

These functions satisfy

$$\lim_{k\to\infty} \underline{\delta}_k = 1, \underline{\delta}_0 \geq 1 \tag{3.58}$$

$$\lim_{k\to\infty} \bar{\delta}_k = 1, \bar{\delta}_0 \geq 1 \tag{3.59}$$

where $\underline{\delta}_0$ and $\bar{\delta}_0$ are the initial values.

The modified convergence zone and the transformed error are now defined as

$$-\underline{\delta}_k\mu_k + \gamma < e_k < \bar{\delta}_k\mu_k - \gamma \tag{3.60}$$

$$\vartheta_k = \frac{1}{2}\ln\left(\frac{\underline{\delta}_k\mu_k + e_k}{\bar{\delta}_k\mu_k - e_k}\right) \tag{3.61}$$

where $0 < \gamma \ll (\bar{\delta}_0 + \underline{\delta}_0)\mu_0$ is a very small positive number.

The steady-state tracking error when ϑ_k is well controlled, i.e., $\vartheta_k \to 0$, becomes

$$e_{ss} = \lim_{k\to\infty} \mu_k\left(\frac{\lim\limits_{k\to\infty} \bar{\delta}_k - \lim\limits_{k\to\infty} \underline{\delta}_k}{2}\right) = 0 \tag{3.62}$$

From (3.62), it can be seen that the initial upper bound $\bar{\delta}_0\mu_0$ and lower bound $-\underline{\delta}_0\mu_0$ can be arbitrarily set to adjust the transient response without causing offset error in steady-state. An illustrative example of the modified convergence zone is shown in Fig. 3.21 with $\mu_0 = 5, \mu_\infty = 1, \kappa = 0.05$ and (a) $\underline{\delta}_0 = \bar{\delta}_0 = 1$; (b) $\underline{\delta}_0 = 1, \bar{\delta}_0 = 2$; (c) $\underline{\delta}_0 = 2.5, \bar{\delta}_0 = 1$.

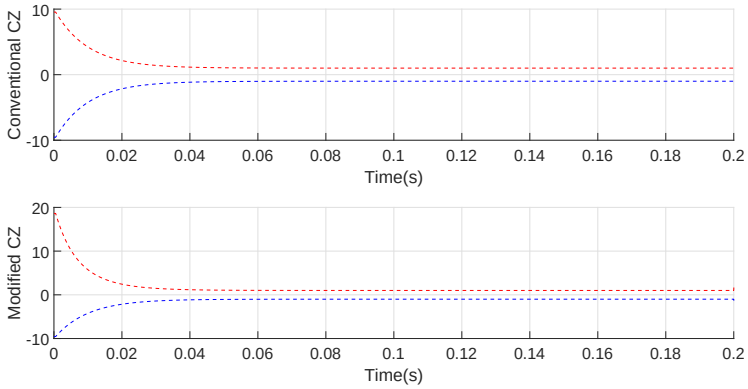

Figure 3.21: An illustrative example of the modified convergence zone

3.5.5 Control Design

Consider the following 1st order sliding variable

$$S_k = \tau_k - \lambda\tau_{k-1} + \lambda - 1 \tag{3.63}$$

where $0 < \lambda < 1$ is a design parameter, τ_k is a variable derived from the transformed error ϑ_k and defined as

$$\tau_k = \frac{\underline{\delta}_k \mu_k + e_k}{\bar{\delta}_k \mu_k - e_k} \tag{3.64}$$

By using τ_k instead of the conventional transformed error ϑ_k described in (3.61), the computation time is reduced since the logarithm function is not employed.

For any real systems, the initial tracking error e_0 is always bounded. Hence, the initial parameters $\underline{\delta}_0$, $\bar{\delta}_0$ and μ_0 which satisfy $-\underline{\delta}_0 \mu_0 + \gamma < e_0 < \bar{\delta}_0 \mu_0 - \gamma$ always exist. Then, τ_0, S_0 are bounded at time step $k = 0$. By assuming that at time instance k, the tracking error e_k satisfies $-\underline{\delta}_k \mu_k + \gamma < e_k < \bar{\delta}_k \mu_k - \gamma$ which means τ_k is bounded, the control action u_k which results in the fulfillment of the PPC at time instance $k+1$ can be obtained as following.

The one step-ahead value S_{k+1} of the sliding variable S_k is

$$S_{k+1} = \tau_{k+1} - \lambda \tau_k + \lambda - 1 \tag{3.65}$$

From (3.64) and (3.65), it yields

$$S_{k+1} = \frac{\underline{\delta}_{k+1} \mu_{k+1} + e_{k+1}}{\bar{\delta}_{k+1} \mu_{k+1} - e_{k+1}} - \lambda \tau_k + \lambda - 1 \tag{3.66}$$

where the one step-ahead tracking error e_{k+1} is computed by (2.19).

The equivalent control signal u_k^{eq} can be obtained by the following reaching law:

$$S_{k+1} = 0 \tag{3.67}$$

Substitute (2.19) and (3.66) into (3.67), a fundamental operation gives

$$y_{d,k+1} + \sum_{i=1}^{n} a_i y_{k-i+1} - \sum_{j=1}^{m} b_j u_{k-j+1} - \hat{p}_k - \tilde{p}_k - \frac{\bar{\delta}_{k+1}(\lambda \tau_k + 1 - \lambda) - \underline{\delta}_{k+1}}{\lambda \tau_k + 2 - \lambda} \mu_{k+1} = 0 \tag{3.68}$$

Since the disturbance estimation error $\tilde{p}_k$ is unknown in practice, the equivalent control signal u_k^{eq} can only be obtained by solving (3.68) with the absence of $\tilde{p}_k$. Then it results in

$$u_k^{eq} = \frac{1}{b_1} \left[y_{d,k+1} + \sum_{i=1}^{n} a_i y_{k-i+1} - \sum_{j=2}^{m} b_j u_{k-j+1} - \hat{p}_k - \frac{\bar{\delta}_{k+1}(\lambda \tau_k + 1 - \lambda) - \underline{\delta}_{k+1}}{\lambda \tau_k + 2 - \lambda} \mu_{k+1} \right] \tag{3.69}$$

The robustness of the system is improved by augmenting the control signal (3.69) with a discontinuous switching term u_k^{sw}. Consequently, the final control action is

$$u_k^{PF} = u_k^{eq} + u_k^{sw} \tag{3.70}$$

The discontinuous switching term u_k^{sw} is as in (3.7) but the switching gain K_{sw} in this case must satisfy

$$K_{sw}^{min} < K_{sw} < K_{sw}^{max} \tag{3.71}$$

with

$$K_{sw}^{min} = \epsilon + \gamma \tag{3.72}$$

$$K_{sw}^{max} = \frac{\mu_\infty(1-\lambda)}{\lambda\frac{(\bar{\delta}_0+\underline{\delta}_0)\mu_0-\gamma}{\gamma} + (2-\lambda)} \tag{3.73}$$

As a result, the final control action is

$$u_k = \frac{1}{b_1}\left[y_{d,k+1} + \sum_{i=1}^{n} a_i y_{k-i+1} - \sum_{j=2}^{m} b_j u_{k-j+1} - \hat{p}_k - \frac{\bar{\delta}_{k+1}(\lambda\tau_k + 1 - \lambda) - \underline{\delta}_{k+1}}{\lambda\tau_k + 2 - \lambda}\mu_{k+1}\right] + \frac{1}{b_1}K_{sw}sign(S_k) \tag{3.74}$$

Theorem 3.3: Given the discrete time uncertain system (2.1) with the sliding variable (3.63). If the control action (3.74) is used and the initial parameters μ_0, $\underline{\delta}_0$, $\bar{\delta}_0$ are chosen such that $-\underline{\delta}_0\mu_0+\gamma < e_0 < \bar{\delta}_0\mu_0-\gamma$, the sliding variable S_k will be driven to a bounded QSMB in finite time and stay within this band afterward. The tracking error e_k always fulfills the requirement of the PPC described by (3.60) for all $k > 0$. The QSMB is defined as:

$$L = \{\tau_k : QSMB_N < S_k < QSMB_P\} \tag{3.75}$$

where $QSMB_P$ and $QSMB_N$ are the upper and lower bounds of the QSMB and described by

$$QSMB_N = \frac{-2K_{sw}\Theta_k^2}{\Gamma_k + 2K_{sw}\Theta_k} \tag{3.76}$$

$$QSMB_P = \frac{2K_{sw}\Theta_k^2}{\Gamma_k - 2K_{sw}\Theta_k} \tag{3.77}$$

, respectively. In which,

$$\Theta_k = (\lambda\tau_k + 2 - \lambda) \tag{3.78}$$

Proof of Theorem 3.3: First, let us prove that at any time instance k, if the tracking error e_k satisfies $-\underline{\delta}_k\mu_k + \gamma < e_k < \bar{\delta}_k\mu_k - \gamma$, then by using the proposed control action (3.74), the one step ahead tracking error e_{k+1} also satisfies the requirement of the PPC, i.e., $-\underline{\delta}_{k+1}\mu_{k+1} + \gamma < e_{k+1} < \bar{\delta}_{k+1}\mu_{k+1} - \gamma$, which means τ_{k+1} and u_{k+1} are also bounded. Hence, the control algorithm can be repeated in the next sampling cycle.

By substituting the control action (3.74) into (2.19), a fundamental operation gives

$$e_{k+1} = \frac{\xi_{1,k}\tau_k + \xi_{2,k}}{\lambda\tau_k + 2 - \lambda} - [\tilde{p}_k + K_{sw}sign(S_k)] \tag{3.79}$$

where $\xi_{1,k}$ and $\xi_{2,k}$ are defined as

$$\xi_{1,k} = \bar{\delta}_{k+1}\mu_{k+1}\lambda \tag{3.80}$$

$$\xi_{2,k} = \left[\bar{\delta}_{k+1}(1-\lambda) - \underline{\delta}_{k+1}\right]\mu_{k+1} \tag{3.81}$$

From (3.71), it can be derived that

$$\gamma - 2K_{sw} < -\{\tilde{p}_k + K_{sw}sign(S_k)\} < 2K_{sw} - \gamma \tag{3.82}$$

Since $-\underline{\delta}_k\mu_k + \gamma < e_k < \bar{\delta}_k\mu_k - \gamma$ holds in this step, it follows from (3.64) that

$$\frac{\gamma}{(\bar{\delta}_0 + \underline{\delta}_0)\mu_0 - \gamma} < \tau_k < \frac{(\bar{\delta}_0 + \underline{\delta}_0)\mu_0 - \gamma}{\gamma} \tag{3.83}$$

which results in

$$K_{sw}^{max} = \frac{\mu_\infty(1-\lambda)}{\lambda\frac{(\bar{\delta}_0+\underline{\delta}_0)\mu_0-\gamma}{\gamma} + (2-\lambda)} < \frac{\mu_\infty(1-\lambda)}{\lambda\tau_k + 2 - \lambda} \tag{3.84}$$

Then, from (3.82) and (3.84), it gives

$$\gamma - \frac{2\mu_\infty(1-\lambda)}{\lambda\tau_k + 2 - \lambda} < -\{\tilde{p}_k + K_{sw}sign(S_k)\} < \frac{2\mu_\infty(1-\lambda)}{\lambda\tau_k + 2 - \lambda} - \gamma \tag{3.85}$$

From (3.79) and (3.85), it yields

$$e_{k+1} < \frac{\xi_{1,k}\tau_k + \xi_{2,k} + 2\mu_\infty(1-\lambda)}{\lambda\tau_k + 2 - \lambda} - \gamma \tag{3.86}$$

Consider the first term of the right hand side of (3.86) as a function of τ_k. It can easily be realized that this term is monotonic increasing with respect to τ_k. Hence,

$$e_{k+1} < \lim_{\tau_k \to \infty} \frac{\xi_{1,k}\tau_k + \xi_{2,k} + 2\mu_\infty}{\lambda\tau_k + 2 - \lambda} - \gamma = \bar{\delta}_{k+1}\mu_{k+1} - \gamma \tag{3.87}$$

Similarly, from (3.79) and (3.85), it also yields

$$e_{k+1} > \frac{\xi_{1,k}\tau_k + \xi_{2,k} - 2\mu_\infty(1-\lambda)}{\lambda\tau_k + 2 - \lambda} + \gamma \tag{3.88}$$

Since the first term of the right hand side of (3.88) is also monotonic increasing with respect to τ_k, it can be deduced that

$$e_{k+1} > \lim_{\tau_k \to 0} \frac{\xi_{1,k}\tau_k + \xi_{2,k} - 2\mu_\infty(1-\lambda)}{\lambda\tau_k + 2 - \lambda} + \gamma \tag{3.89}$$

$$= \frac{\xi_{2,k} - 2\mu_\infty(1-\lambda)}{2 - \lambda} + \gamma \tag{3.90}$$

Adding both sides of (3.90) with $\underline{\delta}_{k+1}\mu_{k+1}$, a fundamental operation gives

$$e_{k+1} + \underline{\delta}_{k+1}\mu_{k+1} > \frac{\{(\bar{\delta}_{k+1} + \underline{\delta}_{k+1})\mu_{k+1} - 2\mu_\infty\}(1-\lambda)}{2 - \lambda} + \gamma \tag{3.91}$$

Due to $\bar{\delta}_{k+1} \geq 1$, $\underline{\delta}_{k+1} \geq 1$, $\mu_{k+1} \geq \mu_\infty$ and $0 < \lambda < 1$, the first term of the right hand side of (3.91) is always positive, then it yields

$$e_{k+1} > -\underline{\delta}_{k+1}\mu_{k+1} + \gamma \tag{3.92}$$

From (3.87) and (3.92), it can be concluded that

$$-\underline{\delta}_{k+1}\mu_{k+1} + \gamma < e_{k+1} < \bar{\delta}_{k+1}\mu_{k+1} - \gamma \tag{3.93}$$

Due to the fact that the initial tracking error e_0 is always bounded in practice, the initial parameters μ_0, $\underline{\delta}_0$ and $\bar{\delta}_0$ can always be found such that the inequality $-\underline{\delta}_0\mu_0 + \gamma < e_0 < \bar{\delta}_0\mu_0 - \gamma$ holds. By using the same manipulation as described above, it can be deduced that the tracking error in the next sampling cycle e_1 is also restricted in the convergence zone, i.e., $-\underline{\delta}_1\mu_1 + \gamma < e_1 < \bar{\delta}_1\mu_1 - \gamma$, and so on. As long as the requirement of the PPC is fulfilled, τ_k is uniformly bounded by (3.83). This means the control action u_k is also uniformly bounded. Therefore, the algorithm can be repeated in every sampling cycle which results

in the fulfillment of the PPC (3.60) $\forall k > 0$. As a result, the transformed error ϑ_k is always well defined.

Sine (3.83) holds $\forall k > 0$, it can be deduced that Θ_k defined in (3.78) is also positive and uniformly bounded by (3.94).

$$\Theta_{min} < \Theta_k < \Theta_{max}, \forall k > 0 \tag{3.94}$$

where Θ_{min} and Θ_{max} are described by

$$\Theta_{min} = \lambda \frac{\gamma}{(\bar{\delta} + \underline{\delta})\mu_0 - \gamma} + 2 - \lambda \tag{3.95}$$

$$\Theta_{max} = \lambda \frac{(\bar{\delta} + \underline{\delta})\mu_0 - \gamma}{\gamma} + 2 - \lambda \tag{3.96}$$

Substitute (2.19), (3.69) and (3.70) into (3.66), it gives

$$S_{k+1} = \frac{-(\tilde{p}_k + b_1 u_k^{sw})\Theta_k^2}{\Gamma_k + (\tilde{p}_k + b_1 u_k^{sw})\Theta_k} \tag{3.97}$$

where Γ_k is defined as

$$\Gamma_k = (\bar{\delta}_{k+1} + \underline{\delta}_{k+1})\mu_{k+1} \tag{3.98}$$

Then, from (3.70) and (3.97), it yields

$$S_{k+1} = \frac{-\{\tilde{p}_k + K_{sw} sign(S_k)\}\Theta_k^2}{\Gamma_k + \{\tilde{p}_k + K_{sw} sign(S_k)\}\Theta_k} \tag{3.99}$$

Case 1: If $S_k > 0$, then

$$S_{k+1} = \frac{-\Theta_k^2 \chi_1}{\Theta_k \chi_1 + \Gamma_k} \tag{3.100}$$

where χ_1 is defined as

$$\chi_1 = \tilde{p}_k + K_{sw} \tag{3.101}$$

From (3.71), it can be derived that

$$\gamma < \chi_1 < 2K_{sw} \tag{3.102}$$

Since (3.100) is monotonic decreasing with respect to χ_1, it yields

$$\frac{-2K_{sw}\Theta_k^2}{\Gamma_k + 2K_{sw}\Theta_k} < S_{k+1} < \frac{-\gamma\Theta_k^2}{\Gamma_k + \gamma\Theta_k} < 0 \tag{3.103}$$

Case 2: If $S_k < 0$, then

$$S_{k+1} = \frac{\Theta_k^2 \chi_2}{-\Theta_k \chi_2 + \Gamma_k} \tag{3.104}$$

where χ_2 is defined as

$$\chi_2 = K_{sw} - \tilde{p}_k \tag{3.105}$$

From (3.71), it can be seen that

$$\gamma < \chi_2 < 2K_{sw} \tag{3.106}$$

Again, since (3.104) is monotonic increasing with respect to χ_2, it can be deduced that

$$\frac{2K_{sw}\Theta_k^2}{\Gamma_k - 2K_{sw}\Theta_k} > S_{k+1} > \frac{\gamma\Theta_k^2}{\Gamma_k - \gamma\Theta_k} > 0 \tag{3.107}$$

From (3.103) and (3.107), it yields

$$\frac{-2K_{sw}\Theta_k^2}{\Gamma_k + 2K_{sw}\Theta_k} < S_{k+1} < \frac{2K_{sw}\Theta_k^2}{\Gamma_k - 2K_{sw}\Theta_k} \tag{3.108}$$

From (3.93) and (3.108), it can be concluded that the sliding variable S_k will approach the bounded QSMB (3.75) in one step and stay inside this band afterward. The tracking error always meets the requirement (3.60) of the PPC. This ends the proof.

3.5.6 Experimental Results

To confirm the validity of the proposed method, experiments on the piezo-actuated positioning system are conducted. The parameters of the controller are shown in Table. 3.1.

The transient response of the system is first investigated by employing a STEP reference output where its value is suddenly changed from 0µm to 5µm. By using the modified convergence zone described by (3.60) with $\underline{\delta}_0 = 1$ and $\bar{\delta}_0 = 2$, both overshoot and offset error no longer exist as seen in Fig. 3.22. The sliding variable S_k also stays within the bounded QSMB. The maximum tracking error (MAXTE) and the root mean square tracking error (RMSTE) in steady-state are 0.02µm and 0.012µm, corresponding to 0.4% and 0.24%of the maximal set-point.

Table 3.1: Parameters of the PPF-DSMC controller

Symbol	Quantity	Value
μ_0	Initial value of the PPF	10.0
μ_∞	Final value of the PPF	0.5
$\bar{\delta}_0$	Initial value of the upper bound	2.0
$\underline{\delta}_0$	Initial value of the lower bound	1.0
λ	Damping factor of the tracking error	0.1
κ	Damping factor of the PPF	0.05
K_{sw}	Switching gain of the DSMC	0.02
T_s	Sampling time	0.5ms

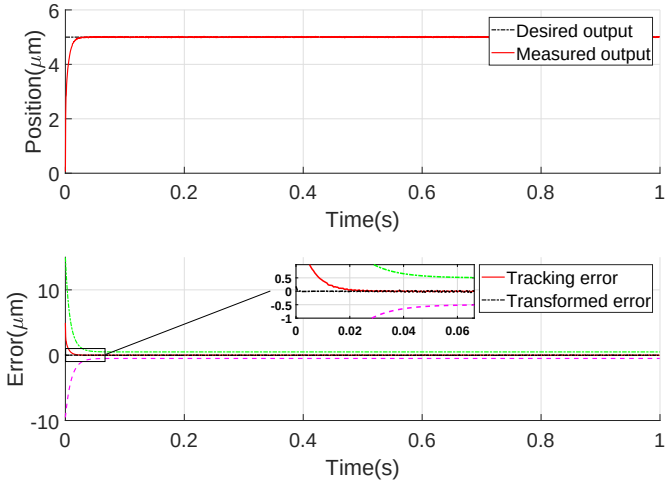

Figure 3.22: Step response of the PPF-DSMC

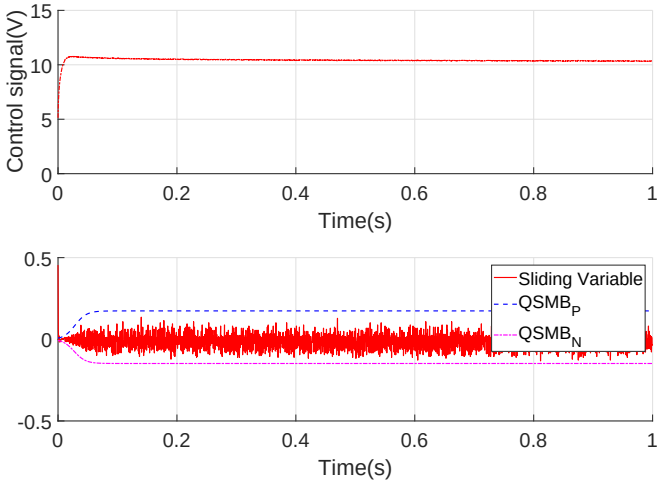

Figure 3.23: The control signal of PPF-DSMC with step desired output

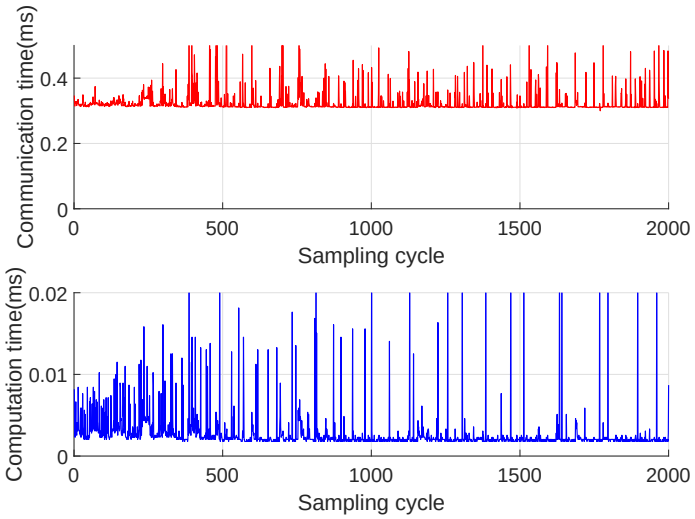

Figure 3.24: The computation time of the PPF-DSMC

The influences of the upper bound $\bar{\delta}$ and lower bound $\underline{\delta}$ of the conventional convergence zone on the transient response of the closed-loop system are shown in Fig. 3.25. As seen in Fig. 3.25(b) where $\bar{\delta} = 1$, $\underline{\delta} = 1.4$ and Fig. 3.25(c) where $\bar{\delta} = 1.6$, $\underline{\delta} = 1$, the overshoot may be increased or avoided if $\bar{\delta} \neq \underline{\delta}$. However, the offset errors always exist in these cases as analyzed in (3.55). In contrast, (3.62) and Fig. 3.26 show that by using the same parameters with the

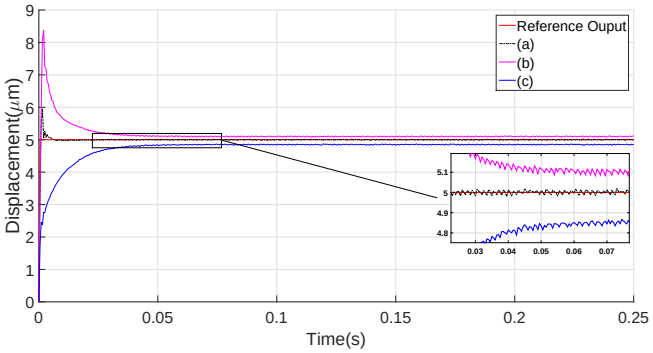

Figure 3.25: Influences of conventional PPF on transient response

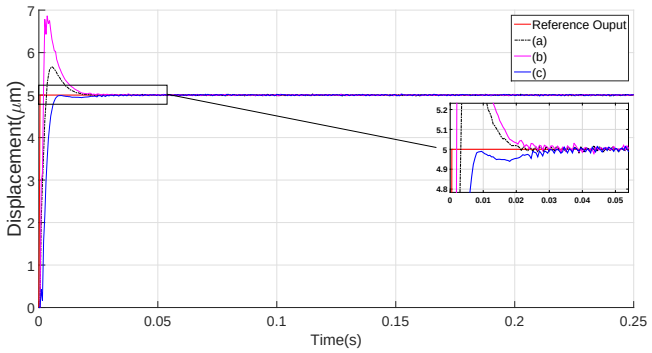

Figure 3.26: Influences of modified PPF on transient response

modified convergence zone, the transient response of the system can be freely adjusted without producing the offset error in the steady-state. In addition, by appropriately selecting the initial values $\bar{\delta}_0$ and $\underline{\delta}_0$, a good transient response can be achieved as seen in Fig. 3.26(c).

In order to investigate the tracking performance of the proposed method, various complicated desired outputs are employed. Figure 3.27 shows the experimental result in which a sinusoidal reference output $y_d = (4 - kT_s)\sin[2\pi(1 + 10kT_s)kT_s - \pi/2] + 5$ with time-varying amplitude and frequency is used. The experimental result with complicated multiple frequencies desired output $y_d = 0.5\cos(2\pi 5kT_s) + 1.5\sin(2\pi 10kT_s) + 0.7\cos(2\pi 25kT_s) + 1.3\cos(2\pi 30kT_s) + 6$ is also shown in Fig. 3.29. In both cases, the closed-loop systems have good transient responses and the RMSTEs at steady-state are less than 0.1µm corresponding to

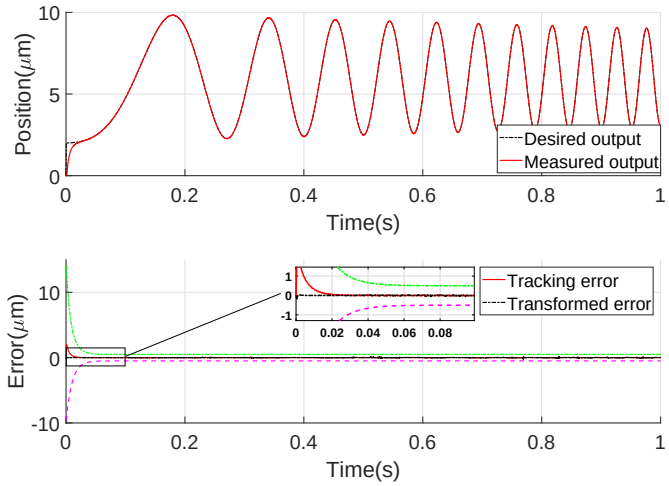

Figure 3.27: Tracking performance of PPF-DSMC with time-varying amplitude and frequency desired output

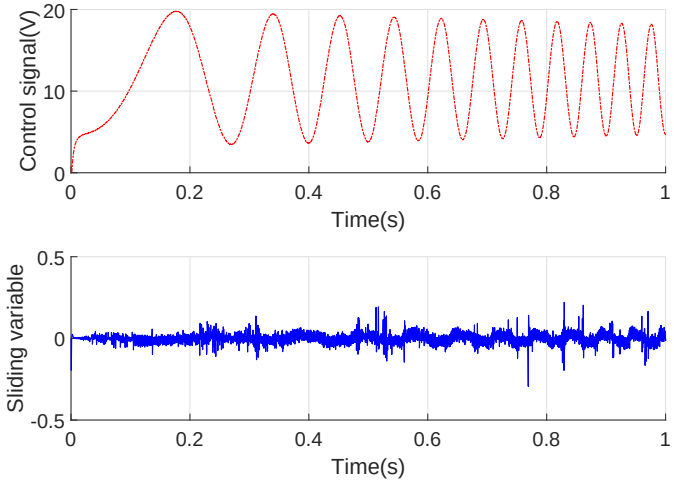

Figure 3.28: The control signal of PPF-DSMC with time-varying amplitude and frequency desired output

1% of the maximal set point.

The proposed method is also compared with the widely used PID controller

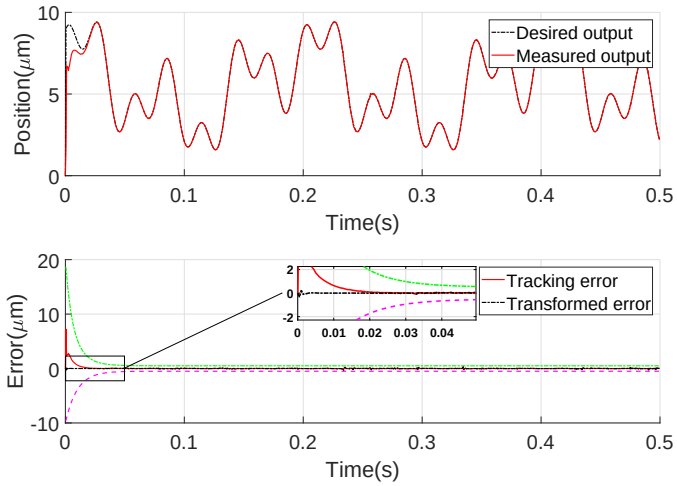

Figure 3.29: Tracking performance of PPF-DSMC with multiple frequency desired output

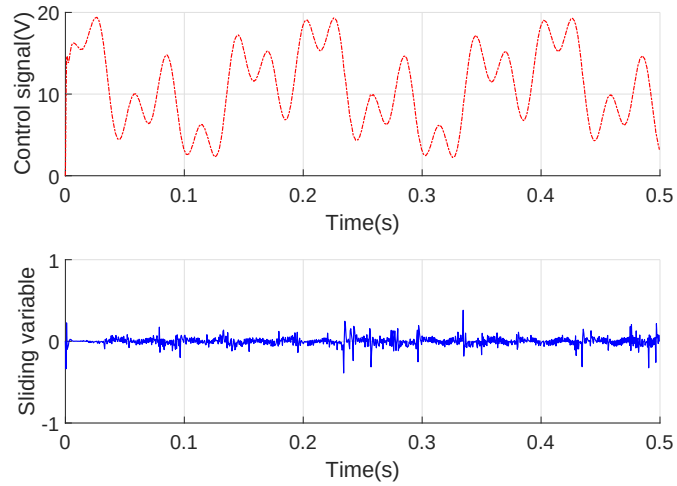

Figure 3.30: The control signal of PPF-SMC with multiple frequency desired output

in term of tracking accuracy. The discrete-time PID controller is described by

$$u_k^{PID} = u_{k-1}^{PID} + K_P(e_k - e_{k-1}) + K_I e_{k-1} + K_D(e_k - 2e_{k-1} + e_{k-2}) \qquad (3.109)$$

A sinusoidal desired output $y_d = \{4\sin(2\pi f k T_s - \pi/2) + 6\}$ is employed to get the comparative results at different frequencies f. After being well tuned, the best

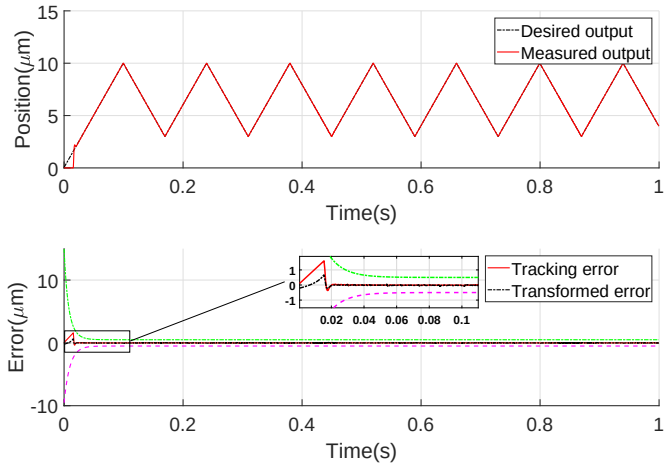

Figure 3.31: Tracking performance of PPF-DSMC with sawtooth desired output

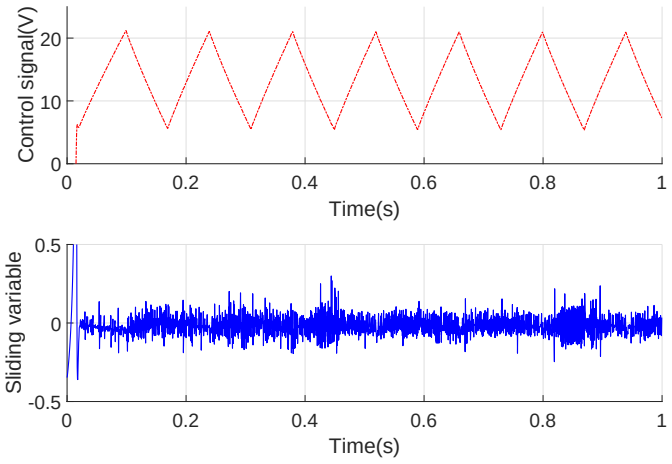

Figure 3.32: The control signal of PPF-SMC with sawtooth desired output

experimental results of the PID controller are achieved with $K_P = 0.1$, $K_I = 0.75$ and $K_D = 1$. The comparative results of both methods are shown in Fig. 3.33. In can be observed that both PID and the proposed method show very good tracking performance at 1Hz where the MAXTE is less than 0.02µm corresponding to 0.2% of the maximal set point. As the tracking frequency increases, the performance of the proposed method is just slightly degraded. In contrast, the PID shows much worse tracking error.

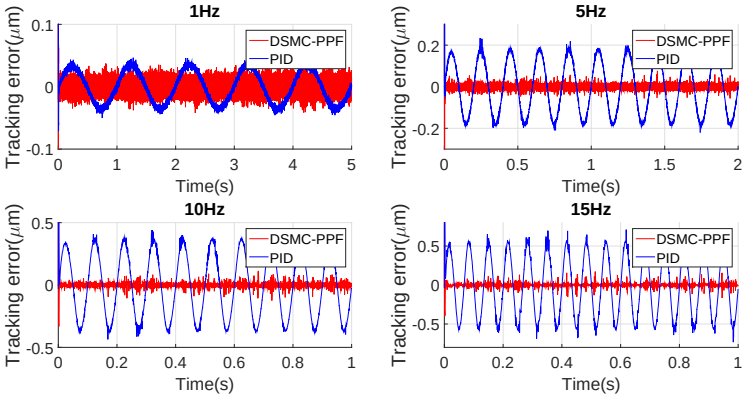

Figure 3.33: Comparative results between PID and PPF-DSMC

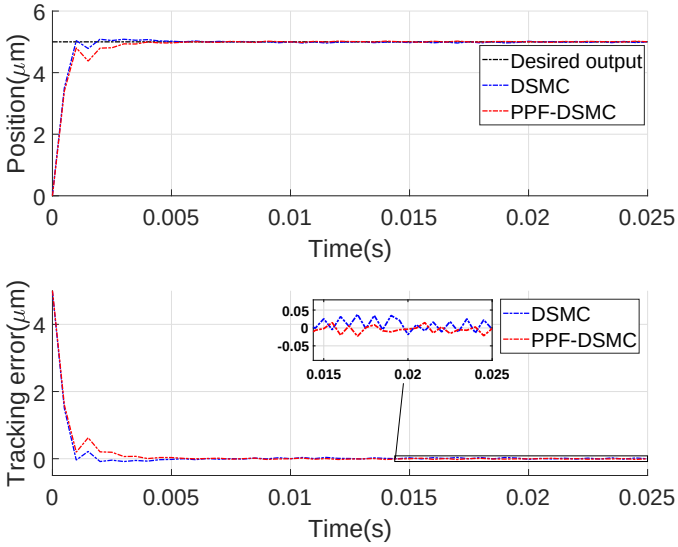

Figure 3.34: Comparative step responses between the proposed PPF-DSMC and the conventional DSMC

The comparative experiment results between the PPF-DSMC and the conventional DSMC are also provided in Fig. 3.34 and Fig. 3.35. As the parameters are chosen such that same transient response can be achieved as seen in Fig. 3.34, the proposed PPF-DSMC shows better tracking performance in term of tracking accuracy as observed in Fig. 3.35. This result comes from additional parameters of the PPF which allows the transient response to be adjusted independently

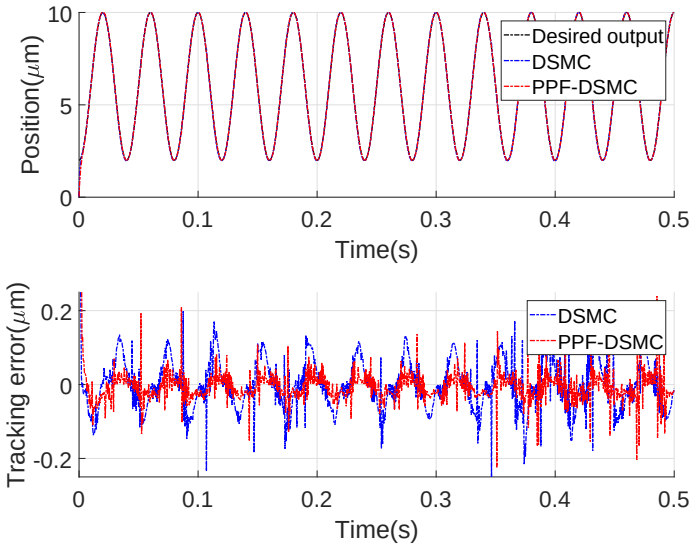

Figure 3.35: Comparative tracking performances between the proposed PPF-DSMC and the conventional DSMC

from the steady-state performance.

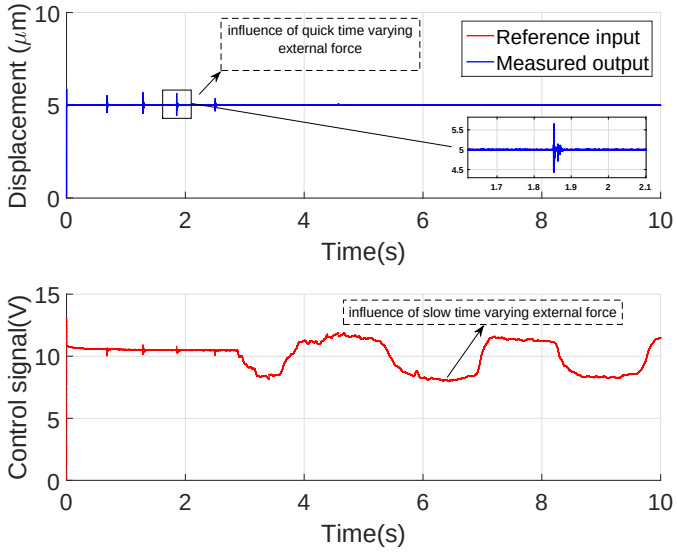

Figure 3.36: Tracking performance under influence of external force

Finally, the robustness of the positioning system is tested by using an external force where the system is impacted by quick time-varying forces from 0s∼3s and by slow time-varying external force from 3s∼10s. As shown in Fig. 3.36, the system is immune from the slow time-varying external force. When impacted by the quick time-varying forces, the system output quickly returns to its desired value. This means the robustness of the DQSMC against the uncertainties is preserved.

3.6 Conclusion

In this chapter, SMC - one of the most well known robust control technique - is employed to handle the nonlinear behavior of the piezo-actuated positioning system. The designs with conventional DSMC and DISMC are presented first. Experimental results are also conducted to confirm the validity as well as investigate the tracking performance of the positioning system. Experimental results show that the transient response and steady-state tracking performance are intimately connected. If the parameter is adjusted to achieve quick response and low tracking error, then the overshoot always occurs. In contrast, a smooth transient response always yields higher tracking error.

To deal with the above mentioned problem, a novel prescribed performance DSMC is proposed in the last section of this chapter. This novel method is capable of maintaining the tracking error in a predefined area under certain initial conditions. Additional parameters are also useful in adjusting the transient-state of the control system without degrading the tracking performance.

Chapter 4

Fractional Order Control Design

4.1 Introduction

Recently, the fractional order calculus, which is a generalization of the integration and differentiation from integer to non-integer order, has become an interesting topic and extensively used in the area of control system [15, 24, 75]. In comparison with the conventional controllers based on integer order integrator and differentiator, the fractional order controller offers more degree of freedom which can be utilized to further improve the performance of the control system. In [67], a review of fractional order PID controller including basic definitions, control design and tuning techniques are presented. The integration of the fractional control into sliding mode control (SMC) for anti-lock breaking and position servo systems are discussed in [71, 73], respectively. This integration utilizes both robustness of SMC and the good performance of fractional dynamic. However, most of those researches are conducted in continuous time domain. The designs in discrete-time domain have not been well investigated yet. Hence, this chapter focuses on discrete-time fractional order controllers including fractional $PI^{\alpha}D^{\beta}$ and fractional order integral sliding mode control (DFISMC).

4.2 Contributions

There are three main contributions in this chapter. First, a new method is proposed to approximate the fractional order integral (FOI) recursively which can easily be implemented in digital controllers. Then, the fractional order $PI^{\alpha}D^{\beta}$ controller with parameters optimized by particle swarm optimization (PSO) is investigated. Specifically, the PSO runs with the real system instead of a mathematical model following that the influence of modeling error is mitigated and the getting result can be used directly without any further calibrations. Finally, a DFISMC with improved transient-response based on fuzzy tuning is presented.

4.3 Fractional Order Calculus

In this section, the definitions which are widely used in the area of control system are introduced.

First, the gamma function $\Gamma(z)$ which is the extension of the factorial for non-integer number z is introduced

$$\Gamma(z) = \int_0^{\infty} e^{-t} t^{z-1} dt \tag{4.1}$$

The most important property of the gamma function is

$$z\Gamma(z) = \Gamma(z+1) \tag{4.2}$$

Then, the definition of derivative of order $\beta \in \Re$ is presented. In continuous-time domain, the most often used one is the *Riemann-Liouville* definition

$${}_{t_0}^{\beta}D_t e(t) = \frac{1}{\Gamma(n-\beta)} \frac{d^n}{dt^n} \int_{t_0}^{t} \frac{e(\tau)}{(t-\tau)^{\beta-n+1}} d\tau \tag{4.3}$$

where t_0 and t are the limits and n is an integer number satisfying $n-1 < \beta < n$. In practical applications where computer-based control devices are used,

the following *Grünwald – Letnikov* definition with *short memory principle* is preferred:

$$ {}_{t_0}^{\beta}D_t e(t) = T_s^{-\beta} \sum_{j=0}^{\left[\frac{t-t_0}{T_s}\right]} (-1)^j \binom{\beta}{j} e(t - jT_s) \tag{4.4} $$

in which [.] means the integer part, T_s is the sampling time and $\binom{\beta}{j}$ is the binomial coefficient defined by

$$ \binom{\beta}{j} = \frac{\Gamma(\beta + 1)}{\Gamma(j + 1)\Gamma(\beta - j + 1)} \tag{4.5} $$

The responses of the fractional order differential (FOD) with various orders β are illustrated in Fig. 4.1. As β decreases, the response of the FOD is smoothen which may reduce the sensitive of the FOD-based controllers to the noise.

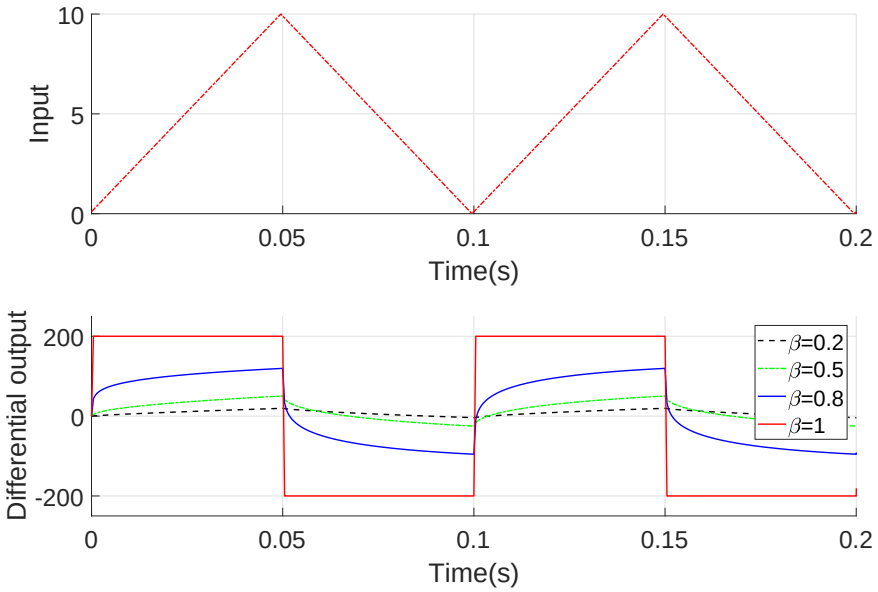

Figure 4.1: Response of FOD with various fractional order β

Finally, the *Riemann-Liouville's definition* for the fractional integral of order $\alpha \in \Re$ of a continuous time function $e(t)$ is

$$ {}^{\alpha}\zeta e(t) = \frac{1}{\Gamma(\alpha)} \int_0^t (t - \tau)^{(\alpha-1)} e(\tau) d\tau \tag{4.6} $$

The simulative step responses of the FOI with various fractional order α are shown in Fig. 4.2. On the contrary to the FOD, the FOI shows stronger influence on the transient response as the fractional order α decreases which may cause fluctuations in transient-state.

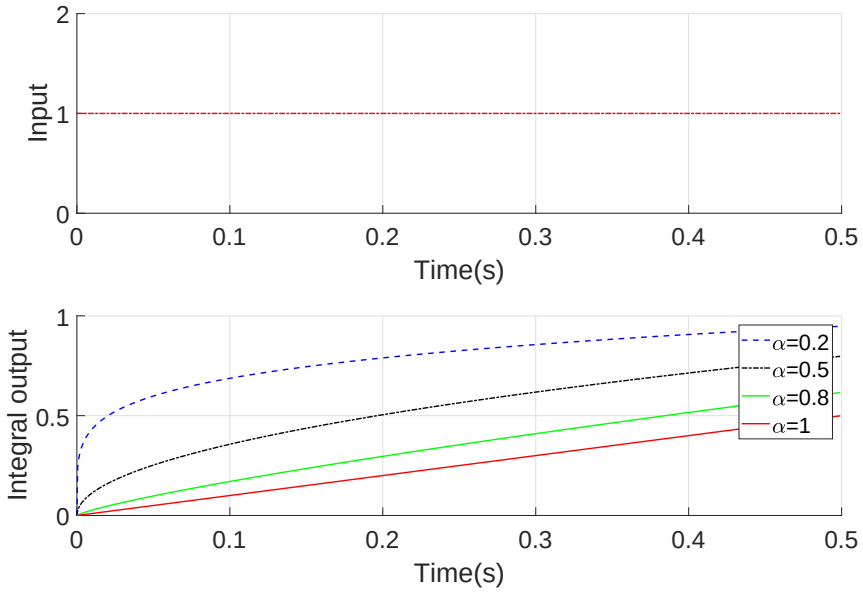

Figure 4.2: Step response of FOI with various fractional orders

In *math.h* library of *C* compiler, the gamma function $\Gamma(z)$ is already supported. The syntax of this function is

$$float \quad tgamma \quad (float \quad z) \tag{4.7}$$

In contrast, FOI is not supported in C compiler. Hence, in order to implement this integration in digital control systems, numerical approximation is needed.

Dividing the interval $(0, t)$ into $k = t/T_s$ sub-intervals, the integral of $e(t)$ can be decomposed into the sum of k integrals

$${}^{\alpha}\zeta e(t) = \frac{1}{\Gamma(\alpha)} \sum_{j=1}^{k} \int_{jT_s}^{(j+1)T_s} (t-\tau)^{\alpha-1} e(\tau) d\tau \tag{4.8}$$

Assume that T_s is sufficient small such that e is constant inside each sub-interval. Then, it yields

$$ {}^{\alpha}\zeta e(t) \approx^{\alpha} \zeta_{e,k} = \frac{1}{\Gamma(\alpha)} \sum_{j=1}^{k} e_j \int_{jT_s}^{(j+1)Ts} (t-\tau)^{\alpha-1} d\tau \tag{4.9} $$

following that

$$ {}^{\alpha}\zeta_{e,k} = \sum_{j=1}^{k} \left[(k-j+1)^{\alpha} - (k-j)^{\alpha} \right] \frac{T_s^{\alpha}}{\alpha\Gamma(\alpha)} e_j \tag{4.10} $$

By using (4.2) and (4.10), it gives

$$ {}^{\alpha}\zeta_{e,k} = \sum_{j=1}^{k} \omega_j e_j \tag{4.11} $$

where $\omega(j)$ is the weighting factor:

$$ \omega_j = \left[(k-j+1)^{\alpha} - (k-j)^{\alpha} \right] \frac{T_s^{\alpha}}{\Gamma(\alpha+1)} \tag{4.12} $$

It can be realized from (4.11) that the FOI is different from its integer counterpart by the weighting factors ω_j in which the weighting factors of new data are larger than of the old data. Since (4.11) can not be implemented directly in practice due to its infinite sample data, an approximation based on finite data length $(t-L, t)$ is proposed in [49] where L is the length of memory. This approximation is based on the observation that for large data, the weighting factors of old data are small enough to be ignored. However, the output of this approximation may be saturated due to the fact that the sum of a finite data set is bounded which prevents the FOI-based controllers from steady-state error compensation as its integer-based counterpart. Hence, this paper proposes a new method to compute the FOI recursively as following.

Denote ${}^{\alpha}\zeta_{e,k-1}$ as the FOI of e_k in previous step. Then, based on (4.10), it gives

$$ {}^{\alpha}\zeta_{e,k} = \omega_1 e_1 + \omega_2 e_2 + \cdots + \omega_{k-1} e_{k-1} + \omega_k e_k \tag{4.13} $$

$$ {}^{\alpha}\zeta_{e,k-1} = \omega_2 e_1 + \omega_3 e_2 + \cdots + \omega_k e_{k-1} \tag{4.14} $$

From (4.13) and (4.14), it yields

$$ {}^{\alpha}\zeta_{e,k} = {}^{\alpha}\ \zeta_{e,k-1} + \sum_{j=2}^{k} \omega_j \tilde{e}_j + \omega_1 e_1 \tag{4.15} $$

with $\tilde{e}_j = e_j - e_{j-1}$. Now, by applying the *short memory principle* to (4.15), it results in

If $k < N$ where $N = \left[\frac{L}{T_s}\right]$ is the number of considered samples data, then

$$ {}^{\alpha}\zeta_{e,k} = {}^{\alpha}\ \zeta_{e,k-1} + \sum_{j=N-k+2}^{N} \Omega_j \tilde{e}_{k-N+j} + \Omega_{N-k+1} e_1 \tag{4.16} $$

If $k \geq N$, then

$$ {}^{\alpha}\zeta_{e,k} = {}^{\alpha}\ \zeta_{e,k-1} + \sum_{j=2}^{N} \Omega_j \tilde{e}_{k-N+j} + \Omega_1 e_{k-N+1} \tag{4.17} $$

with

$$ \Omega_j = \left[(N-j+1)^{\alpha} - (N-j)^{\alpha}\right] \frac{T_s^{\alpha}}{\Gamma(\alpha+1)} \tag{4.18} $$

The simulative response of the proposed approximation with unit step and exponential inputs are shown in Fig. 4.3 and Fig. 4.4, respectively. It can be realized that the proposed FOI is actually a hybrid of the exact FOI (4.15) and the conventional integer order integral. This approximation exactly reflects the behavior of the FOI in first N step and acts like an integer order integral after that. Which means the controllers based on this proposed FOI is able to improved the transient response while maintaining the steady-state error compensation ability. In contrast, the output of the method in [49] is either saturated with unit step input or slowly increasing with exponential input, which obviously affects the steady-state error compensation ability.

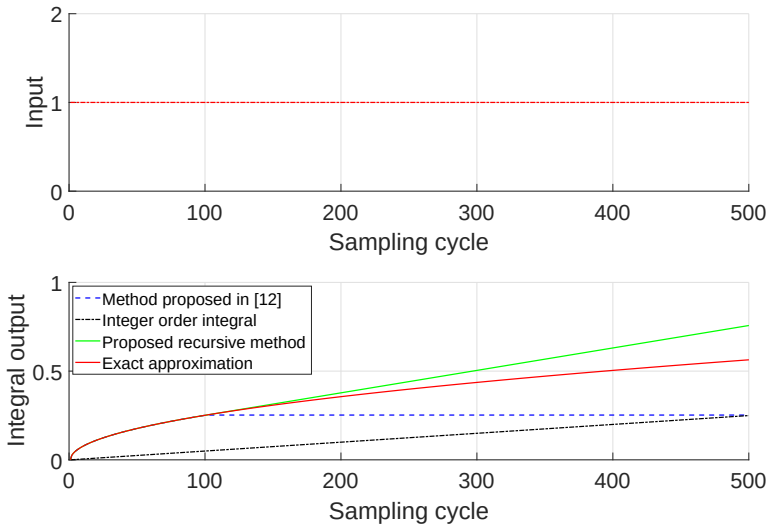

Figure 4.3: Behavior of the proposed FOI approximation with unit step input and $N = 100$

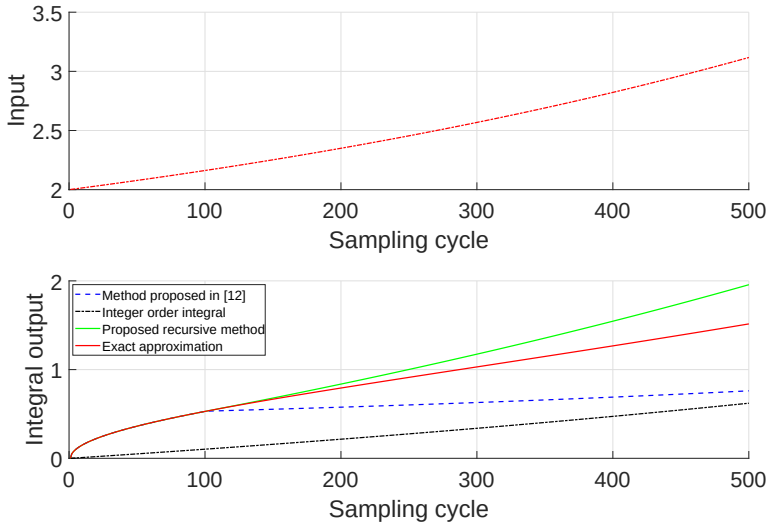

Figure 4.4: Behavior of the proposed FOI with $input = 1 + e^{3t}$ and $N = 100$

4.4 Discrete-Time Fractional Order $PI^{\alpha}D^{\beta}$ with Particle Swarm Optimization Tuning

4.4.1 Introduction

In continuous-time case, the systematical design of the fractional order $PI^{\alpha}D^{\beta}$ has been introduced in many researches, in both frequency [16, 48, 56, 76, 89, 93] and time domain [60]. Besides, optimization techniques such as PSO [63, 92] or genetic algorithm (GA) [36] are also good solutions for tuning the parameters of the controller. However, these optimization techniques require a quite good model and the algorithm runs off-line with the mathematical model in most cases. Since the modeling error always exists, especially with uncertain model like piezo-actuated positioning system, further tuning is also needed to apply the parameters getting from the optimization process to experiment. To overcome the aforementioned problem, this section presents a new approach to get the optimal parameters of the discrete-time fractional order $PI^{\alpha}D^{\beta}$ controller. The algorithm is based on PSO technique and developed for piezo-actuated system only. The main concept of the optimization is based on the observation that the fractional order $PI^{\alpha}D^{\beta}$ can also be regarded as a model-free controller since the parameters of the control plant are not included in the control signal. Consequently, the PSO can run on-line with real system instead of the mathematical model. To protect the system from instability during optimization process, a safe zone which can easily be obtained by experiments is required. The result getting from this optimization process is optimal for real system and can be used directly without any further adjustments.

4.4.2 Discrete-Time Fractional Order $PI^{\alpha}D^{\beta}$ Investigation

Consider the following discrete-time $PI^{\alpha}D^{\beta}$ controller of fractional order α and β:

$$u_k^{fPID} = u_k^p + u_k^{fI} + u_k^{fD} \tag{4.19}$$

with

$$u_k^p = K_P e_k \tag{4.20}$$

$$u_k^{fI} = u_{k-1}^{fI} + K_I \left[\sum_{j=N-k+2}^{N} \Omega_j \tilde{e}_{k-N+j} + \Omega_1 e_{k-N+1} \right] \tag{4.21}$$

$$u^{fD} = \frac{K_D}{T_s^\beta} \sum_{j=0}^{N} (-1)^j \binom{\beta}{j} e(t-N) \tag{4.22}$$

$$\Omega_j = \left[(N-j+1)^\alpha - (N-j)^\alpha \right] \frac{T_s^\alpha}{\Gamma(\alpha+1)} \tag{4.23}$$

and K_P, K_I, K_D are positive proportional, integral and differential gain, respectively. By using "trial and error" technique, several experiment results are achieved to investigate the influences of the fractional order on the response of the control system. In these experiments, the parameters of the PID controller are intentionally chosen such that the closed-loop system is closed to the verge of instability. In this case, the change of parameters has strong influence on the system response and can be seen clearly.

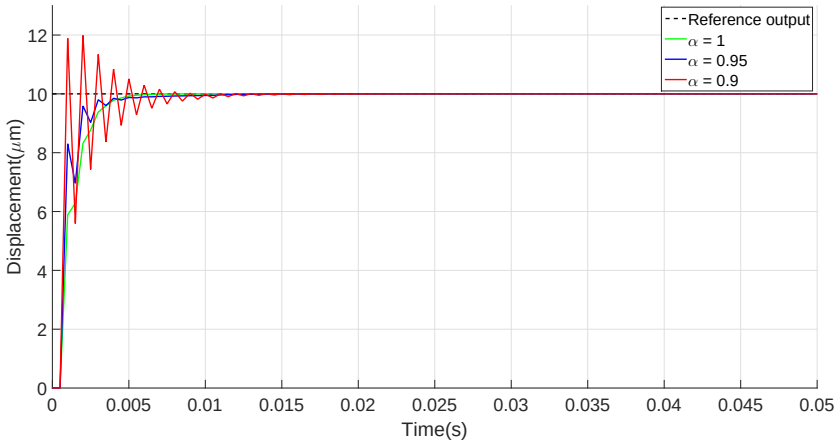

Figure 4.5: Influence of fractional order integral α

The influence of the fractional order integral α to the transient state is shown in Fig. 4.5. It can be seen that as α decrease, the system response tends to be faster. However, the amplitude of oscillation also increases and the system may be unstable if α is too small.

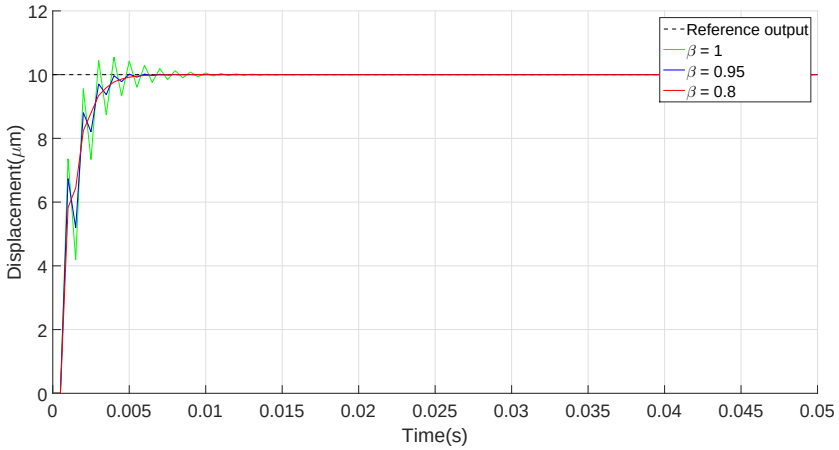

Figure 4.6: Influence of fractional order β

The influence of fractional order β in transient-state is shown in Fig. 4.6. As can be observed, the decrement of β leads to the reduction of the oscillation amplitude which results in an improved transient response.

4.4.3 PSO Implementation

PSO is a population-based evolutionary algorithm [37] developed based on the behavior of social animals. The basic PSO algorithm is introduced in [52] in detail. This sub-section only shows the implementation of the PSO to on-line optimize the parameters of the fractional order controller (4.19). The performance index which needs to be minimized in this case is the integral of time multiplied by absolute value of the error (ITAE)

$$ITAE(t) = \int_0^{\infty} t|e(t)|dt \tag{4.24}$$

The discrete-time version of (4.24) used in this research is

$$ITAE_k = T_s \sum_0^M kT_s|e_k| \tag{4.25}$$

where M is a finite sampling cycles.

Each particle has a position vector represented by

$$X_i(k) = \begin{bmatrix} \alpha_i(k) & \beta_i(k) & K_{P,i}(k) & K_{I,i}(k) & K_{D,i}(k) \end{bmatrix} \tag{4.26}$$

and a velocity vector represented by

$$V_i(k) = \begin{bmatrix} V_{\alpha,i}(k) & V_{\beta,i}(k) & V_{P,i}(k) & V_{I,i}(k) & V_{D,i}(k) \end{bmatrix} \tag{4.27}$$

Each particle remembers its own best position in a vector P_{best}

$$P_{best,i}(k) = \begin{bmatrix} P_{\alpha,i}(k) & P_{\beta,i}(k) & P_{P,i}(k) & P_{I,i}(k) & P_{D,i}(k) \end{bmatrix} \tag{4.28}$$

In (4.26), (4.27) and (4.28), i is an integer index satisfying $i \in (0, NumofPo)$ in which $NumofPo$ is the number of population.

The best position vector among all the neighbors of a particle is then stored in a global best vector G_{best}

$$G_{best,j} = \begin{bmatrix} G_{\alpha,j} & G_{\beta,j} & G_{P,j} & G_{I,j} & G_{D,j} \end{bmatrix} \tag{4.29}$$

in which j is an positive integer index satisfying $j \in (0, NumofIter)$ and $NumofIter$ is the number of iterations.

In each iteration, the velocity and position of each particle are manipulated by the following relations

$$V_i(k+1) = J(k)V_i(k) + c_1 \left(P_{best,i}(k) - X_i(k)\right) \mathbf{R}_1 + c_2 \left(G_{best,j} - X_i(k)\right) \mathbf{R}_2 \tag{4.30}$$

$$X_i(k+1) = X_i(k) + V_i(k+1) \tag{4.31}$$

in which $J(k)$ is an inertia weight computed by

$$J(k) = 0.5 + rand \tag{4.32}$$

where $rand$ generates a random number in $[0, 1]$ range and c_1, c_2 are normally called *cognitive* and *social* coefficient, usually in the range $0 \leq c_1, c_2 \leq 4$. The two matrices $\mathbf{R}_1$ and $\mathbf{R}_2$ are diagonal matrices of random numbers in $[0, 1]$. The step by step implementation of the PSO is as follows
Step 1: Initialization.

a. Initialize the position $X_i(0)$ $\forall$ i $\in$ 1:NumOfPo.

b. Initialize the best position to its initial position: $P_{best,i}(0) = X_i(0)$.

c. Run the closed-loop system with parameters $X_i(0)$ to calculate the $ITAE(X_i(0))$ for each particle and initialize the global best $G_{best}(0) = min(ITAE_i(0))$.

Step 2: Repeat the following tasks in $NumofIter$ iterations.

a. Update the global best $G_{best}(k) = Gbest(k-1)$.

b. Update the particle velocity according to (4.30).

c. Restrict the particle velocity in $[v_{min}, v_{max}]$ range.

d. Update the particle position as (4.31).

e. Restrict the particle position in safe zone to guarantee that the closed-loop system is stable during optimization process.

f. Run the closed-loop system with new particle position to compute the $ITAE(X_i(k+1))$ performance index.

g. If $ITAE(X_i(k+1)) \geq ITAE(P_{best,i}(k))$, update the personal best: $P_{best,i}(k) = X_i(k+1)$.

h. If $ITAE(X_i(k+1)) \geq ITAE(G_{best}(k))$, update the personal best: $G_{best}(k) = X_i(k+1)$.

Step 3: Obtain the best solution from G_{best} at the end of the iterative process.

4.4.4 Experiment results

To show the effectiveness of the PSO algorithm described in the previous subsection, experiments are conducted on system (2.1) with different number of population and iteration. The safe zone in which the system is stable can easily

be found by several experiments and expressed by

$$0 < K_P \leq 0.5 \tag{4.33}$$

$$0 < K_I \leq 1.0 \tag{4.34}$$

$$0 < K_D \leq 1.0 \tag{4.35}$$

$$0.9 < \alpha \leq 1.0 \tag{4.36}$$

$$0 < \beta \leq 1.0 \tag{4.37}$$

The optimization results are shown in Table 4.1.

Table 4.1: PSO results

PSO initial condition	K_P	K_I	K_D	α	β
$NumofPo = 5$, $NumofIter = 15$	0.3635	0.8845	0.4924	0.9875	0.1125
$NumofPo = 15$, $NumofIter = 15$	0.2133	0.9721	0.4641	0.9841	0.2178
$NumofPo = 15$, $NumofIter = 15$	0.2096	0.84522	0.49985	1.0	1.0

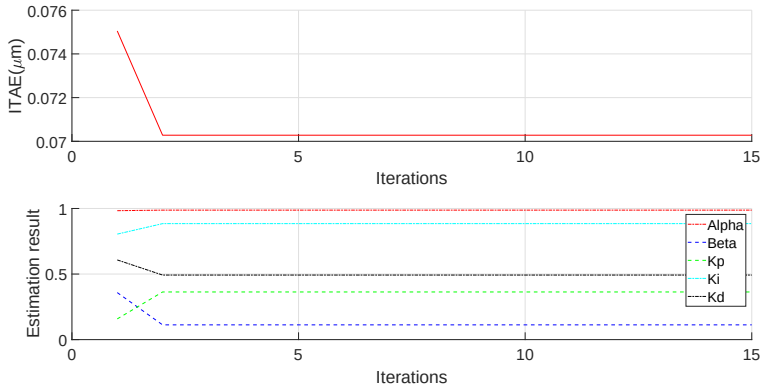

Figure 4.7: PSO result with $NumofPo = 5$ and $NumofIter = 15$

The experiment result with $NumofPo = 5$ and $NumofIter = 15$ is shown Fig. 4.7. As can be observed, the ITAE converges to its minimum value in just

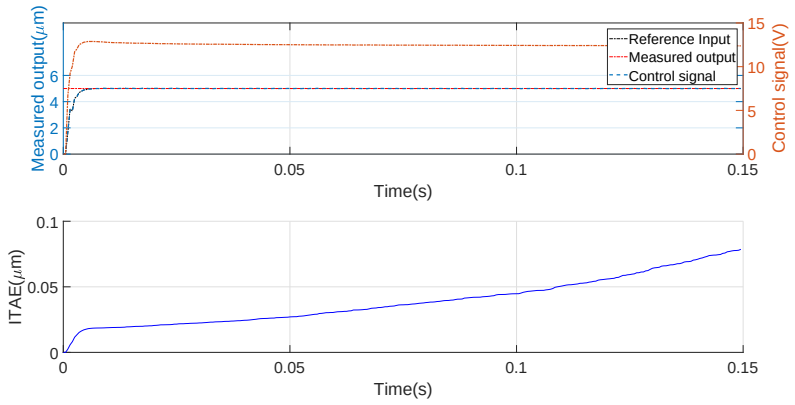

Figure 4.8: Step response of the $PI^{\alpha}D^{\beta}$ with $NumofPo = 5$ and $NumofIter = 15$

one iteration. It can also be seen that the fractional order of integral α is always close to 1 to mitigate the oscillation amplitude. In contrast, the fractional order of differential β is always close to 0 to remove the fluctuation may caused by the differential gain K_D. As a result, the step response of the closed-loop system is quite smooth without overshoot and steady-state tracking error as seen in Fig. 4.8.

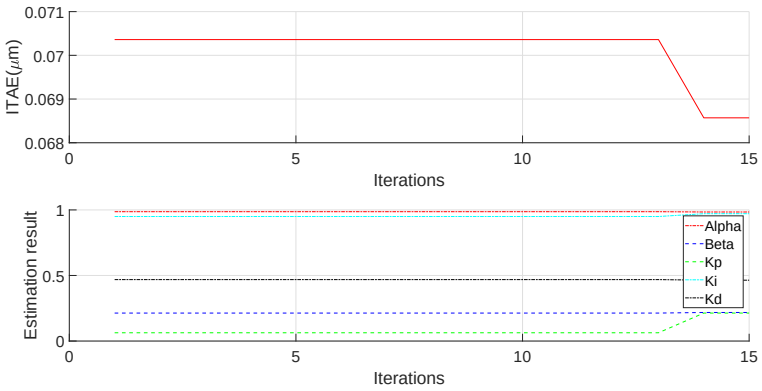

Figure 4.9: PSO result with $NumofPo = 15$ and $NumofIter = 15$

As the number of population increases, i.e, $NumofPo = 15$ and $NumofIter = 15$, it can be observed from Fig. 4.9 that the convergence time of the ITAE is a little bit slower, i.e, 13 iterations. However, the experimental step response is

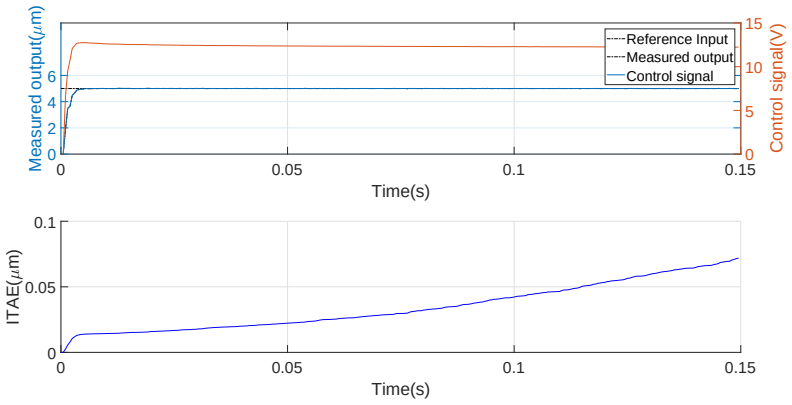

Figure 4.10: Step response of the $PI^{\alpha}D^{\beta}$ with $NumofPo = 15$ and $NumofIter = 15$

almost same as seen in Fig. 4.10. This means the PSO algorithm can give good result with few computational effort.

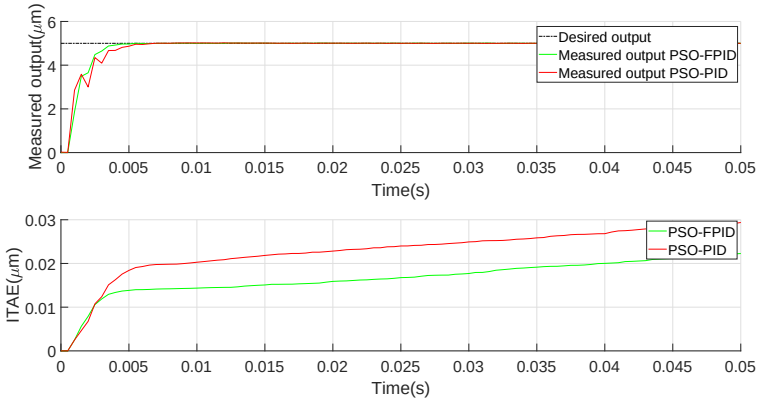

Figure 4.11: Comparative experiment results between PSO-$PI^{\alpha}D^{\beta}$ and PSO-PID

The comparative step response between the optimal fractional order $PI^{\alpha}D^{\beta}$ and the optimal conventional PID is shown in Fig. 4.11. The parameters of the conventional PID is also obtained by running the PSO with same restrictions expressed by (4.33), (4.34) and (4.35). It can obviously be seen that with two more degree of freedoms, the $PI^{\alpha}D^{\beta}$ controller always shows better response than its integer order counterpart and achieves lower $ITAE$ as well.

Finally, experiments with other complicated desired outputs are conducted.

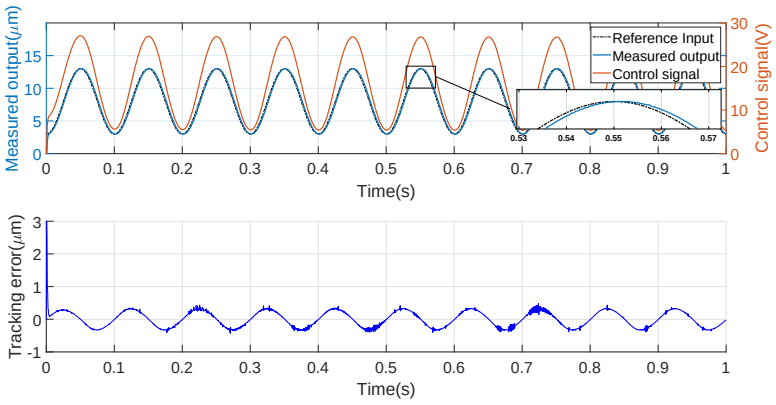

Figure 4.12: Tracking performance of $PI^{\alpha}D^{\beta}$ with 10Hz sinusoidal desired output

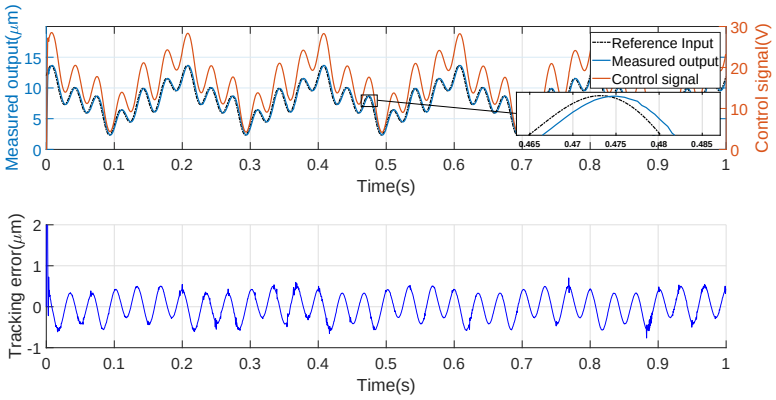

Figure 4.13: Tracking performance of of $PI^{\alpha}D^{\beta}$ with mixed amplitude and frequency desired output

The experiment result with 10Hz sinusoidal reference output is shown in Fig. 4.12. The result achieved with other complicated desired output such as mixed amplitude-frequency, time-varying amplitude and frequency, sawtooth desired outputs are shown in Fig. 4.13, Fig. 4.14 and Fig. 4.15, respectively. It can be seen that as the tracking frequency increases, the tracking performance is degraded due to the phase shift and the reduction of the system gain. Hence, a DF-PIDSMC is introduced in the next section to enhance the tracking performance of the system.

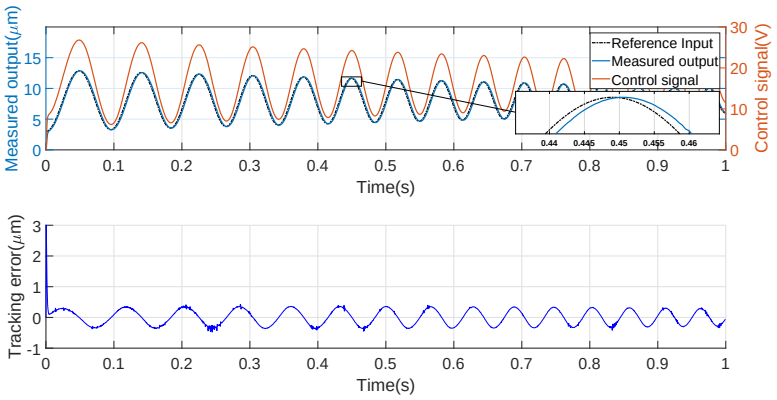

Figure 4.14: Tracking performance of of $PI^{\alpha}D^{\beta}$ with time-varying amplitude and frequency desired output

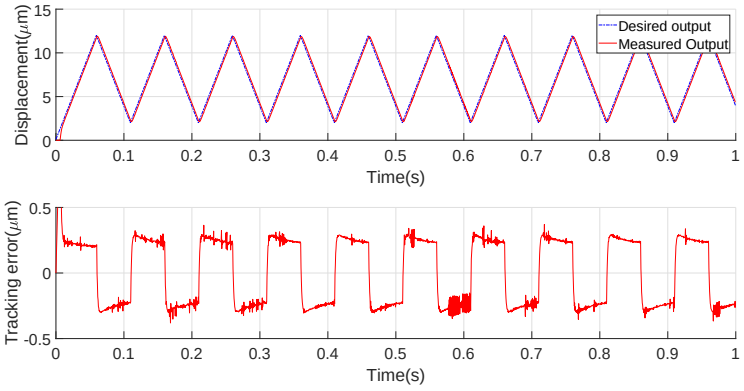

Figure 4.15: Tracking performance of of $PI^{\alpha}D^{\beta}$ controller with sawtooth desired output

4.5 DFISMC Design

In this section, the design of DFISMC with fuzzy tuning is presented.

4.5.1 Control Design

Consider the following fractional order variable:

$$\Lambda_k = e_k +^{\alpha} \Xi_{e,k} \tag{4.38}$$

where ${}^{\alpha}\Xi_{e,k}$ is the integral of the tracking error with fractional order α and integral gain K_I

$$ {}^{\alpha}\Xi_{e,k} = {}^{\alpha}\ \Xi_{e,k-1} + K_I \left(\sum_{j=2}^{N} \Omega_j \tilde{e}_{k-N+j} + \Omega_1 e_{k-N+1} \right) \tag{4.39} $$

and ${}^{\alpha}\Xi_{e,0} = \omega_N e_0$ at initial state.

The one-step ahead value of Λ is

$$ \Lambda_{k+1} = e_{k+1} + {}^{\alpha}\ \Xi_{e,k+1} \tag{4.40} $$

with

$$ {}^{\alpha}\Xi_{e,k+1} = {}^{\alpha}\ \Xi_{e,k} + K_I \left(\sum_{j=2}^{N} \Omega_j \tilde{e}_{k-N+j+1} + \Omega_1 e_{k-N+2} \right) \tag{4.41} $$

From (4.38), it can be deduced that

$$ {}^{\alpha}\Xi_{e,k} = \Lambda_k - e_k \tag{4.42} $$

Hence, (4.40) can be rewritten based on (4.41) and (4.39) as

$$ \Lambda_{k+1} = e_{k+1} + \Lambda_k - e_k + K_I \left(\sum_{j=2}^{N} \Omega_j \tilde{e}_{k-N+j+1} + \Omega_1 e_{k-N+2} \right) \tag{4.43} $$

which yields

$$ \Lambda_{k+1} - \Lambda_k = (1 + K_I \Omega_N) e_{k+1} - (1 + K_I \tilde{\Omega}_N) e_k - K_I \sum_{j=2}^{N-1} \tilde{\Omega}_j e_{k-N+j} \tag{4.44} $$

Now, define the sliding variable S_{k+1} as

$$ S_{k+1} = \Lambda_{k+1} - \Lambda_k \tag{4.45} $$

and by substituting (2.19) and (2.16) into (4.45), it gives

$$ \begin{aligned} S_{k+1} = & -(1 + K_I \tilde{\Omega}_N) e_k - K_I \sum_{j=2}^{N-1} \tilde{\Omega}_j e_{k-N+j} \\ & + (1 + K_I \Omega_N) \left[y_{d,k+1} + \sum_{i=0}^{n-1} a_i y_{k-i} - \sum_{j=0}^{m-1} b_j u_{k-j} - \hat{p}_k - \tilde{p}_k \right] \end{aligned} \tag{4.46} $$

The control action is obtained based on the following reaching law

$$S_{k+1} = 0 \tag{4.47}$$

By neglecting the unknown disturbance estimation error $\tilde{p}_k$, the solution for (4.47) is

$$\begin{aligned} u_k = & \frac{1}{b_1}\left(y_{d,k+1} + \sum_{i=0}^{n-1} a_{i+1} y_{k-i} - \sum_{j=1}^{m-1} b_{j+1} u_{k-j} - \hat{p}_k\right) \\ & - \frac{(1 + K_I\tilde{\Omega}_N)e_k + K_I \sum_{j=2}^{N-1} \tilde{\Omega}_j e_{k-N+j}}{b_1(1 + K_I\Omega_N)} \end{aligned} \tag{4.48}$$

The dynamic of the tracking error is obtained by substituting (4.48) into (2.19). Then, a fundamental operations gives

$$\begin{aligned} e_{k+1} &= \frac{1 + K_I\tilde{\Omega}_N}{1 + K_I\Omega_N} e_k + \frac{K_I}{1 + K_I\Omega_N} \sum_{j=2}^{N-1} \tilde{\Omega}_j e_{k-N+j} - \tilde{p}_k \\ &= \frac{1 + K_I\tilde{\Omega}_N}{1 + K_I\Omega_N} e_k + \frac{K_I}{1 + K_I\Omega_N} \sum_{j=2}^{N-1} \tilde{\Omega}_j e_{k-N+j} + O(T_s^2) \end{aligned} \tag{4.49}$$

with

$$\tilde{\Omega}_j = \Omega_j - \Omega_{j-1} \tag{4.50}$$

It can be seen that the dynamic of the tracking error (4.49) is high order and complicated. Besides, it is not so difficult to realize that (4.49) is also the generalized error dynamic of the conventional DISMC, i.e, if $\alpha = 1$ then $\tilde{\Omega}_j = 0 \; \forall j > 0$ and $\Omega_N = T_s$ which results in the error dynamic of the DISMC

$$e_{k+1} = \frac{1}{1 + K_I T_s} e_k + O(T_s^2) \tag{4.51}$$

To illustrate the dynamic of the tracking error described by (4.49), simulations are conducted for the identified model (2.2) of the positioning system. The simulative unit impulse response of the error is shown in Fig. 4.16. It can be observed that as α decreases, the transient time increases.

The simulative step response of the control system where the nominal plant used in control design and the plant used in simulation are same is shown in Fig.

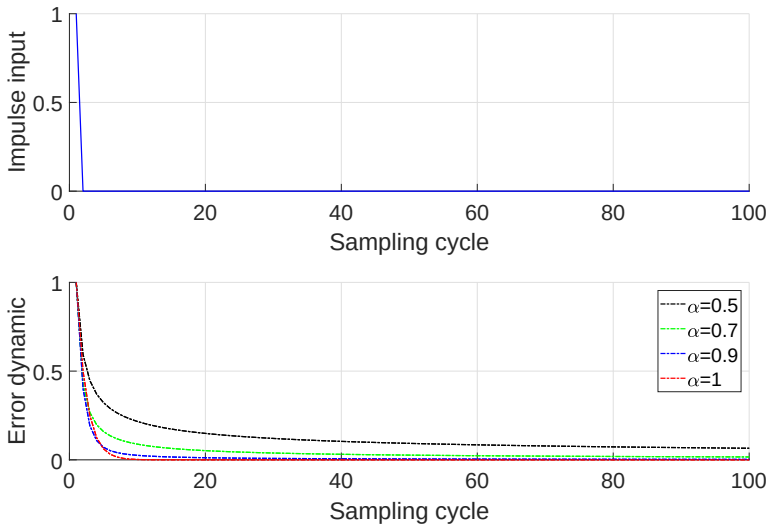

Figure 4.16: Influence of α on the error dynamic

4.17. When the model is perfect, the overshoot does not occur and the behavior of the system in transient-state is similar to what described by the error dynamic. This means the reduction of α yields a worse transient response with large ITAE. Hence, the fractional order α should be kept close to 1 in this case.

$$y_{k+1} = -0.95 \times 0.19 y_k - 1.05 \times 0.009 y_{k-1} + 0.5 \times 0.49 u_k + 1.5 \times 0.047 u_{k-1} \tag{4.52}$$

Figure (4.18) shows the simulation results in a more practical circumstance: the model used in simulation (4.52) is different from the nominal model of the plant (2.2) used in control design which means the modeling error exists. It can be seen that the overshoot occurs and α is useful in this situation since it can be used to reduce the overshoot.

The integral gain K_I also has influence on the system response as illustrated in Fig. (4.19). Large K_I yields faster response along with large overshoot. Thus, adjusting K_I and α simultaneously may give a balance solution in which small overshoot and quick response can be achieved.

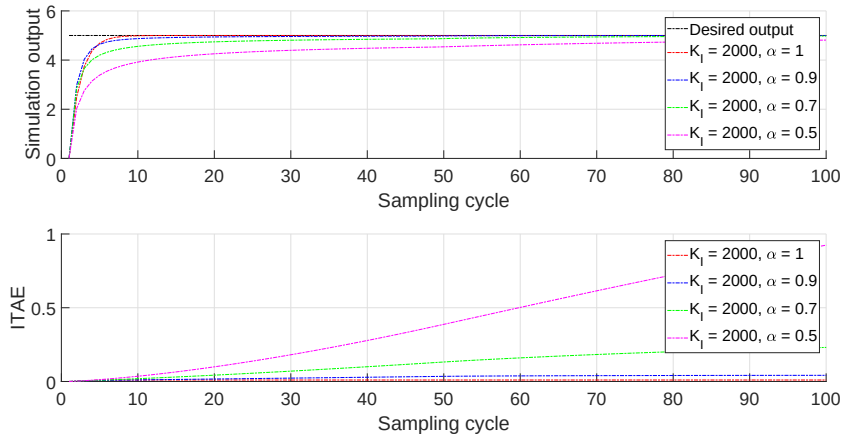

Figure 4.17: Simulative step response of DFISMC with accurate model

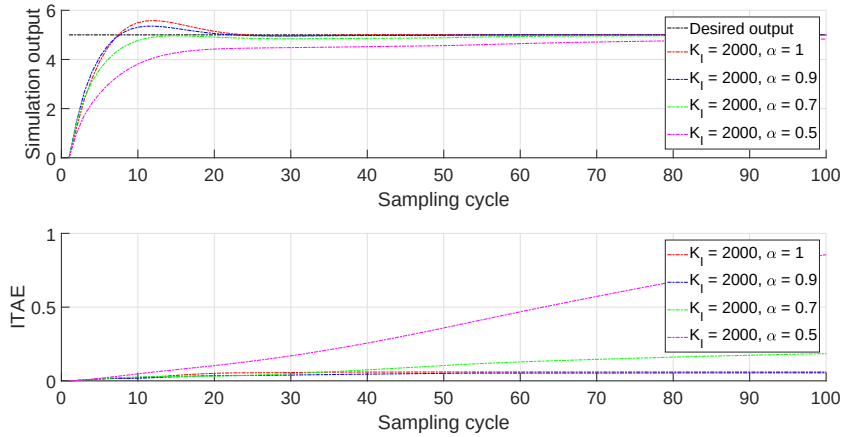

Figure 4.18: Simulative step response of DFISMC with inaccurate model

4.5.2 Fuzzy Tuning

To effectively utilize the integral gain K_P and the fractional order of integral α in improving the transient response of the control system, fuzzy technique is employed in this research. The absolute of the tracking error is used as the input of the fuzzy block whist K_P and α are outputs. The following rules based on the

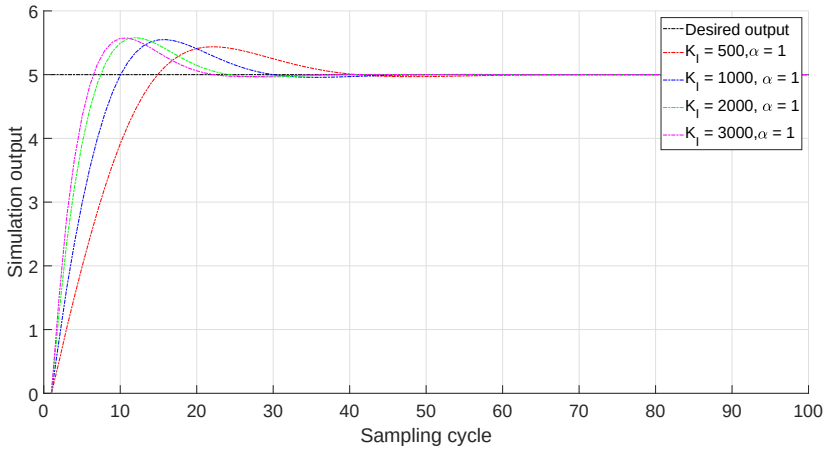

Figure 4.19: Influence of the integral gain K_I on transient response

Mamdani fuzzy inference method [51, 54] is employed

$$\begin{aligned}
&\textit{rule 1}\text{: If } |e_k| \text{ is PZ Then } K_I \text{ is PZ and } \alpha \text{ is PH}\\
&\textit{rule 1}\text{: If } |e_k| \text{ is PS Then } K_I \text{ is PZ and } \alpha \text{ is PL}\\
&\textit{rule 1}\text{: If } |e_k| \text{ is PM Then } K_I \text{ is PZ and } \alpha \text{ is PM}\\
&\textit{rule 1}\text{: If } |e_k| \text{ is PL Then } K_I \text{ is PZ and } \alpha \text{ is PS}\\
&\textit{rule 1}\text{: If } |e_k| \text{ is PH Then } K_I \text{ is PZ and } \alpha \text{ is PZ}
\end{aligned} \tag{4.53}$$

Then, the fuzzy sets are designed as shown in Fig. 4.20, Fig. 4.21 and Fig. 4.22. To reduce the computation cost, symmetrical input and output membership functions (MFs) are chosen. The general form of these MFs are described by

$$MF_r(x) = \begin{cases} \frac{2x-2c_{r,x}+w_{r,x}}{w_{r,x}} & for \quad c_{r,x} - \frac{w_{r,x}}{2} \leq x \leq c_{r,x} \\ \frac{2c_{r,x}-2x+w_{r,x}}{w_{r,x}} & for \quad c_{r,x} < x \leq c_{r,x} + \frac{w_{r,x}}{2} \\ 0 & otherwise \end{cases} \tag{4.54}$$

in which, $r = \{1, \cdots, 5\}$ is the index of the rule, $x = \{|e_k|, \alpha_k, K_{I,k}\}$ stands for the input variables of the MFs, $c_{r,x}$ and $w_{r,x}$ are center and width of each MF.

Finally, the central of gravity method is used for defuzzification. Since the

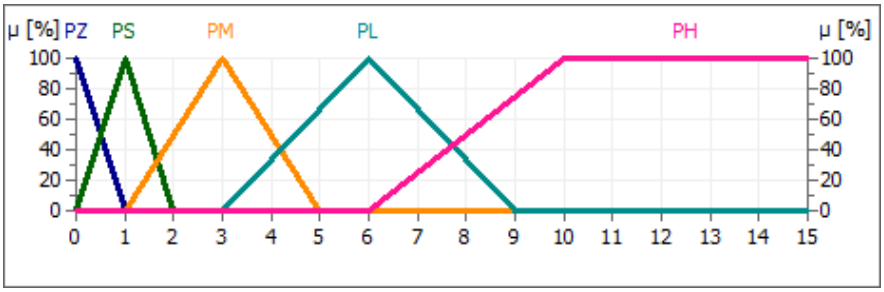

Figure 4.20: Membership functions of fuzzy input $|e_k|$

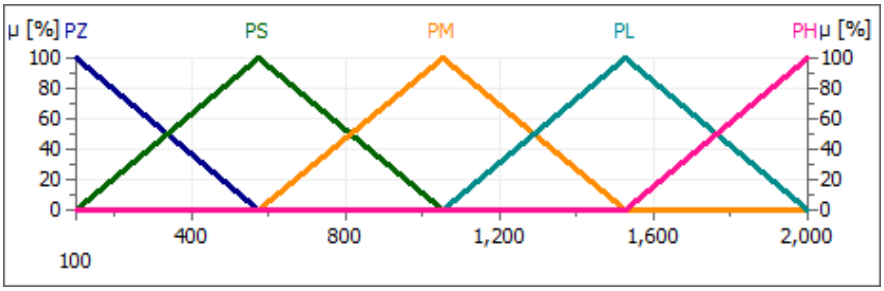

Figure 4.21: Membership functions of fuzzy output $|K_I|$

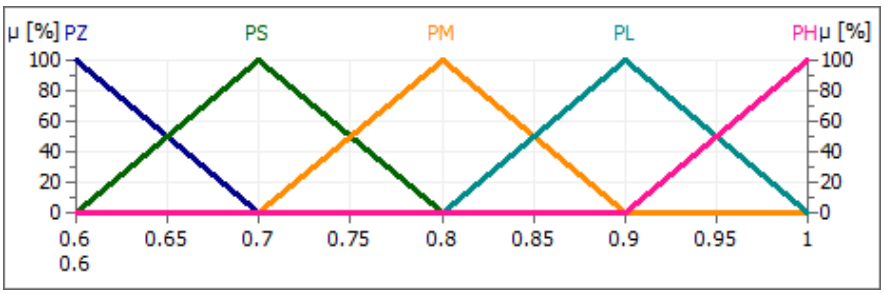

Figure 4.22: Membership functions of fuzzy output α

output MFs are symmetrical triangles, the solutions for the defuzzification is

$$\alpha_k = \frac{\sum_{r=1}^{5} MF_r(|e_k|) w_{(r,\alpha_k)} c_{(r,\alpha_k)}}{\sum_{r=1}^{5} MF_r(|e_k|) w_{(r,\alpha_k)}} \tag{4.55}$$

$$K_{I,k} = \frac{\sum_{r=1}^{5} MF_r(|e_k|) w_{(r,K_{I,k})} c_{(r,K_{I,k})}}{\sum_{r=1}^{5} MF_r(|e_k|) w_{(r,K_{I,k})}} \tag{4.56}$$

4.5.3 Experimental results

In this section, experimental results on the piezo-actuated positioning system are conducted to confirm the validity and feasibility of the proposed FDISMC.

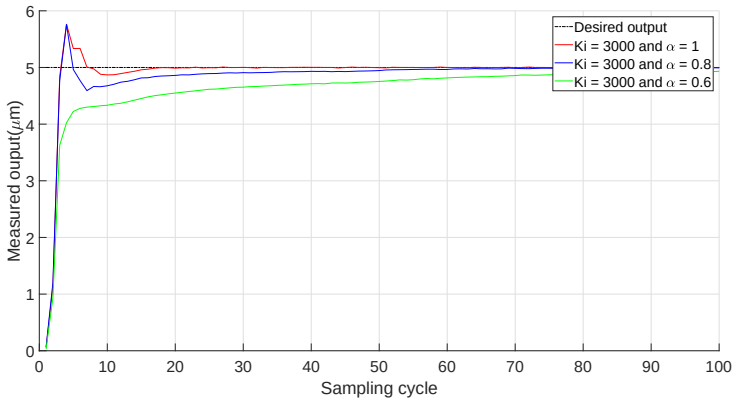

Figure 4.23: Experimental influence of the fractional order α

The influence of the fractional order α is first investigated and shown in Fig. 4.23. It can be seen that the behavior of the control system is same as described in the simulation where the overshoot can be avoided by reducing α.

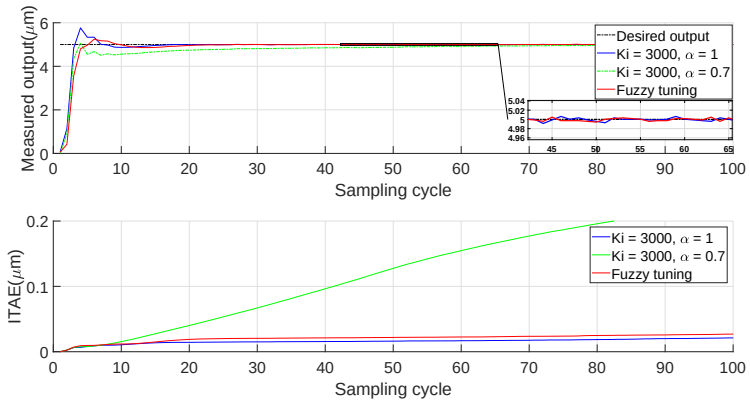

Figure 4.24: Comparative step responses

Then, the comparative step responses of the control system are depicted in Fig. 4.24 whist the outputs of the fuzzy block are shown in Fig. 4.25. If K_I and α are fixed (the blue and green line), either overshoot nor large ITAE are

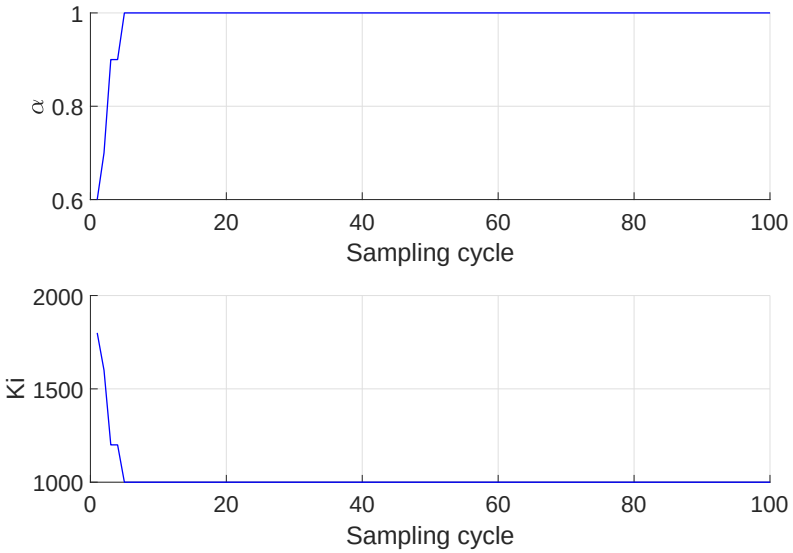

Figure 4.25: Fuzzy inference during transient-state

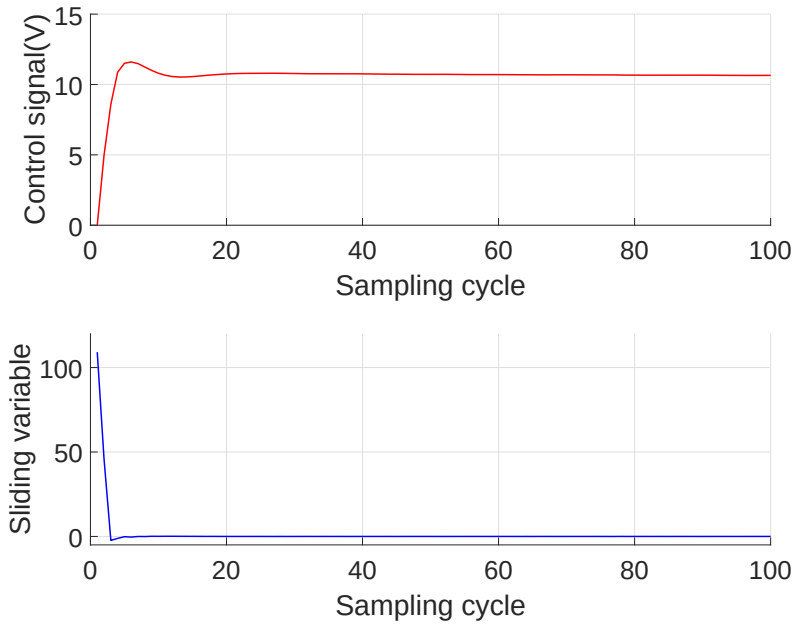

Figure 4.26: The control signal of FDISMC with step desired output

unavoidable. In contrast, improved transient response with low overshoot and

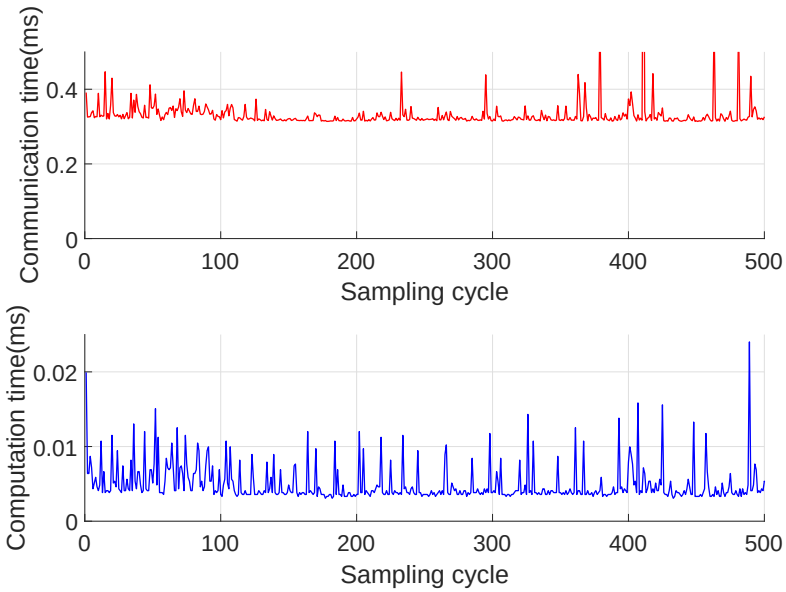

Figure 4.27: The computation time of the FDISMC algorithm

ITAE can be achieved by using the fuzzy tuning (the red line).

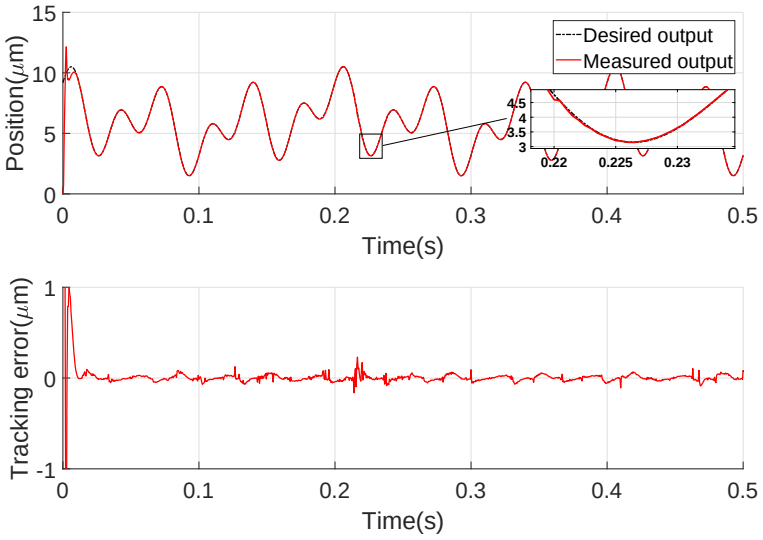

Figure 4.28: Tracking performance of the FDISMC with mixed amplitude-frequency desired output

Finally, the tracking performance is verified by using complicated desired out-

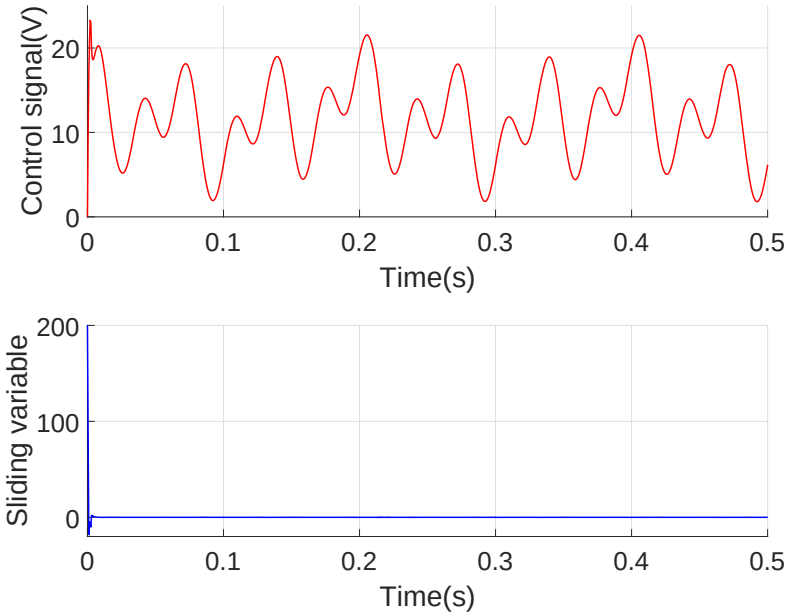

Figure 4.29: The control signal of the FDISMC with mixed amplitude-frequency desired output

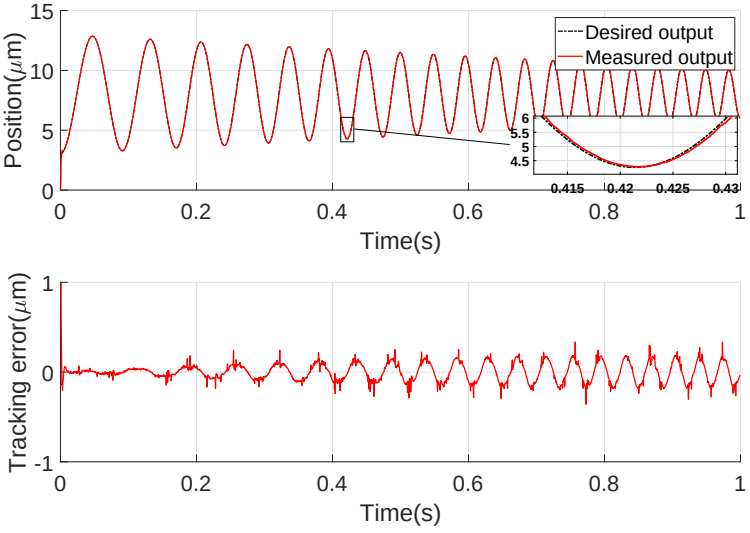

Figure 4.30: Experiment result of FDISMC with time-varying amplitude and frequency desired output

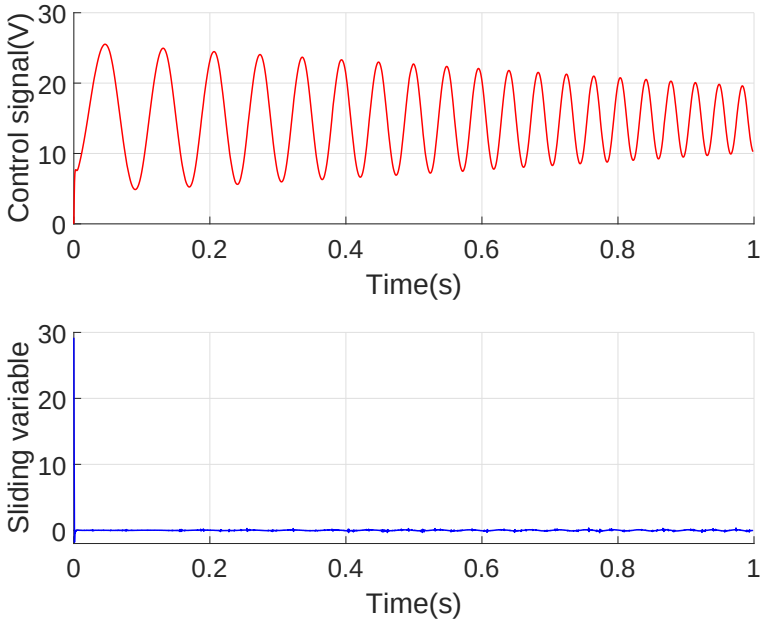

Figure 4.31: The control signal of FDISMC with time-varying amplitude and frequency desired output

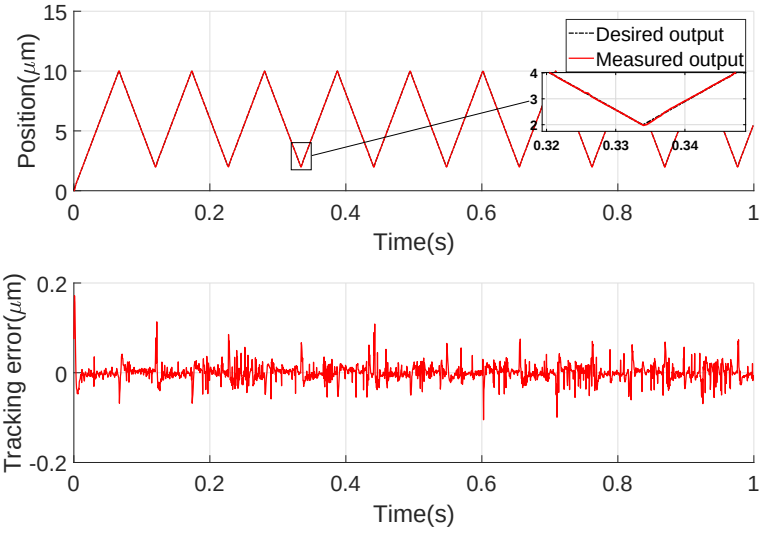

Figure 4.32: Experiment result of FDISMC with sawtooth desired output

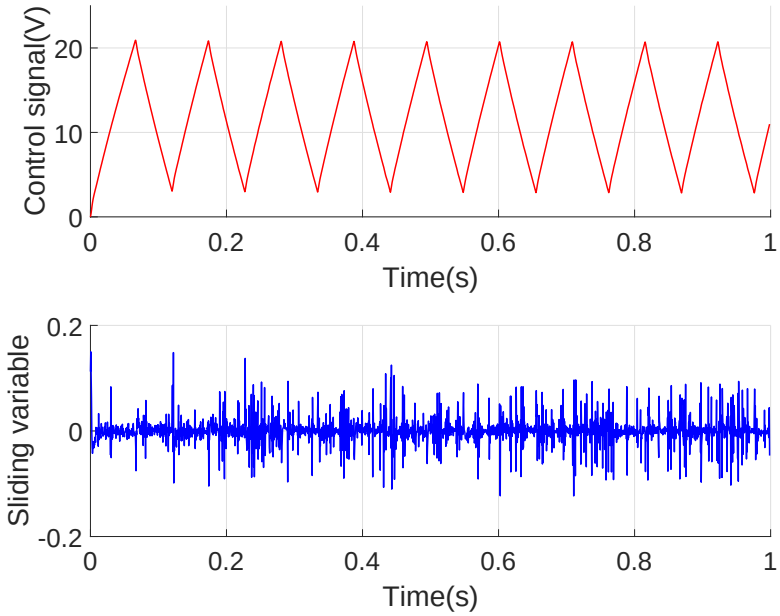

Figure 4.33: The control signal of FDISMC with sawtooth desired output

puts including sawtooth, time-varying amplitude and frequency, mixed amplitude-frequency as seen in Fig. 4.28 → Fig. 4.33. As long as the ratio between the sampling and tracking frequency is less than 100, the RMSTE is less than 0.1µm, corresponding to 1% of the maximal set-point. This result is acceptable for most practical applications.

4.6 Conclusion

In this chapter, the design and implementation of discrete-time fractional oder-based controllers are presented. First, a simple approximation of FOI which computes the FOI recursively is proposed. The proposed approximation does not require much computational effort and can easily be implemented in digital control platforms. Based on the proposed approximation, the discrete-time $PI^{\alpha}D^{\beta}$ controller of fractional order α and β is investigated. To optimize the parameters of this controller, the PSO technique is adopted. In advance, the optimization

process runs with real system instead of a mathematical model. Thus, the influence of the modeling error is trivial. However, as the conventional integer order PID controller, the tracking performance of the system with complicated desired outputs is always degraded as the tracking frequency increases due to the phase shift and gain reduction. To enhance the tracking performance, the DFISMC is considered. Fuzzy tuning is adopted to adjust the integral gain and the fractional order of integral such that the transient response of the control system is improved, i.e, both low overshoot and ITAE are achieved. The validity and effectiveness of the proposed methods are confirmed by experiments.

Chapter 5

Conclusions and Future Works

5.1 Conclusions

Aiming to practical and implementable control schemes which are capable of replacing the conventional PID controller widely installed in commercial devices in the area of micro/nano positioning, as well as achieving excellent tracking performance, various advanced control methods have been proposed in this study. First, the pseudo MPC is proposed and presented in *Chapter 2*. This scheme requires less tuning effort. In advanced, high tracking performance and robust against the modeling error are fulfilled. Second, the prescribed performance DSMC is proposed in *Chapter 3*. In comparison with the conventional DSMC and DISMC, this proposed method offers more degree of freedom which allows the transient response to be adjusted without influences of steady-state. Besides, the tracking performance is as good as the conventional DSMC. At last, the fractional order-based controllers are discussed in *Chapter 3*. This type of controller can be regarded as a generalization of their integer order-based counterparts and offers more degree of freedoms which may lead to the improvement of the control performance. In details, the $PI^{\alpha}D^{\beta}$ of fractional order α and β with a new FOI approximation technique is proposed. All parameters of the controller are optimized by PSO running on real system instead of the mathematical model. As a results, the influences of modeling error are removed. The achieved result is

quite nice with faster response, without overshoot and lower ITAE. However, the tracking performance with complicated desired outputs is still not improved in comparison with the conventional PID. Hence, to achieve a better results with complicated desired trajectories, the DFISMC with fuzzy tuning is also discussed.

Throughout this dissertation, all the control designs as well as analyses are carried out in discrete-time domain. This approach allows the control action to be easily implemented in any embedded systems. On the other hand, the disturbance estimation based on one-step delay technique also plays a very important role in compensating the uncertainties as well as improving the robustness of the control system.

Finally, a lot of experiments employing complicated desired trajectories and external disturbances are conducted to carefully verify the validity and effectiveness of the proposed control schemes. Comparative experiments are also carried out to show the advantages of the proposed method over their conventional counterparts. The effectiveness of the proposed controllers can be summarized by comparative experiments shown in Fig. 5.1 and Fig. 5.2. As can be observed in Fig. 5.1, the pseudo MPC, PPF-DSMC and FDISMC show much better tracking performance in comparison with the conventional PID controller as well as the fractional PID controller since advanced techniques such as adaptive control, disturbance estimation are utilized in combination with conventional controllers. The computation times of each method are provided in Fig. 5.2. Among such proposed methods, the computation cost of the pseudo MPC is highest because of the matrix multiplications in update laws. Right behind the pseudo MPC is the FDISMC. The reason is that the fractional order calculus itself requires large number of past data. Besides, fuzzification and defuzzification algorithms are also complicated. Although exhibit lowest computation cost, the fractional PID can not achieve high tracking performance with complicated desired output. Hence, the proposed PPF-DSMC seems to be a balance method due to its good performance and acceptable computation cost.

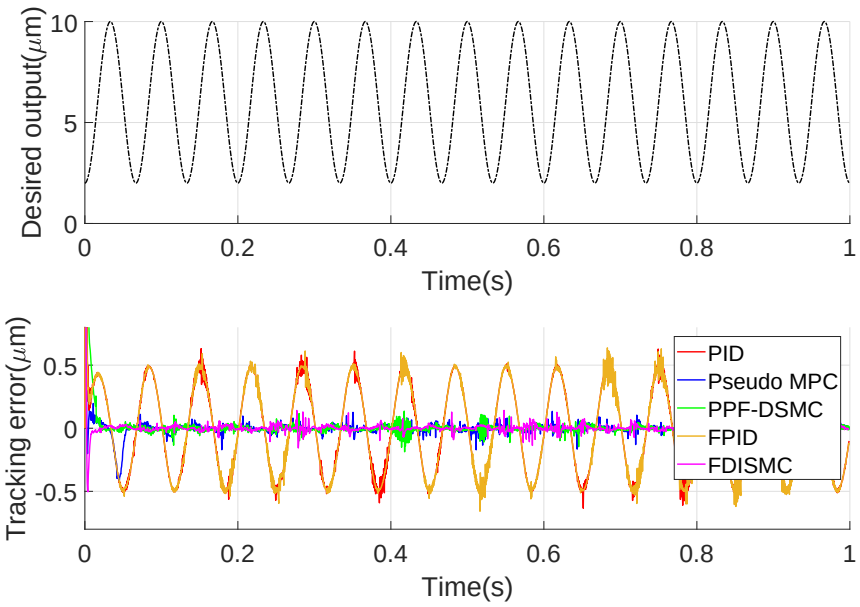

Figure 5.1: Comparative tracking errors

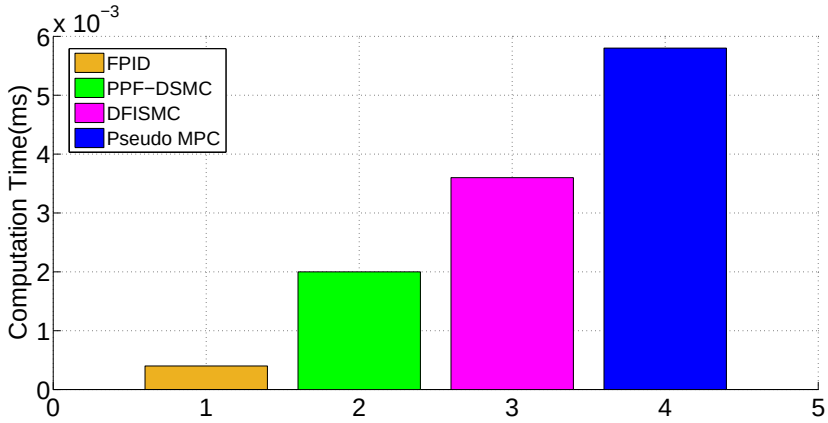

Figure 5.2: Comparative computation times

5.2 Future works

Throughout this study, all the control algorithms are implemented an run on a personal computer (PC). Due to the communication delay between the PC and the interface card, the sampling frequency is restricted at 2kHz. This fact prevents

the authors from using systematical identification methods which is capable of capturing the behavior of the positioning system at higher frequency to get a better model. On the other hand, investigating the tracking performance using high frequency desired output is also impossible. Other type of actuators in the field of micro/nano positioning have not also been investigated yet. Finally, due to the complicated and high order of the DFISMC, a systematic design method to optimize the parameters of the controller has not been well studied. Hence, the following issues are going to be considered in near future:

a. To verify the developed control schemes for other type of actuators in the area of micro/nano positioning.

b. To implement the developed control methods on an embedded system which has similar configuration with the commercial controllers such that fair comparative experiments can be conducted.

c. To investigate the behavior of the positioning system at high frequency.

d. To propose a systematic design method for the DFISMC.

e. To develop a *plug and run* controller based on an effective identification and optimization procedure.

References

[1] PI Digital Motion Controller, https://www.physikinstrumente.com/en/technology/controllers-software/precision-motion-control.

[2] K. Abidi, J. X. Xu, and Y. Xinghuo. On the discrete-time integral sliding-mode control. *IEEE Transactions on Automatic Control*, **52**(4):709–715, April 2007.

[3] I. Ahmad. Two degree-of-freedom robust digital controller design with bouc-wen hysteresis compensator for piezoelectric positioning stage. *IEEE Access*, **6**:17275–17283, 2018.

[4] Wei Tech Ang, F. A. Garmon, P. K. Khosla, and C. N. Riviere. Modeling rate-dependent hysteresis in piezoelectric actuators. In *Proceedings 2003 IEEE/RSJ International Conference on Intelligent Robots and Systems (IROS 2003) (Cat. No.03CH37453)*, **2**, pages 1975–1980 vol.2, Oct 2003.

[5] A. Badel, J. Qiu, and T. Nakano. A new simple asymmetric hysteresis operator and its application to inverse control of piezoelectric actuators. *IEEE Transactions on Ultrasonics, Ferroelectrics, and Frequency Control*, **55**(5):1086–1094, May 2008.

[6] A. Bartoszewicz and P. Leniewski. Reaching law approach to the sliding mode control of periodic review inventory systems. *IEEE Transactions on Automation Science and Engineering*, **11**(3):810–817, July 2014.

[7] A. Bartoszewicz and P. Leniewski. New switching and nonswitching type reaching laws for smc of discrete time systems. *IEEE Transactions on Control Systems Technology*, **24**(2):670–677, March 2016.

[8] C. P. Bechlioulis and G. A. Rovithakis. Robust partial-state feedback prescribed performance control of cascade systems with unknown nonlinearities. *IEEE Transactions on Automatic Control*, **56**(9):2224–2230, Sept 2011.

[9] Charalampos P. Bechlioulis and George A. Rovithakis. Adaptive control with guaranteed transient and steady state tracking error bounds for strict feedback systems. *Automatica*, **45**(2):532 – 538, 2009.

[10] J. Cao, S. Q. Xie, and R. Das. Mimo sliding mode controller for gait exoskeleton driven by pneumatic muscles. *IEEE Transactions on Control Systems Technology*, **26**(1):274–281, Jan 2018.

[11] Sohom Chakrabarty and Bijnan Bandyopadhyay. A generalized reaching law for discrete time sliding mode control. *Automatica*, **52**:83 – 86, 2015.

[12] Sohom Chakrabarty and Bijnan Bandyopadhyay. A generalized reaching law with different convergence rates. *Automatica*, **63**:34 – 37, 2016.

[13] S. Y. Chen and C. Y. Lee. Digital signal processor based intelligent fractional-order sliding-mode control for a linear voice coil actuator. *IET Control Theory Applications*, **11**(8):1282–1292, 2017.

[14] X. Chen, C. Y. Su, Z. Li, and F. Yang. Design of implementable adaptive control for micro/nano positioning system driven by piezoelectric actuator. *IEEE Transactions on Industrial Electronics*, **63**(10):6471–6481, Oct 2016.

[15] Y. Chen, I. Petras, and D. Xue. Fractional order control - a tutorial. In *2009 American Control Conference*, pages 1397–1411, June 2009.

[16] YangQuan Chen, Huifang Dou, Blas M. Vinagre, and Concha. A. Monje. A robust tuning method for fractional order pi controllers. *IFAC Proceedings Volumes*, **39**(11):22 – 27, 2006. 2nd IFAC Workshop on Fractional Differentiation and its Applications.

[17] A. Chotai, P. C. Young, and M. A. Behzadi. Self-adaptive design of a nonlinear temperature control system. *IEE Proceedings D - Control Theory and Applications*, **138**(1):41–49, Jan 1991.

[18] M. L. Corradini, G. Ippoliti, S. Longhi, and G. Orlando. A quasi-sliding mode approach for robust control and speed estimation of pm synchronous motors. *IEEE Transactions on Industrial Electronics*, **59**(2):1096–1104, Feb 2012.

[19] M. Curkovic, K. Jezernik, and R. Horvat. Fpga-based predictive sliding mode controller of a three-phase inverter. *IEEE Transactions on Industrial Electronics*, **60**(2):637–644, Feb 2013.

[20] J. de Jess Rubio. Sliding mode control of robotic arms with deadzone. *IET Control Theory Applications*, **11**(8):1214–1221, 2017.

[21] S. Devasia, E. Eleftheriou, and S. O. R. Moheimani. A survey of control issues in nanopositioning. *IEEE Transactions on Control Systems Technology*, **15**(5):802–823, Sept 2007.

[22] Haibo Du, Xinghuo Yu, Michael Z.Q. Chen, and Shihua Li. Chattering-free discrete-time sliding mode control. *Automatica*, **68**:87 – 91, 2016.

[23] M. Edardar, X. Tan, and H. K. Khalil. Design and analysis of sliding mode controller under approximate hysteresis compensation. *IEEE Transactions on Control Systems Technology*, **23**(2):598–608, March 2015.

[24] M. O. Efe. Fractional order systems in industrial automation: A survey. *IEEE Transactions on Industrial Informatics*, **7**(4):582–591, Nov 2011.

[25] Weibing Gao, Yufu Wang, and A. Homaifa. Discrete-time variable structure control systems. *IEEE Transactions on Industrial Electronics*, **42**(2):117–122, Apr 1995.

[26] Jorge L. Garriga and Masoud Soroush. Model predictive control tuning methods: A review. *Industrial & Engineering Chemistry Research*, **49**(8):3505–3515, 2010.

[27] Ping Ge and Musa Jouaneh. Tracking control of a piezoceramic actuator. *IEEE Transactions on Control Systems Technology*, **4**(3):209–216, May 1996.

[28] Ping Ge and Musa Jouaneh. Tracking control of a piezoceramic actuator. *IEEE Transactions on Control Systems Technology*, **4**(3):209–216, May 1996.

[29] M. Goldfarb and N. Celanovic. Modeling piezoelectric stack actuators for control of micromanipulation. *IEEE Control Systems*, **17**(3):69–79, June 1997.

[30] Q. P. Ha, Q. H. Nguyen, D. C. Rye, and H. F. Durrant-Whyte. Fuzzy sliding-mode controllers with applications. *IEEE Transactions on Industrial Electronics*, **48**(1):38–46, Feb 2001.

[31] D. Habineza, M. Rakotondrabe, and Y. Le Gorrec. Bouc-wen modeling and feedforward control of multivariable hysteresis in piezoelectric systems: Application to a 3-dof piezotube scanner. *IEEE Transactions on Control Systems Technology*, **23**(5):1797–1806, Sept 2015.

[32] J. Y. Hung, W. Gao, and J. C. Hung. Variable structure control: a survey. *IEEE Transactions on Industrial Electronics*, **40**(1):2–22, Feb 1993.

[33] G. P. Incremona, A. Ferrara, and L. Magni. Mpc for robot manipulators with integral sliding modes generation. *IEEE/ASME Transactions on Mechatronics*, **22**(3):1299–1307, June 2017.

[34] Mohammed Ismail, Fayçal Ikhouane, and José Rodellar. The hysteresis bouc-wen model, a survey. *Archives of Computational Methods in Engineering*, **16**(2):161–188, Jun 2009.

[35] M. Al Janaideh and P. Krej. Inverse rate-dependent prandtl-ishlinskii model for feedforward compensation of hysteresis in a piezomicropositioning actuator. *IEEE/ASME Transactions on Mechatronics*, **18**(5):1498–1507, Oct 2013.

[36] Isabel S. Jesus and Ramiro S. Barbosa. Genetic optimization of fuzzy fractional pd+i controllers. *ISA Transactions*, **57**:220 – 230, 2015.

[37] J. Kennedy and R. Eberhart. Particle swarm optimization. In *Neural Networks, 1995. Proceedings., IEEE International Conference on*, **4**, pages 1942–1948 vol.4, Nov 1995.

[38] P. Krejci and K. Kuhnen. Inverse control of systems with hysteresis and creep. *IEE Proceedings - Control Theory and Applications*, **148**(3):185–192, May 2001.

[39] K. Kuhnen and H. Janocha. 1compensation of the creep and hysteresis effects of piezoelectric actuators with inverse systems.

[40] K. Kuhnen and H. Janocha. Adaptive inverse control of piezoelectric actuators with hysteresis operators. In *1999 European Control Conference (ECC)*, pages 791–796, Aug 1999.

[41] Klaus Kuhnen. Modeling, identification and compensation of complex hysteretic nonlinearities: A modified prandtl-ishlinskii approach. *European Journal of Control*, **9**(4):407 – 418, 2003.

[42] Z. Li and J. Shan. Modeling and inverse compensation for coupled hysteresis in piezo-actuated fabry-perot spectrometer. *IEEE/ASME Transactions on Mechatronics*, **22**(4):1903–1913, Aug 2017.

[43] Z. Li, X. Zhang, C. Y. Su, and T. Chai. Nonlinear control of systems preceded by preisach hysteresis description: A prescribed adaptive control approach. *IEEE Transactions on Control Systems Technology*, **24**(2):451–460, March 2016.

[44] Z. Li, X. Zhang, C. Y. Su, and T. Chai. Nonlinear control of systems preceded by preisach hysteresis description: A prescribed adaptive control approach. *IEEE Transactions on Control Systems Technology*, **24**(2):451–460, March 2016.

[45] L. Liu, K. K. Tan, S. Chen, C. S. Teo, and T. H. Lee. Discrete composite control of piezoelectric actuators for high-speed and precision scanning. *IEEE Transactions on Industrial Informatics*, **9**(2):859–868, May 2013.

[46] Y. Liu, J. Shan, Y. Meng, and D. Zhu. Modeling and identification of asymmetric hysteresis in smart actuators: A modified ms model approach. *IEEE/ASME Transactions on Mechatronics*, **21**(1):38–43, Feb 2016.

[47] Yanfang Liu, Jinjun Shan, Ulrich Gabbert, and Naiming Qi. Hysteresis and creep modeling and compensation for a piezoelectric actuator using a fractional-order maxwell resistive capacitor approach. *Smart Materials and Structures*, **22**(11):115020, 2013.

[48] Ying Luo and YangQuan Chen. Stabilizing and robust fractional order pi controller synthesis for first order plus time delay systems. *Automatica*, **48**(9):2159 – 2167, 2012.

[49] Chengbin Ma and Yoichi Hori. The time-scaled trapezoidal integration rule for discrete fractional order controllers. *Nonlinear Dynamics*, **38**(1):171–180, Dec 2004.

[50] H. Ma, J. Wu, and Z. Xiong. A novel exponential reaching law of discrete-time sliding-mode control. *IEEE Transactions on Industrial Electronics*, **64**(5):3840–3850, May 2017.

[51] E.H. Mamdani and S. Assilian. An experiment in linguistic synthesis with a fuzzy logic controller. *International Journal of Man-Machine Studies*, **7**(1):1 – 13, 1975.

[52] Federico Marini and Beata Walczak. Particle swarm optimization (pso). a tutorial. *Chemometrics and Intelligent Laboratory Systems*, **149**:153 – 165, 2015.

[53] I. D. Mayergoyz and G. Friedman. Generalized preisach model of hysteresis. *IEEE Transactions on Magnetics*, **24**(1):212–217, Jan 1988.

[54] J. L. Meza, V. Santibanez, R. Soto, and M. A. Llama. Fuzzy self-tuning pid semiglobal regulator for robot manipulators. *IEEE Transactions on Industrial Electronics*, **59**(6):2709–2717, June 2012.

[55] . Milosavljevic, B. Perunicic-Drazenovic, and B. Veselic. Discrete-time velocity servo system design using sliding mode control approach with disturbance compensation. *IEEE Transactions on Industrial Informatics*, **9**(2):920–927, May 2013.

[56] Concepcin A. Monje, Blas M. Vinagre, Vicente Feliu, and YangQuan Chen. Tuning and auto-tuning of fractional order controllers for industry applications. *Control Engineering Practice*, **16**(7):798 – 812, 2008.

[57] J. Na, Q. Chen, X. Ren, and Y. Guo. Adaptive prescribed performance motion control of servo mechanisms with friction compensation. *IEEE Transactions on Industrial Electronics*, **61**(1):486–494, Jan 2014.

[58] Y. Niu, D. W. C. Ho, and Z. Wang. Improved sliding mode control for discrete-time systems via reaching law. *IET Control Theory Applications*, **4**(11):2245–2251, November 2010.

[59] J. Peng and X. Chen. A survey of modeling and control of piezoelectric actuators. *Modern Mechanical Engineering*, **3**(1):1–20, February 2013.

[60] I. Podlubny. Fractional-order systems and pi/sup /spl lambda//d/sup /spl mu//-controllers. *IEEE Transactions on Automatic Control*, **44**(1):208–214, Jan 1999.

[61] E. Psomopoulou, A. Theodorakopoulos, Z. Doulgeri, and G. A. Rovithakis. Prescribed performance tracking of a variable stiffness actuated robot. *IEEE Transactions on Control Systems Technology*, **23**(5):1914–1926, Sept 2015.

[62] M. Rakotondrabe. Bouc-wen modeling and inverse multiplicative structure to compensate hysteresis nonlinearity in piezoelectric actuators. *IEEE Transactions on Automation Science and Engineering*, **8**(2):428–431, April 2011.

[63] Hadi Ramezanian, Saeed Balochian, and Asef Zare. Design of optimal fractional-order pid controllers using particle swarm optimization algorithm for automatic voltage regulator (avr) system. *Journal of Control, Automation and Electrical Systems*, **24**(5):601–611, Oct 2013.

[64] J. B. Rawlings. Tutorial overview of model predictive control. *IEEE Control Systems*, **20**(3):38–52, Jun 2000.

[65] A. Sabanovic. Variable structure systems with sliding modes in motion control: A survey. *IEEE Transactions on Industrial Informatics*, **7**(2):212–223, May 2011.

[66] L. Schirone, F. Celani, and M. Macellari. Discrete-time control for dc-ac converters based on sliding mode design. *IET Power Electronics*, **5**(6):833–840, July 2012.

[67] Pritesh Shah and Sudhir Agashe. Review of fractional pid controller. *Mechatronics*, **38**(Supplement C):29 – 41, 2016.

[68] H. J. Shieh, Y. J. Chiu, and Y. T. Chen. Optimal pid control system of a piezoelectric microspitioner. In *2008 IEEE/SICE International Symposium on System Integration*, pages 1–5, Dec 2008.

[69] G. Song, Jinqiang Zhao, Xiaoqin Zhou, and J. A. De Abreu-Garcia. Tracking control of a piezoceramic actuator with hysteresis compensation using inverse preisach model. *IEEE/ASME Transactions on Mechatronics*, **10**(2):198–209, April 2005.

[70] Wu-Chung Su, S. V. Drakunov, and U. Ozguner. An o(t2) boundary layer in sliding mode for sampled-data systems. *IEEE Transactions on Automatic Control*, **45**(3):482–485, Mar 2000.

[71] Yinggan Tang, Xiangyang Zhang, Dongli Zhang, Gang Zhao, and Xinping Guan. Fractional order sliding mode controller design for antilock braking systems. *Neurocomputing*, **111**(Supplement C):122 – 130, 2013.

[72] A. Theodorakopoulos and G. A. Rovithakis. Low-complexity prescribed performance control of uncertain mimo feedback linearizable systems. *IEEE Transactions on Automatic Control*, **61**(7):1946–1952, July 2016.

[73] Nasim Ullah, Wang Shaoping, Muhammad Irfan Khattak, and Muhammad Shafi. Fractional order adaptive fuzzy sliding mode controller for a position servo system subjected to aerodynamic loading and nonlinearities. *Aerospace Science and Technology*, **43**(Supplement C):381 – 387, 2015.

[74] V. Utkin. Variable structure systems with sliding modes. *IEEE Transactions on Automatic Control*, **22**(2):212–222, Apr 1977.

[75] D. Valerio and J. S. Costa. Introduction to single-input, single-output fractional control. *IET Control Theory Applications*, **5**(8):1033–1057, May 2011.

[76] D. Valerio and J. S. Costa. Introduction to single-input, single-output fractional control. *IET Control Theory Applications*, **5**(8):1033–1057, May 2011.

[77] B. Veselic, B. Perunicic-Drazenovic, and C. Milosavljevic. High-performance position control of induction motor using discrete-time sliding-mode control. *IEEE Transactions on Industrial Electronics*, **55**(11):3809–3817, Nov 2008.

[78] R. P. Vieira, C. C. Gastaldini, R. Z. Azzolin, and H. A. Grundling. Discrete-time sliding mode speed observer for sensorless control of induction motor drives. *IET Electric Power Applications*, **6**(9):681–688, November 2012.

[79] Liuping Wang and Peter C. Young. An improved structure for model predictive control using non-minimal state space realisation. *Journal of Process Control*, **16**(4):355 – 371, 2006.

[80] W. Wang, D. Wang, Z. Peng, and T. Li. Prescribed performance consensus of uncertain nonlinear strict-feedback systems with unknown control directions. *IEEE Transactions on Systems, Man, and Cybernetics: Systems*, **46**(9):1279–1286, Sept 2016.

[81] Z. Wang, Z. Zhang, and J. Mao. Precision tracking control of piezoelectric actuator based on bouc-wen hysteresis compensator. *Electronics Letters*, **48**(23):1459–1460, November 2012.

[82] Z. Wang, Z. Zhang, and J. Mao. Precision tracking control of piezoelectric actuator based on bouc-wen hysteresis compensator. *Electronics Letters*, **48**(23):1459–1460, November 2012.

[83] J. X. Xu and K. Abidi. Discrete-time output integral sliding-mode control for a piezomotor-driven linear motion stage. *IEEE Transactions on Industrial Electronics*, **55**(11):3917–3926, Nov 2008.

[84] Q. Xu. Piezoelectric nanopositioning control using second-order discrete-time terminal sliding-mode strategy. *IEEE Transactions on Industrial Electronics*, **62**(12):7738–7748, Dec 2015.

[85] Q. Xu. Piezoelectric nanopositioning control using second-order discrete-time terminal sliding-mode strategy. *IEEE Transactions on Industrial Electronics*, **62**(12):7738–7748, Dec 2015.

[86] Q. Xu. Precision motion control of piezoelectric nanopositioning stage with chattering-free adaptive sliding mode control. *IEEE Transactions on Automation Science and Engineering*, **14**(1):238–248, Jan 2017.

[87] Q. Xu and Y. Li. Micro-/nanopositioning using model predictive output integral discrete sliding mode control. *IEEE Transactions on Industrial Electronics*, **59**(2):1161–1170, Feb 2012.

[88] Q. Xu and Y. Li. Model predictive discrete-time sliding mode control of a nanopositioning piezostage without modeling hysteresis. *IEEE Transactions on Control Systems Technology*, **20**(4):983–994, July 2012.

[89] C. Yeroglu and N. Tan. Note on fractional-order proportional-integral-differential controller design. *IET Control Theory Applications*, **5**(17):1978–1989, Nov 2011.

[90] X. Yu and O. Kaynak. Sliding-mode control with soft computing: A survey. *IEEE Transactions on Industrial Electronics*, **56**(9):3275–3285, Sept 2009.

[91] X. Yu, B. Wang, and X. Li. Computer-controlled variable structure systems: The state-of-the-art. *IEEE Transactions on Industrial Informatics*, **8**(2):197–205, May 2012.

[92] Guo-Qiang Zeng, Jie Chen, Yu-Xing Dai, Li-Min Li, Chong-Wei Zheng, and Min-Rong Chen. Design of fractional order pid controller for automatic regulator voltage system based on multi-objective extremal optimization. *Neurocomputing*, **160**:173 – 184, 2015.

[93] WeiJia Zheng, Ying Luo, XiaoHong Wang, YouGuo Pi, and YangQuan Chen. Fractional order pid controller design for satisfying time and frequency domain specifications simultaneously. *ISA Transactions*, **68**:212 – 222, 2017.

[94] H. Zhou, K. K. Tan, and T. H. Lee. Micro-positioning of linear piezoelectric motors based on a learning nonlinear pid controller. In *Proceedings of the 39th IEEE Conference on Decision and Control (Cat. No.00CH37187)*, **1**, pages 913–918 vol.1, 2000.

Research Achievements

[P.1] M. L. Nguyen and X. Chen, "High precision motion control of piezo-actuated stages using discrete-time sliding mode control with prescribed performance function",*2016 14th International Conference on Control*, Automation, Robotics and Vision (ICARCV), Phuket, 2016, pp. 1-6.

[P.2] M. L. Nguyen and X. Chen, "Enhanced Discrete Time Sliding Mode Predictive Control for Micro/Nano Positioning Devices Based on Piezoelectric Actuators", *2016 Regional Conference on Electrical and Electronics Engineering (RCEEE)*, Hanoi, 2016.

[P.3] M. L. Nguyen and X. Chen, "Tracking Control of Piezo-Actuated Stage Based On Model Predictive Control and Disturbance Observer, *ICEE / The International Conference on Electrical Engineering*, Okinawa, Japan, 2016.

[P.4] M. L. Nguyen, X. Chen, "Discrete Time Quasi Sliding Mode Control For Piezo-Actuated Positioning Systems: A Prescribed Performance Control Approach, in *IFAC-Papers OnLine*, Volume 50, Issue 1, 2017, Pages 5121-5126, ISSN 2405-8963, https://doi.org/10.1016/j.ifacol.2017.08.780.

[P.5] M. L. Nguyen and X. Chen, "Digital Control of Single Phase UPS Inverters Based on Discrete-Time State and Disturbance Observer, *CASD2017 Symposium on Control and Automation for Sustainable Development*, Hanoi, 2017

[P.6] M. L. Nguyen and X. Chen, "Discrete-Time Fractional Order Integral Sliding Mode Control for Piezoelectric Actuators with Improved Performance Based on Fuzzy Tuning, *IEEE WCICA2018 The World Congress on Intelligent Control and Automation*, Changsha China, 2018.

[P.7] M. L. Nguyen, X. Chen and F. Yang, "Discrete-Time Quasi-Sliding-Mode Control With Prescribed Performance Function and its Application to Piezo-Actuated Positioning Systems," in *IEEE Transactions on Industrial Electronics*, vol. 65, no. 1, pp. 942-950, Jan. 2018. doi: 10.1109/TIE.2017.2708024